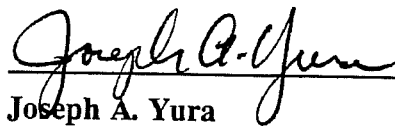


**BEHAVIOR OF REINFORCED CONCRETE PIER CAPS
UNDER CONCENTRATED BEARING LOADS**

APPROVED:



Joseph A. Yura



Michael E. Kreger

**To all the people who have encouraged
me to further my education,
and to my grandparents who I miss very much.**

**BEHAVIOR OF REINFORCED CONCRETE PIER CAPS
UNDER CONCENTRATED BEARING LOADS**

by

RICHARD JOHNATHAN DENIO, B.S.

THESIS

Presented to the Faculty of the Graduate School of

The University of Texas at Austin

in Partial Fulfillment

of the Requirements

for the Degree of

MASTER OF SCIENCE IN ENGINEERING

THE UNIVERSITY OF TEXAS AT AUSTIN

August 1993

ACKNOWLEDGEMENTS

This research project was funded by the Texas Department of Transportation. The author would like to thank TxDOT for funding the research project, and specifically thank Mike Lynch for working with me through the course of this project, finding bridge plans and calculations, and for his helpful comments. It was also a pleasure to work with David McDonald.

The author is deeply appreciative of his supervising professors for their guidance throughout the course of his stay at UT. It was a pleasure to work with Dr. Joe Yura who simplified numerous problems with his insight, and gave the author constant advice throughout testing and writing. Thanks also to Dr. Mike Kreger for his involvement and advice throughout the course of the project. Several professors were also extremely helpful to the author during his tenure in the lab. Thanks go in particular to Dr. Mike Engelhardt, Dr. Karl Frank, and Dr. James Jirsa for answering numerous questions.

Thanks must be extended to the other students working on this research project: Joe Ales, and Jason Olson. It was a pleasure to work with two dedicated students who took an interest in the overall project. The author greatly appreciates all the help on the lab floor making forms, tying steel, placing strain gages, pouring concrete, and running tests. Thanks go to Joe who continually answered questions on creating and operating a test set-up. Thanks go to Jason for help getting output from ANSYS. The author also appreciates the work of Emad Uddin Ahmed, who did everything possible to help out while working with the author.

The author is forever indebted to the lab staff who offered help whenever needed. From the upstairs group, sincere thanks go to April Jenkins for answering a million questions and keeping the author registered, Laurie Golding for getting all required materials and for dealing with suppliers, and Charon Cunningham for teaching the author everything needed to publish a thesis.

The author is greatly appreciative of the efforts of Bake Stassney to keep the lab running smoothly, and forever thankful that Bake fixed the 600 kip machine. Thanks much to Ray Madonna for helping the author deal with circuitry and the data acquisition systems, and Wayne Fontenot for the machining and the expert forklift maneuvering needed to place the spreader beam. Thanks to Pat Ball for the welding and help with the cameras, and to Wayne Little for helping order concrete, and run the crane and forklift. Lastly, thanks to Ryan Green who helped deal with the data acquisition systems, and for keeping the lab computers operating amongst the chaos. The author

enjoyed working with a talented group, and especially appreciates the patience of the staff as a new student adjusted to the lab environment.

It was the author's great pleasure to work with and relax with his fellow students. The pain of final exams and project deadlines was eased by a group that also looked forward to lulls in the grind. Several friends should be recognized for keeping the author sane in Texas and in good spirits. It was a hoot to live with Stacy Bartoletti and Jeff Borger who always were willing to forget school for awhile. Thanks also to Jim Light, Tom Pechillo, Bruce English, and all the others (especially the softball team) for all the good times. The author was thankful to have a chance to learn with a diverse group of students that were willing to share their ideas.

Finally, thanks Mom, Dad, Sue, and Tom, for being there all these years. Your love and support have made all this possible.

Richard J. Denio

May 24, 1993

TABLE OF CONTENTS

List of Tables	ix
List of Figures	x
Chapter 1 Introduction	1
1.1 Background/Problem Statement	1
1.2 Objectives and Scope	2
Chapter 2 Research Program	4
2.1 Typical TxDOT Pier Cap Design	4
2.2 Description of Test Specimens	6
2.2.1 Dimensions and Rebar Sizes for the Scale Specimens	6
2.2.2 Tested Reinforcing Patterns	7
2.3 Differences Between the Test Specimens and Full Size Piers	11
2.4 Materials	12
2.5 Fabrication of Specimens	13
2.6 Instrumentation	14
2.7 Test Set-Up	16
2.8 Loading Procedure	17
Chapter 3 Test Results	19
3.1 Nomenclature for Specimen Tests	19
3.2 Terminology for Discussing Test Results	19
3.3 Specimen Capacity	20
3.4 Load-Deflection Behavior	22
3.5 Cracking Loads	29
3.6 Failure Modes	30
3.7 Strain Gages	36
Chapter 4 Analysis of Results	41
4.1 Introduction	41

4.2	Discussion of Test Results	41
4.3	Corbel Analysis	43
4.4	Deep Beam Analysis	44
4.5	The Strut and Tie Design Method	45
4.5.1	Introduction	45
4.5.2	Major Assumptions of the Strut and Tie Method	47
4.5.3	Creation of a Strut and Tie Model	47
4.5.4	Individual Elements of the Strut and Tie Model	49
4.5.4.1	Ties	49
4.5.4.2	Struts	49
4.5.4.3	Nodes	51
4.6	Strut and Tie Model 1	53
4.6.1	Geometry and Assumptions of Model 1	53
4.6.2	Analysis Results from Strut and Tie Model 1	60
4.7	Strut and Tie Model 2	62
4.8	Summary of Strut and Tie Results	64
4.9	Design Example Using Strut and Tie Model 1	67
4.10	Comparison of Example Problem Reinforcing Steel to a Typical TxDOT Detail	75
Chapter 5	Summary and Conclusions	79
5.1	Objectives and Scope	79
5.2	Observed Behavior	79
5.3	Comparison of Design Methods	80
5.4	Areas for Additional Research	81
Appendix A	Tensile Tests of Rebar	82
Appendix B	Load - Displacement Graphs	83
Appendix C	Photos of the Failed Specimens	90
Appendix D	Load - Strain Graphs	102
Bibliography	109

LIST OF TABLES

Table 2.1	Rebar Sizes for Full Size and <u>Standard Scale Piers</u> (see Figure 2.3 for bar layout)	7
Table 2.2	Static Yield Strengths of Rebar	12
Table 2.3	Concrete Cylinder Compressive Strengths	12
Table 3.1	Summary of Specimen Reinforcement Patterns	21
Table 3.2	Specimen Capacities and Concrete Strengths	21
Table 3.3	Specimen Cracking Loads	29
Table 3.4	Comparison of Strain for the First and Second Tests on a Specimen	40
Table 4.1	Test Specimen Strengths	41
Table 4.2	Test Specimen Capacity Compared to the Strength Predicted by Conventional Design Methods	44
Table 4.3	Specimen Capacity and Member Forces for Strut and Tie Model 1	60
Table 4.4	Tested Capacities for Pier A and Pier C	61
Table 4.5	Limitations on the Components of T2 Based on Reinforcing in the Test Specimens	61
Table 4.6	Specimen Capacity and Member Forces for Strut and Tie Model 2	63
Table 4.7	Predicted Specimen Capacities when a V_c Term is Added to Strengths from Strut and Tie Model 1	65
Table 4.8	Comparison of Average Ratio of Theory/Test Capacity for Different Design Methods	66
Table 4.9	Strut and Tie Capacity and Member Forces for a Typical TxDOT Steel Detail (Figure 4.29)	77

LIST OF FIGURES

Figure 1.1	A Typical TxDOT Bridge Support	1
Figure 1.2	Application of Bridge Loads to the Pier Cap	1
Figure 1.3	Arch Action When the Span/Depth Ratio < 1	2
Figure 1.4	Test Set-Up for Scale Specimens	3
Figure 2.1	Pier Cap Geometry and Terminology	4
Figure 2.2	Typical Pier Geometry	4
Figure 2.3	Typical Pier Steel Reinforcing Pattern	5
Figure 2.4	Geometry of the Scale Test Specimens	6
Figure 2.5	Steel Reinforcing Detail for the Standard Scale Specimen (Pier A2)	8
Figure 2.6	Improper Placement of Bars U in Specimens A1 and A2	9
Figure 2.7	Top Layer Pier Cap Reinforcing in Specimen B	9
Figure 2.8	Lap Weld of Bar T	9
Figure 2.9	Specimen D Reinforcing	10
Figure 2.10	Relocation of Bars Z1 in the Test Specimens	11
Figure 2.11	Relocation of Bars B in the Test Specimens	12
Figure 2.12	Steel Reinforcing Cage for Specimen A2	13
Figure 2.13	Placement of Reinforcing Cages in Forms	14
Figure 2.14	Strain Gage Locations in Specimens C and D	15
Figure 2.15	Reduction in Rebar Cross Section Due to Strain Gage Placement	15
Figure 2.16	Location of Linear Pots	16
Figure 2.17	Test Set-Up Geometry	16
Figure 2.18	Placement of Test Specimens in the Test Machine	17
Figure 3.1	Load Paths for the Pier Cap	19
Figure 3.2	Patterns of Concrete Distress	20
Figure 3.3	Load Deflection Behavior for Pier A1-1	23
Figure 3.4	Crack Distribution on the Face of Pier A1-1 After Failure	24
Figure 3.5	Crack Distribution at the Top of Pier A1-1 After Failure	25

Figure 3.6	Crushing of Pier A1-1 After Failure	25
Figure 3.7	Comparison of Resultant Load vs. Deflection at Linear Pot #1	26
Figure 3.8	Comparison of Resultant Load vs. Deflection at Linear Pot #2	27
Figure 3.9	Comparison of Resultant Load vs. Deflection at Linear Pot #3	28
Figure 3.10	Specimens A1-1 and C-1 at Failure	31
Figure 3.11	Redistribution of Internal Forces in the Pier Cap	32
Figure 3.12	Development Lengths for Top Layer Reinforcing in Specimen B	32
Figure 3.13	Splitting Cracks Due to Bond Distress in Specimen B	33
Figure 3.14	Opening of Flexure/Shear for Pier B-2 - Spalled Cover Removed	33
Figure 3.15	Punching of the Base Plate into Pier B2-2	34
Figure 3.16	Crack Distribution on the Face of Pier D-1 After Failure	34
Figure 3.17	Force Distribution in Specimen D After Opening of the Flexural Crack	35
Figure 3.18	Cracking and Punching Under the Base Plate for Pier C-2	36
Figure 3.19	Strain Gage Locations in Specimens C and D	36
Figure 3.20	Resultant Load vs. Strain on Gages 1 - 4 for Pier C-1	37
Figure 3.21	Resultant Load vs. Strain on Gages 9 - 12 for Pier D-1	38
Figure 3.22	Resultant Load vs. Strain in Gages 5 - 8 for Pier C-2	39
Figure 3.23	Resultant Load vs. Strain in Gages 5 - 8 for Pier D-2	40
Figure 4.1	Force Distribution Assumed in Corbel Code Provisions (Salmon 1985)	43
Figure 4.2	Examples of Strut and Tie Models (from Schlaich 1987)	46
Figure 4.3	B and D Regions (Shaded) of a Structure (from Schlaich 1987)	48
Figure 4.4	Use of the Load Path Method to form a Strut and Tie Model (from Schlaich 1987)	48
Figure 4.5	The Good Strut and Tie Model has Shorter Ties Than the Bad Model (from Schlaich 1987)	49
Figure 4.6	The Three Compression Struts (a) The Fan (b) The Bottle (c) The Prism (from Schlaich 1987)	50
Figure 4.7	Strut and Tie Model Considering Transverse Tensile Stresses (from Schlaich 1987)	51
Figure 4.8	CCC Node with Unequal Pressure (from Barton 1988)	52
Figure 4.9	CCC Node Under Hydrostatic Stress (adapted from Anderson 1988)	52

Figure 4.10	CCT Node With Multiple Layers of Reinforcing (from Bergmeister 1990) . . .	53
Figure 4.11	Mesh Used for the Finite Element Analysis	54
Figure 4.12	Loading Applied to the Finite Element Model	54
Figure 4.13	Contour of Principal Tensile Stresses	54
Figure 4.14	Contour of Principal Compressive Stresses	55
Figure 4.15	Failure Pattern for a Typical Specimen	55
Figure 4.16	Shear Span Modelled in the Finite Element Analysis	56
Figure 4.17	Configuration of Strut and Tie Model 1	57
Figure 4.18	Determination of the Compression Field Width	57
Figure 4.19	Centroid Location for the Column Compression Strut	58
Figure 4.20	Layout of Compression Steel at the Edge of the Column	59
Figure 4.21	Configuration of Strut and Tie Model 2	62
Figure 4.22	Pier Cap Geometry for the Example Problem	67
Figure 4.23	Strut and Tie Model for the Example Problem	68
Figure 4.24	Cross Section of Strut C5	69
Figure 4.25	Location of Node 2 in the Strut and Tie Model	70
Figure 4.26	Geometry of the CCC Node (Node 2 in the Strut and Tie Model)	71
Figure 4.27	Steel Reinforcing Pattern from the Example Problem	72
Figure 4.28	Geometry of the CCT Node (Node 1 in the Strut and Tie Model)	73
Figure 4.29	Typical Steel Reinforcing Pattern Used by TxDOT	76
Figure A.1	Typical Stress - Strain Curve for a Tensile Test of Rebar	82
Figure B.1	Location of Linear Pots	83
Figure B.2	Resultant Load vs. Deflection at Linear Pots 1 through 4 for Pier A1-1	84
Figure B.3	Resultant Load vs. Deflection at Linear Pots 1 through 4 for Pier A2-2	85
Figure B.4	Resultant Load vs. Deflection at Linear Pots 1 through 4 for Pier A2-3	85
Figure B.5	Resultant Load vs. Deflection at Linear Pots 1 through 4 for Pier B-1	86
Figure B.6	Resultant Load vs. Deflection at Linear Pots 1 through 4 for Pier B-2	86
Figure B.7	Resultant Load vs. Deflection at Linear Pots 1 through 4 for Pier C-1	87
Figure B.8	Resultant Load vs. Deflection at Linear Pots 1 through 4 for Pier C-2	87
Figure B.9	Resultant Load vs. Deflection at Linear Pots 1 through 4 for Pier D-1	88

Figure B.10	Resultant Load vs. Deflection at Linear Pots 1 through 4 for Pier D-2	88
Figure B.11	Resultant Load vs. Deflection at Linear Pots 1 through 4 for Pier E-1	89
Figure B.12	Resultant Load vs. Deflection at Linear Pots 1 through 4 for Pier E-2	89
Figure C.1	Damage to Pier A1-1 After Failure	91
Figure C.2	Damage to Pier A2-2 After Failure	92
Figure C.3	Damage to Pier A2-3 After Failure	93
Figure C.4	Damage to Pier B-1 After Failure	94
Figure C.5	Damage to Pier B-2 After Failure	95
Figure C.6	Damage to Pier C-1 After Failure	96
Figure C.7	Damage to Pier C-2 After Failure	97
Figure C.8	Damage to Pier D-1 After Failure	98
Figure C.9	Damage to Pier D-2 After Failure	99
Figure C.10	Damage to Pier E-1 After Failure	100
Figure C.11	Damage to Pier E-2 After Failure	101
Figure D.1	Location of Strain Gages	102
Figure D.2	Resultant Load vs. Strain in Gages 1 through 4 for Pier C-1	103
Figure D.3	Resultant Load vs. Strain in Gages 5 through 8 for Pier C-1	103
Figure D.4	Resultant Load vs. Strain in Gages 9 through 12 for Pier C-1	104
Figure D.5	Resultant Load vs. Strain in Gages 2 and 4 for Pier C-2	104
Figure D.6	Resultant Load vs. Strain in Gages 5 through 8 for Pier C-2	105
Figure D.7	Resultant Load vs. Strain in Gages 9 through 12 for Pier C-2	105
Figure D.8	Resultant Load vs. Strain in Gages 1 through 4 for Pier D-1	106
Figure D.9	Resultant Load vs. Strain in Gages 5 through 8 for Pier D-1	106
Figure D.10	Resultant Load vs. Strain in Gages 9 through 12 for Pier D-1	107
Figure D.11	Resultant Load vs. Strain in Gages 1 through 4 for Pier D-2	107
Figure D.12	Resultant Load vs. Strain in Gages 5 through 8 for Pier D-2	108
Figure D.13	Resultant Load vs. Strain in Gages 9 through 12 for Pier D-2	108

CHAPTER 1

INTRODUCTION

1.1 BACKGROUND/PROBLEM STATEMENT

An increasing number of bridges are being constructed in urban areas where the bridge geometry is controlled by space limitations from existing roads, bridges, or other obstacles. When designing the bridge supports in these congested areas, lateral and vertical space constraints often dictate the configuration used for the bridge piers and bents. A typical bridge support detail used by the Texas Department of Transportation (TxDOT) when space is limited is shown in Figure 1.1.

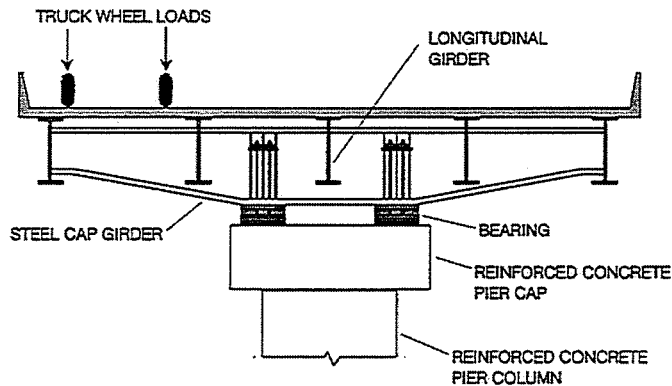


Figure 1.1 A Typical TxDOT Bridge Support

In this detail, longitudinal steel girders frame into a steel bent cap which is supported by a reinforced concrete pier cap. Compressive load is transferred from the steel bent to the pier cap through bearing plates whose reactions do not lie within the column as shown in Figure 1.2. Because the projection of the bearing load does not lie within the column, the pier cap design must consider shear. The capacity of the pier cap to withstand the eccentric compressive loads from the steel bent cap is the focus of this research.

When examining the compressive load carrying capacity of the pier cap, the nature of the

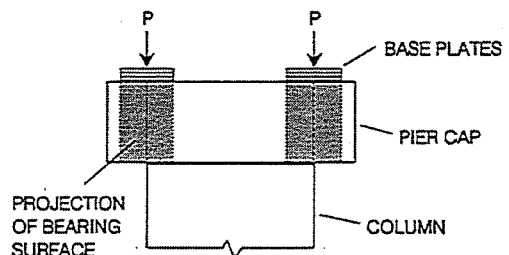


Figure 1.2 Application of Bridge Loads to the Pier Cap

transfer of load from the steel bent cap to the concrete pier cap is critical. The steel bent cap typically is supported on disc bearings, pot bearings, or bearing plates which are subject to factored loads on the order of 2,000 kips. All of these supports are relatively small compared to the area on top of the pier cap, and place highly concentrated compressive loads on the top of the pier cap. There are two basic problems to solve with respect to these concentrated loads. First, the concrete under the bearing plate must not crush. Second, the concentrated loads on the pier cap must be transferred to the column. The design for bearing capacity is clearly outlined in the AASHTO Bridge Specifications (AASHTO 1992). The design of the pier cap region to allow transfer of load to the column is much more difficult for the engineer, since it is an atypical section whose design is not explicitly covered in design codes. With the bearings placed outside of the interior of the column, the load is slightly eccentric to the column as shown in Figure 1.2. For the piers studied, the shear span is very small, with a span to depth ratio below 0.1. For reinforced concrete cantilevers with such small span to depth ratios, loads will be transferred primarily by the action of a tied arch as shown in Figure 1.3 (Salmon 1985). However, existing code provisions aimed at beams with span to depth ratios less than one do not consider arching action as a primary load carrying mechanism. Instead, existing code provisions for beams with span/depth ratios less than one focus on the capacity of concrete in shear. Thus, a design based on existing code provisions will be overly conservative because concrete can carry much less load in shear than in direct compression.

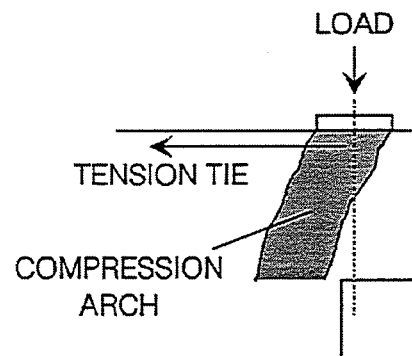


Figure 1.3 Arch Action When the Span/Depth Ratio < 1

1.2 OBJECTIVES AND SCOPE

The behavior of the entire connection shown in Figure 1.1 is being studied under a project for the Texas Department of Transportation (TxDOT). The research considers the distribution of forces within the bridge system, the behavior of the anchor bolt system, and the behavior of the concrete pier cap. This report focuses on the behavior and design of the reinforced concrete pier cap used by TxDOT subject to compressive loads. The objectives of this research are a determination of the strength and behavior of the reinforced concrete pier cap under compression loads, and the formulation of design recommendations for the pier cap.

To assess the capacity of the pier cap to sustain extreme compression loads, six pier caps at a 30 percent scale were tested in compression as shown in Figure 1.4. Steel reinforcement designs in the pier cap were altered to examine extremes in capacity, and to examine the contributions of different types and quantities of reinforcing steel to the strength of the pier cap. Three techniques that could be used to analyze the pier cap are compared. The two conventional design solutions that are applicable are a corbel analysis and deep beam analysis. As an alternative design method, a strut and tie model will be presented for comparison. Also, bearing stresses from testing will be compared with stresses allowed in the 1992 AASHTO provisions.

The test set-up is summarized in Chapter 2 of this report, which describes sizes of the specimens, steel reinforcement patterns, and loading geometry.

Results from the test program are summarized in Chapter 3 and are discussed in Chapter 4. Also in Chapter 4, pier cap strengths predicted by the different design techniques are compared, and a design example using the strut and tie method is presented. Full data from the tests and photos of the failed specimens are presented in the appendices.

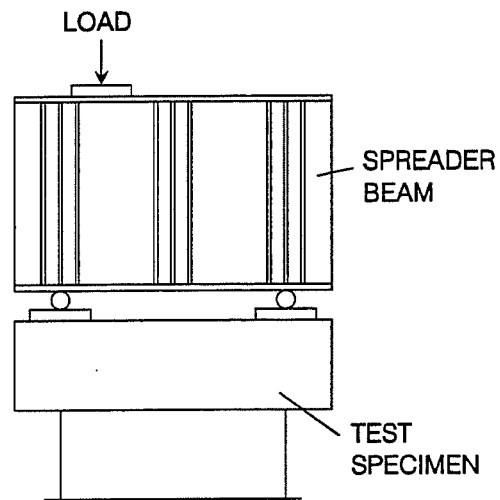


Figure 1.4 Test Set-Up for Scale Specimens

CHAPTER 2

RESEARCH PROGRAM

2.1 TYPICAL TxDOT PIER CAP DESIGN

The basic geometry of the pier cap and column studied and terminology used for the detail is shown in Figure 2.1. To study the behavior and strength of the pier cap, six one-third scale specimens were built and tested to failure.

With a known pier cap strength from experimental results, an improved design guideline to more accurately predict the strength of the detail can be produced.

The steel reinforcing patterns used by TxDOT for slightly different pier cap and column configurations are very similar, so the single pier cap geometry shown in Figure 2.2 was chosen as the focus of study. This configuration has a large extension of the pier cap beyond the column, with the centerline of the loading coinciding with the edge of the column. This layout produces a load eccentricity, which requires an inclined load path to transfer load from the pier cap into the column. The loading geometry shown represents the maximum eccentricity currently used by TxDOT for the pier cap/column configuration studied, so results can be applied to piers with a smaller load eccentricity.

The pattern and sizes of reinforcing that are usually used in the typical pier cap and column are shown in Figure 2.3. The top layer of

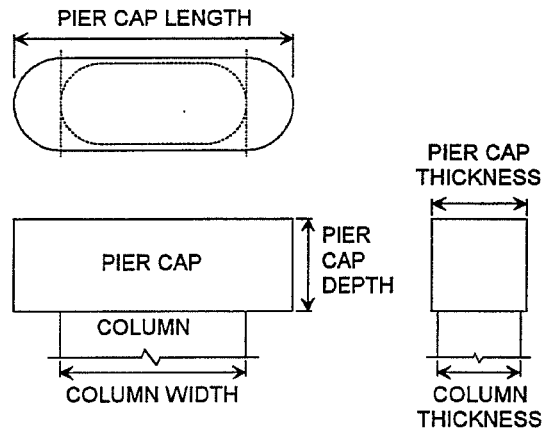


Figure 2.1 Pier Cap Geometry and Terminology

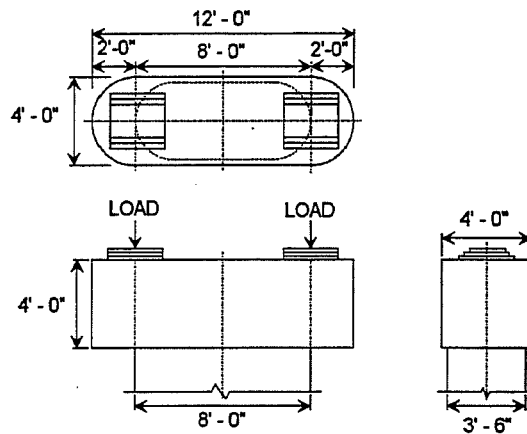
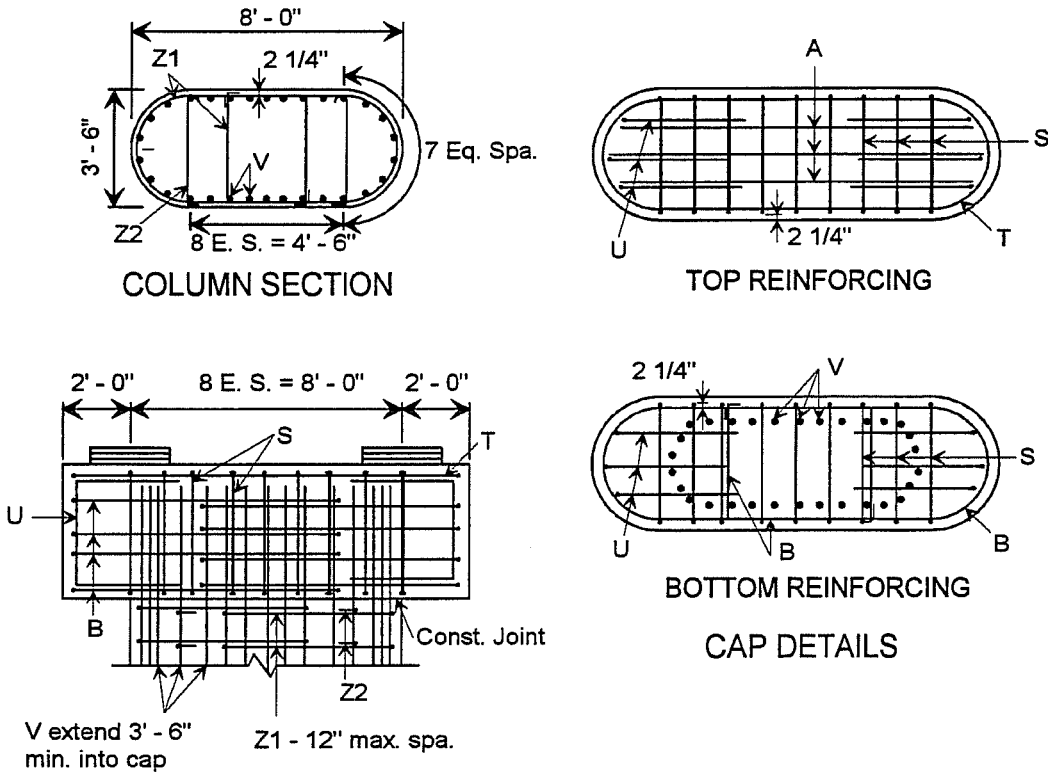


Figure 2.2 Typical Pier Geometry



PIER ELEVATION

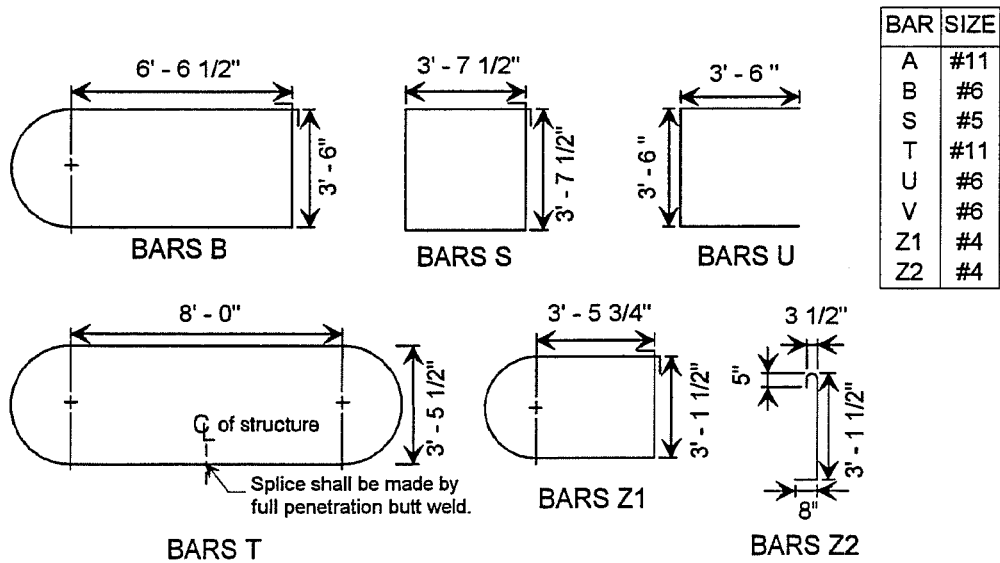


Figure 2.3 Typical Pier Steel Reinforcing Pattern

the pier cap is very heavily reinforced with a combination of #11 straight bars and a #11 continuous loop (bar T) to resist high tensile loads. Bar T is made continuous by a full penetration butt weld that is located in the middle of the pier cap. The pier cap has both horizontal (bars B) and vertical stirrups (bars S) evenly distributed over the depth and length of the pier cap, respectively. The horizontal stirrups (bars B) have semi-circular ends to provide confinement all the way around the end of the pier.

2.2 DESCRIPTION OF TEST SPECIMENS

2.2.1 Dimensions and Rebar Sizes for the Scale Specimens

The geometry of the detail shown in Figure 2.2 was used as the reference for creation of test specimens. Since the estimated loads needed to fail a full size specimen exceeded the capacity of testing machines available in the laboratory, model specimens were constructed at a 30% scale. The thickness and depth of the pier cap, the column thickness, and base plate size for the test specimens were obtained by direct proportioning from the standard detail presented in section 2.1. The width of the column was set at 36 inches (which also sets the length of the pier cap) for convenience in application of the load. The final pier size used for all the scale specimens is shown in Figure 2.4. Note that the test specimens have a column width equal to the pier cap width. This larger column size will slightly increase the strength of the specimens by providing a greater area over which to transfer load from the pier cap to the column.

Rebar sizes for the scale specimens were obtained by choosing the size rebar with an area closest to 30% of the full size

of the rebar. Table 2.1 shows the sizes of the rebar used in the standard scale specimens, and the actual scale (based on area) of the rebar used. The hooped stirrups in the column (bars Z) are not at an appropriate scale because a minimum number of rebar sizes was desired. This discrepancy

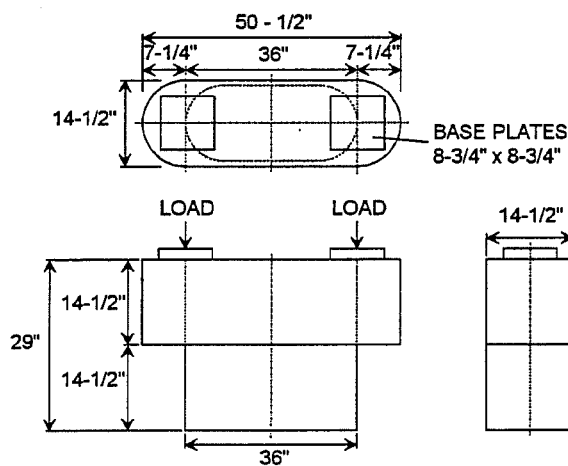


Figure 2.4 Geometry of the Scale Test Specimens

Table 2.1 Rebar Sizes for Full Size and Standard Scale Piers (see Figure 2.3 for bar layout)

Bar	Full Size	Scale Size	Actual Scale
A	#11 $A_b = 1.56 \text{ in}^2$	#6 $A_b = 0.44 \text{ in}^2$	28.2 %
B	#6 $A_b = 0.44 \text{ in}^2$	#3 $A_b = 0.11 \text{ in}^2$	25.0 %
S	#5 $A_b = 0.31 \text{ in}^2$	#3 $A_b = 0.11 \text{ in}^2$	35.4 %
T	#11 $A_b = 1.56 \text{ in}^2$	#6 $A_b = 0.44 \text{ in}^2$	28.2 %
U	#6 $A_b = 0.44 \text{ in}^2$	#3 $A_b = 0.11 \text{ in}^2$	25.0 %
V	#11 $A_b = 1.56 \text{ in}^2$	#6 $A_b = 0.44 \text{ in}^2$	28.2 %
Z	#4 $A_b = 0.20 \text{ in}^2$	#3 $A_b = 0.11 \text{ in}^2$	55.0 %

in scale was accepted since the column stirrups will have a negligible effect on the strength of the pier cap.

2.2.2 Tested Reinforcing Patterns

Six specimens were cast, all using the exterior dimensions shown in Figure 2.4. The layout of steel reinforcing for each specimen is detailed below.

SPECIMEN A2

- all rebar sizes in this specimen were scaled directly from the standard detail, using the rebar sizes listed in Table 2.1.
- this specimen is referred to as the standard scale specimen.
- the steel detail used for this specimen is shown in Figure 2.5.
- bars U have inadvertently been misplaced in this specimen, as they were placed outside of bars B as shown in Figure 2.6.

SPECIMEN A1

- this specimen is identical to specimen A2, except that there are five sets of evenly spaced stirrups in the column portion.
- again, bars U were inadvertently misplaced as shown in Figure 2.6.

SPECIMEN B

- the curved loop (bar T) in the top layer of the pier cap was replaced by 2 straight bars, also #6 bars, as shown in Figure 2.7.
- all other reinforcing follows the standard scale specimen.

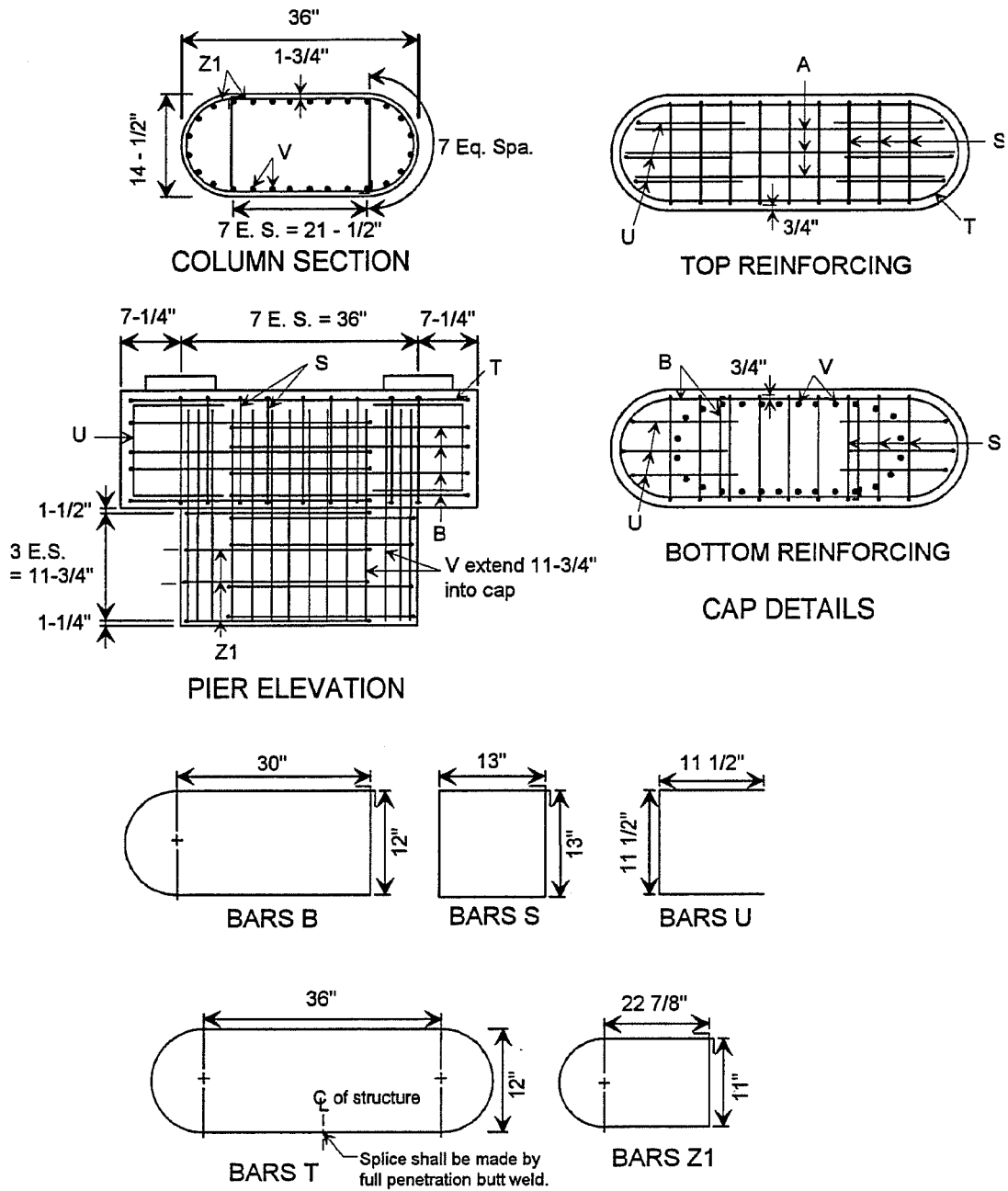


Figure 2.5 Steel Reinforcing Detail for the Standard Scale Specimen (Pier A2)

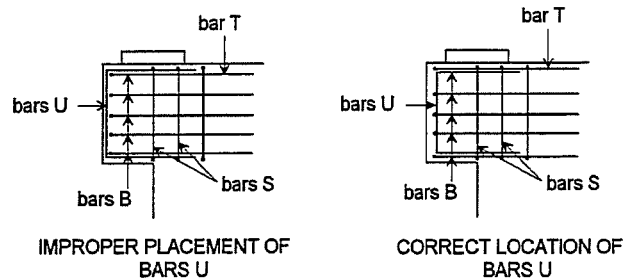


Figure 2.6 Improper Placement of Bars U in Specimens A1 and A2

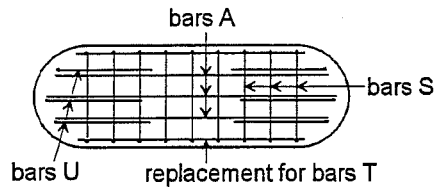


Figure 2.7 Top Layer Pier Cap Reinforcing in Specimen B

SPECIMEN C

- all steel in the top layer of the pier cap was decreased from #6 to #3 bars (bars A and T are now #3 bars).
- since bar T was changed to a #3 bar, it was made continuous by a lap weld, as opposed to the butt weld used for the standard scale specimen. The length of the weld was sized to develop the full capacity of the bar, and is shown in Figure 2.8.

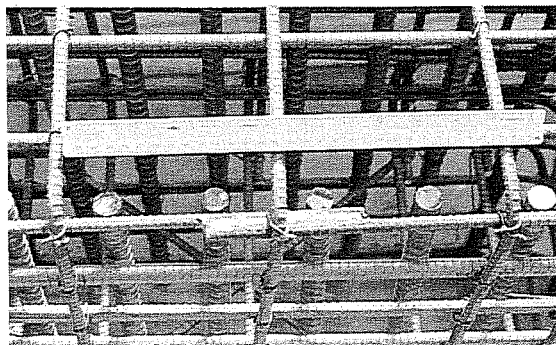


Figure 2.8 Lap Weld of Bar T

SPECIMEN D

- all steel in the top layer was decreased in size from #6 to #3 bars (bars A and bars T), and bar T was lap welded as for specimen C.
- bars U were omitted.
- three sets of the pier cap horizontal stirrups (bars B) were omitted.
- this detail is shown in Figure 2.9.

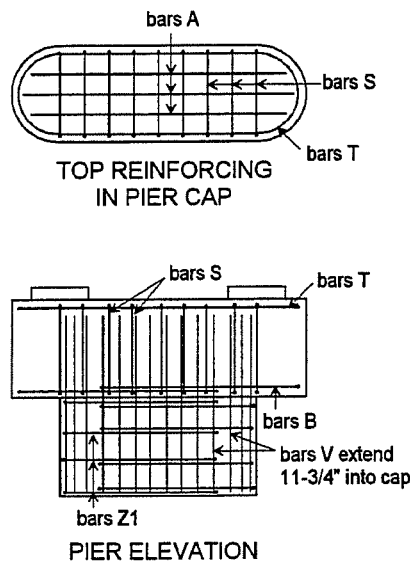


Figure 2.9 Specimen D Reinforcing

SPECIMEN E

- bars A in the top layer of the pier cap were reduced to #3 bars.
- bar T was replaced by a pair of overlapping bars B, which were #3 bars.

The different specimens were designed to determine the strength and behavior of the standard detail, and the contribution of different types of reinforcing to the overall strength of the pier. The A specimens were made to provide a direct test of the standard detail, and to compare the variability between specimens. Specimen B examines the ability of the looped bar to provide confinement for the end of the pier. Specimen C examines the effect of less top layer reinforcing on the behavior and strength of the specimen. Specimen D is used to set a minimum bound for

the strength of the pier cap. Finally, specimen E considers the necessity of a welded bar in the top layer of the pier cap.

2.3 DIFFERENCES BETWEEN THE TEST SPECIMENS AND FULL SIZE PIERS

There were some differences between the construction of the scale specimens and actual piers. For the test specimens, cover was only $3/4"$ for the pier cap, as opposed to $2\ 1/4"$ for the full size pier cap, a 33% scale. A smaller cover was used for the test specimens to maintain a constant proportion of concrete subject to spalling. For the column section, cover was $1\ 3/4"$ for the test specimens. This larger cover was a result of the formwork used for the scale specimens. The column steel must be inset relative to the sides of the pier cap to avoid intersecting the reinforcing in the pier cap. Since the column for the scale specimens was the same thickness as the pier cap, extra cover in the column region was produced.

In the scale specimens, the amount of column steel in the rectangular portion of the column was reduced to relieve congestion of the reinforcing. The number of column bars (bars V) in the center portion of the column was decreased from nine on a side in the actual piers to eight on a side in the scale specimens. Thus, there were 28 total bars V in the test specimens as opposed to 30 total for the full scale piers. Such a change should have no noticeable effect on the specimens performance.

Additionally, location of reinforcement in the scale specimens was slightly modified from that of the field placement. For the scale specimens, bars Z2 were omitted to ease fabrication. As shown in Figure 2.10, bars Z2 had been anchored at bar 1 near the column edge. To maintain the same confining effect at the end of the column for the test specimens, bars Z1 were made longer and anchored at bar 1. Finally, bars B in the test specimens were anchored farther in the scale specimens than in full size piers by placing them around column bar 1 as shown in Figure 2.11. Previously, bars B had been anchored around bar 2 of Figure 2.11. The change was made to facilitate test specimen fabrication. Thus, bars B and Z1 in the scale specimen are physically anchored around the same column bar.

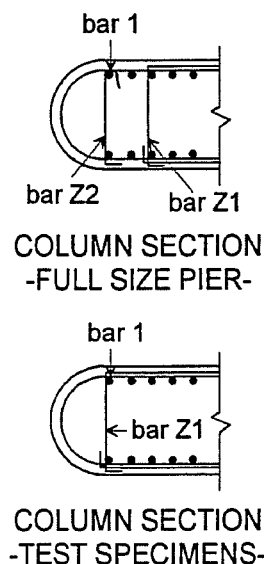


Figure 2.10 Relocation of Bars Z1 in the Test Specimens

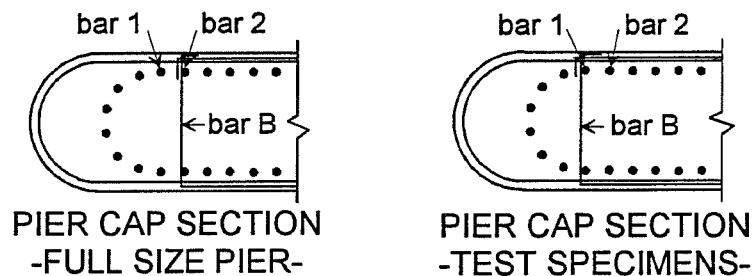


Figure 2.11 Relocation of Bars B in the Test Specimens

2.4 MATERIALS

All bars in the test specimens were either #3 or #6 in size. Specimens were constructed in two sets, so steel for each set of specimens was ordered from the same lot. Static yield strengths obtained from tensile tests on the bars are listed in Table 2.2. For specimens B through E, the #3 bars had a low yield strength of 47.4 ksi. Inspection of stamps on these bars showed that the bars were not grade 60, but a lower grade of steel. Testing of the rebar is described in Appendix A.

Table 2.2 Static Yield Strengths of Rebar

Specimens	f_y for #3 bars	f_y for #6 bars
A1 and A2	60.8	60.0
B through E	47.4	60.0

The concrete design strength for the TxDOT pier caps is 3,600 psi at 28 days, so a 4,000 psi mix was ordered from a local concrete supplier. The concrete had a maximum aggregate size of 3/4" to allow placement in the congested rebar cage, and to fit within the 3/4" cover. Two different pours were made, with the first pour for specimens A1 and A2, and the second for specimens B through E. The cylinder compressive strengths are shown in Table 2.3. The cylinders

Table 2.3 Concrete Cylinder Compressive Strengths

Specimens	7 day strength	28 day strength	long term strength
A1 and A2	2939 psi	3905 psi	4050 psi
B through E	2820 psi	3554 psi	4016 psi

tested were 6 inches by 12 inches, and were loaded using neoprene pads. The long term strength

is taken as the average of all cylinders tested after 35 days, and represents 7 cylinders for specimens A and 18 cylinders for specimens C-E. Cylinders were stored with the specimens.

2.5 FABRICATION OF SPECIMENS

All specimens were constructed at the Ferguson Lab. The reinforcing cage for specimen A2 is shown in Figure 2.12. All of the bent bars were ordered from a local fabricator, and met a

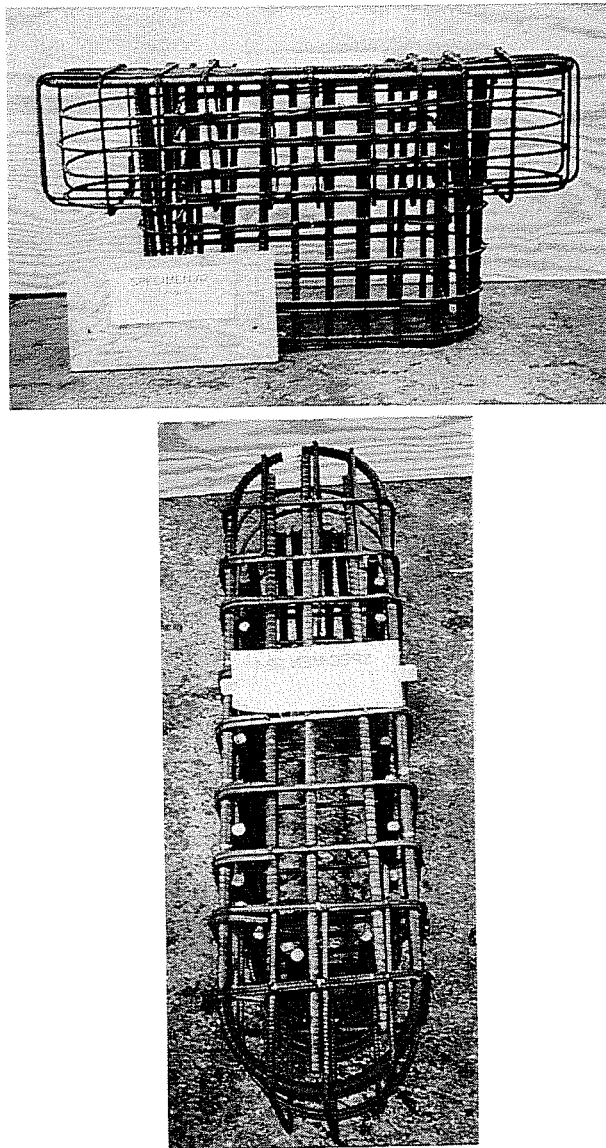


Figure 2.12 Steel Reinforcing Cage for Specimen A2

reasonable tolerance - $\sim 3/8"$ - for the out to out dimensions. Spacers were placed on rebar parallel to the straight edges of the specimen to ensure equal cover on opposite sides of the specimen. Forms were made right side up, so the effect of bleeding and segregation would be the same as for actual piers. The circular end of the column was formed using sheet metal placed within a wood frame. The placement of the reinforcing in the forms is shown in Figure 2.13.

The specimens were poured monolithically, with no construction joint as used in the field. Concrete was placed using an overhead crane and bucket, and thoroughly consolidated using internal vibration. After pouring, the exposed concrete on the top of the forms was covered with plastic. After one week, the forms and cylinders were stripped and left to cure in air. Removal of the forms showed that there were no defects such as honeycombing in the concrete.

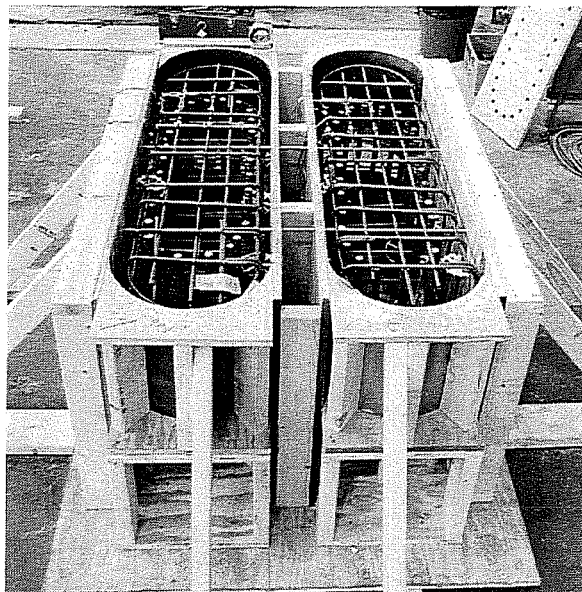


Figure 2.13 Placement of Reinforcing Cages in Forms

2.6 INSTRUMENTATION

Strain gages were placed on reinforcing in the top layer of the pier cap of specimens C and D. The gage locations are shown in Figure 2.14. The strain gages were not located under the bearing plates, so strain gage readings represent a basically uniaxial state of stress. The strain gages had a 6 mm gage length, with a 12 mm by 4 mm backing. The size of the gage backing mandated significant grinding of the #3 bars to produce a flat surface for the strain gages. Since the gages were placed on the top and bottom of a bar, the area of the bar at the gage location was reduced as shown in Figure 2.15. To protect the gages from moisture and the casting process, the gages

were covered by a water-proofing sealer and mastic. All gages were still active after concrete was placed. The initial strain gage accuracy was approximately ± 10 microstrains.

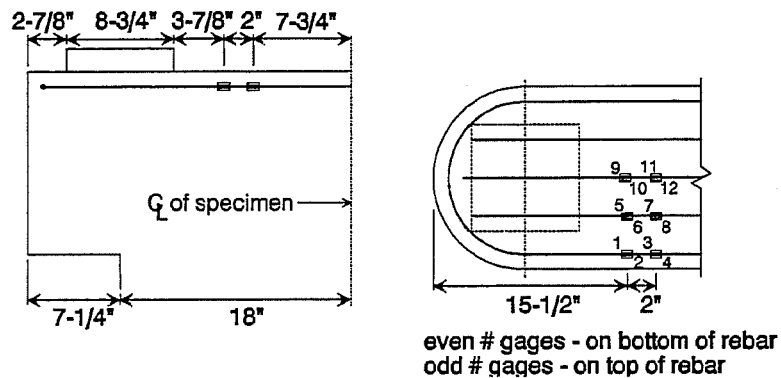


Figure 2.14 Strain Gage Locations in Specimens C and D

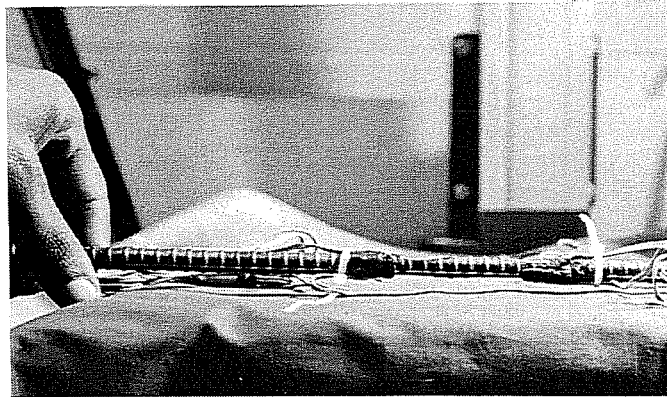


Figure 2.15 Reduction in Rebar Cross Section Due to Strain Gage Placement

Six linear potentiometers (pots) were placed on the specimen to measure deflections as shown in Figure 2.16. The accuracy of the linear pots is ± 0.001 inches. The identification of the potentiometers was kept constant with respect to the point of load application, so pots 1 and 2 always refer to the pots at the tip of the tested end of the specimen. Thus, pots 3 and 4 are always at the center of the base plate, and pots 5 and 6 are always at the far end of the specimen. For the first test on a specimen, pots 1 and 2 were at the south side of the pier, while pots 5 and 6 were at

the north end of the pier. For the second test on a specimen, pots 1 and 2 were at the north end of the specimen, and pots 5 and 6 were at the south end of the specimen.

2.7 TEST SET-UP

The test set-up was designed to allow two tests on each specimen. The configuration for applying load to the specimen is shown in Figure 2.17. The specimen and spreader beam were placed inside the frame of a 600 kip load machine as shown in Figure 2.18. The test machine was fitted with a swivel head so rotation of the girder would not be restrained. A spreader beam was used to place load from the test machine on each end of the pier cap to prevent overturning of the specimen.

The loading head of the 600 kip machine was offset from the centerline of the spreader beam to place most of the load at one end of the pier. The end of the pier cap with the smaller portion of load did not sustain any damage while the opposite end was tested, so test results for the two ends of the specimens are directly comparable. Once one end of the pier was tested, the specimen was repositioned on the floor of the test machine and the other end of the specimen was tested.

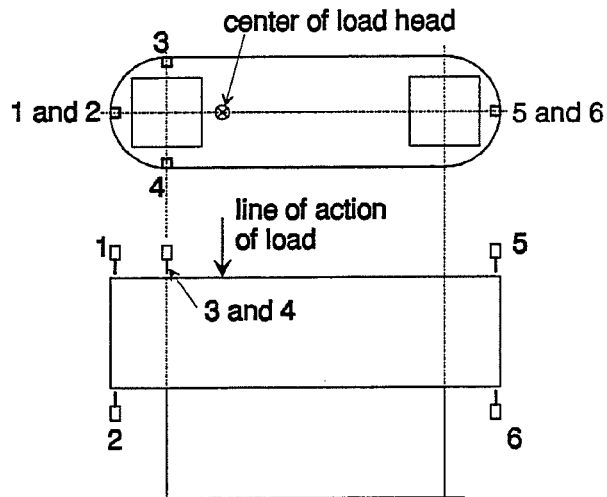


Figure 2.16 Location of Linear Pots

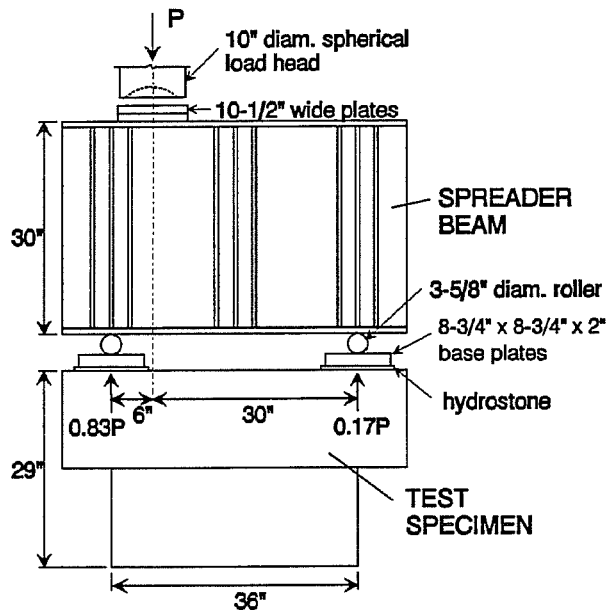


Figure 2.17 Test Set-Up Geometry

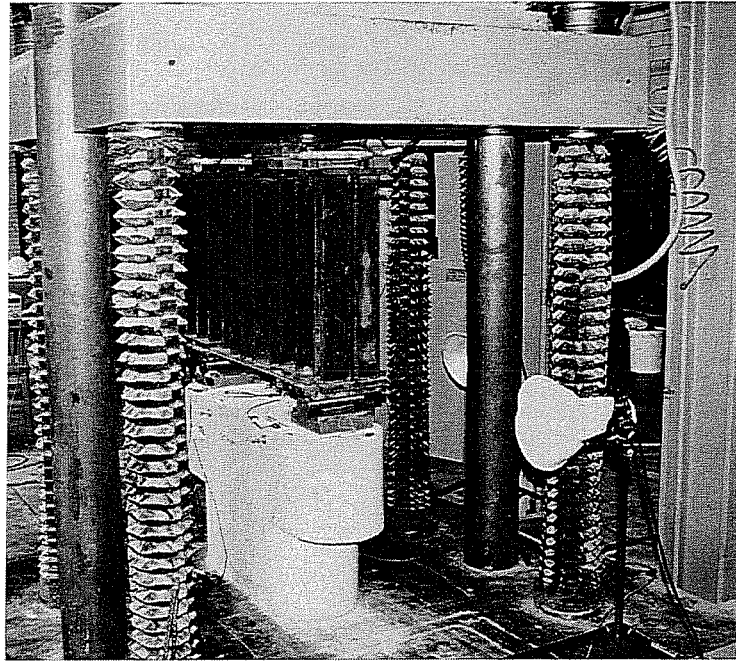


Figure 2.18 Placement of Test Specimens in the Test Machine

The 3 5/8 inch diameter rollers under the spreader beam place two distinct line loads on the base plates. By idealizing load from the test machine as a line load on the spreader beam, the test set-up is statically determinate. Therefore, the net load on each end of the pier cap can be found as a proportion of the total load measured by the test machine.

To level the spreader beam and provide full contact between the top of the pier cap and the base plates, a 5/16 inch layer of hydrostone was poured under the base plates. Also, for some of the piers a thin film of hydrostone was poured under the semi-circular end of the column, at the end of the specimen being tested. This layer of hydrostone produced full contact between the floor and specimen, preventing any rigid body rotations of the specimen due to a non planar surface on the bottom of the specimen.

2.8 LOADING PROCEDURE

Loading was applied in discrete increments, typically 20 to 30 kips on the linear portion of the load-deflection curve. After an increment in load was applied, about five minutes passed while

cracks were marked and inspected. At the end of this delay, load and deflection readings were taken electronically, giving the static capacity. The next load step was then applied.

Loading was controlled while examining a plot of the total load versus deflection at linear pot #1. For the linear portion of the load-deflection plot, load control was used to determine the size of load increments before changing to deflection control near the peak capacity. The first test on a specimen was stopped shortly after the peak load had been reached to avoid excessive damage to the specimen which could affect the second test. For specimens B through E, the second test on the specimen was run to large deflections to examine the specimen ductility.

CHAPTER 3

TEST RESULTS

3.1 NOMENCLATURE FOR SPECIMEN TESTS

Eleven tests were conducted to failure on the six specimens, with the most significant results presented in this chapter and detailed results for each test in Appendices B, C, and D. As discussed in Chapter 2, each end of a specimen was tested separately, allowing two possible tests to failure on each pier. Specimens were named with a letter as presented in Chapter 2. A specific test on a specimen is denoted by placing a number after the name of the specimen, with the number indicating the time of that test. For instance, Pier B-1 refers to the first test on specimen B, while Pier B-2 refers to the second test on specimen B, at the opposite end of the specimen.

The only specimen tested three times was specimen A2. This pier was first tested with the load head centered on the spreader beam, placing nearly equal loads on each end of the pier (test Pier A2-1). This first loading was large enough to originate cracking, but did not cause failure. Thus, Pier A2-2 was the first loading to failure on specimen A2, and Pier A2-3 was the second loading to failure on specimen A2.

3.2 TERMINOLOGY FOR DISCUSSING TEST RESULTS

Load Paths. The load applied at the bearing plates was directly transmitted to the column by a compression strut in the pier cap. To maintain equilibrium at the base plate, a tension tie must form at the top of the pier cap as shown in Figure 3.1.

Cracking Patterns. During testing of the specimens, four distinct types of concrete distress were observed. Their location and shape are defined below for clarity in examining test results.

Flexural Cracks. Flexural cracks were seen extending across the top of the pier, and sometimes extended down the face of the pier as shown as failure "A" in Figure 3.2. These cracks are what one would observe on the tension side of a reinforced concrete beam tested in bending.

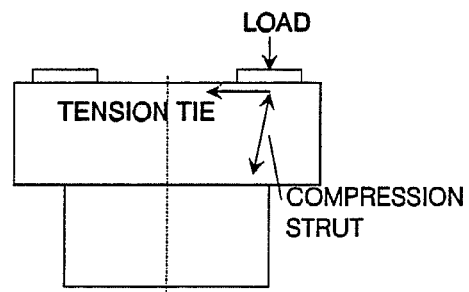


Figure 3.1 Load Paths for the Pier Cap

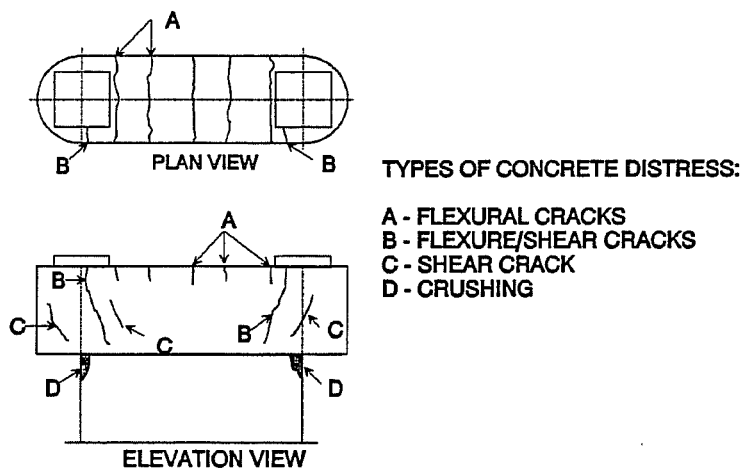


Figure 3.2 Patterns of Concrete Distress

Flexure/Shear Cracks. These cracks were observed on the top and faces of the pier cap, shown as failure "B" in Figure 3.2. The flexural component typically originated between the edges of a base plate, and the component on the top of the pier cap only extended from the base plate to the edge of the pier. The cracks formed a small flexural component on the face of the pier (up to about 3 inches long) before the crack sloped in towards the center of the pier. These cracks typically grew to extend across the depth of the pier cap.

Shear Cracks. These inclined cracks formed on the faces of the pier cap as shown as failure "C" in Figure 3.2. The shear cracks were distinguished from flexure/shear cracks as they had no flexural component when they initially formed. A crack that began as a pure shear crack would often extend across the depth of the pier cap so that it eventually resembled a flexure/shear crack.

Crushing. Crushing of concrete was located at the interface between the pier cap and column, and is shown as failure "D" in Figure 3.2. The crushing was easily observed, with flaking of the concrete the first indication of failure followed by further spalling of the concrete with additional loading.

3.3 SPECIMEN CAPACITY

A summary of steel reinforcing patterns used in the specimens is given in Table 3.1. The specimens static ultimate strengths and concrete cylinder strengths on the day of testing are listed in Table 3.2. The specimen strength refers to the resultant load on the end of the pier being tested,

Table 3.1 Summary of Specimen Reinforcement Patterns

Specimen	Description
A1	directly scaled from the standard detail
A2	directly scaled from the standard detail
B	straight #6 bars in the top layer of the pier cap
C	all #3 bars in the top layer of the pier cap, continuous loop provides confinement
D	minimal reinforcing, horizontal stirrups omitted
E	all #3 bars in the top layer of the pier cap, lapped hoops provide confinement

Table 3.2 Specimen Capacities and Concrete Strengths

* - only two cylinders tested

Test	Static Capacity (kips)	Cylinder Strength (psi)	Average Capacity (kips)	Effective f'_c (psi)	Age of Concrete (days)
A1-1	387	3961*	395	4050	83
A2-2	368	3916	395	4050	51
A2-3	430	4211*	395	4050	69
B-1	304	3930	323	4016	39
B-2	341	3869	323	4016	45
C-1	299	4141	299	4016	85
C-2	298	4100	299	4016	87
D-1	203	4032	209	4016	53
D-2	214	4021	209	4016	74
E-1	258	3554	269	3651	23
E-2	279	3747	269	3651	30

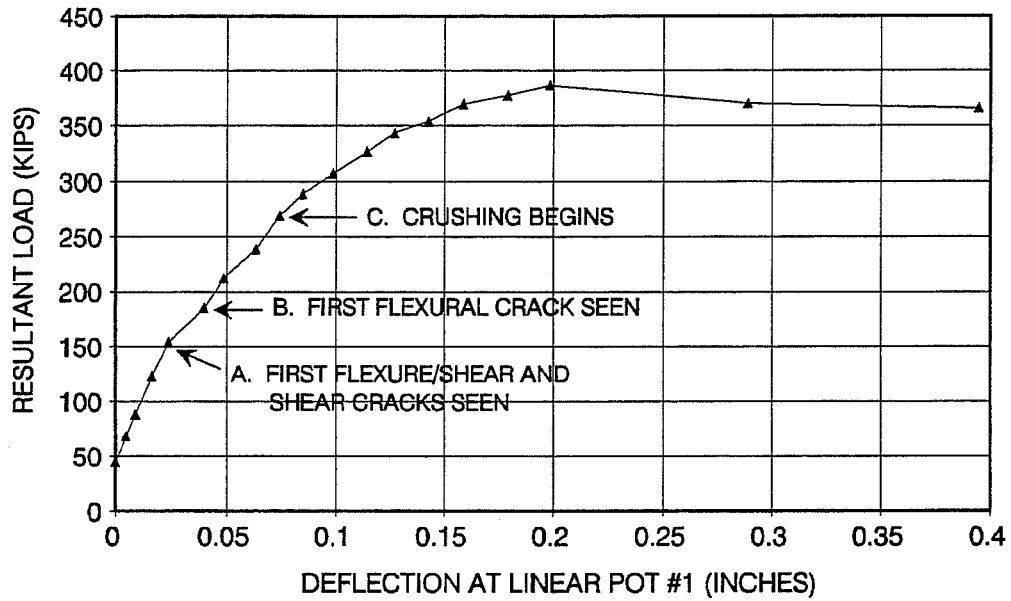
not the total load applied to the spreader beam. Cylinder compressive strengths are the average of three cylinders unless noted. Also shown in Table 3.2 are the average capacities for the

specimens, and the "effective concrete strength" for the specimens (effective f_c'). To calculate an average strength for the A series specimens, test results for specimens A1 and A2 are combined since pier cap reinforcing was identical for the two specimens. The effective concrete strength presented in Table 3.2 represents an average strength for a concrete pour, and is presented to remove the small variability in concrete strength after prolonged curing. For tests run on specimens more than 35 days old, the effective f_c' is the average compressive strength of all cylinders tested after 35 days (the long term average strength from Chapter 2). Only specimen E was tested at less than 35 days, so the effective f_c' for specimen E was taken as the average of Pier E-1 and Pier E-2 cylinders. All specimens except for specimen E had essentially the same concrete strength, so only results for specimen E need to be normalized.

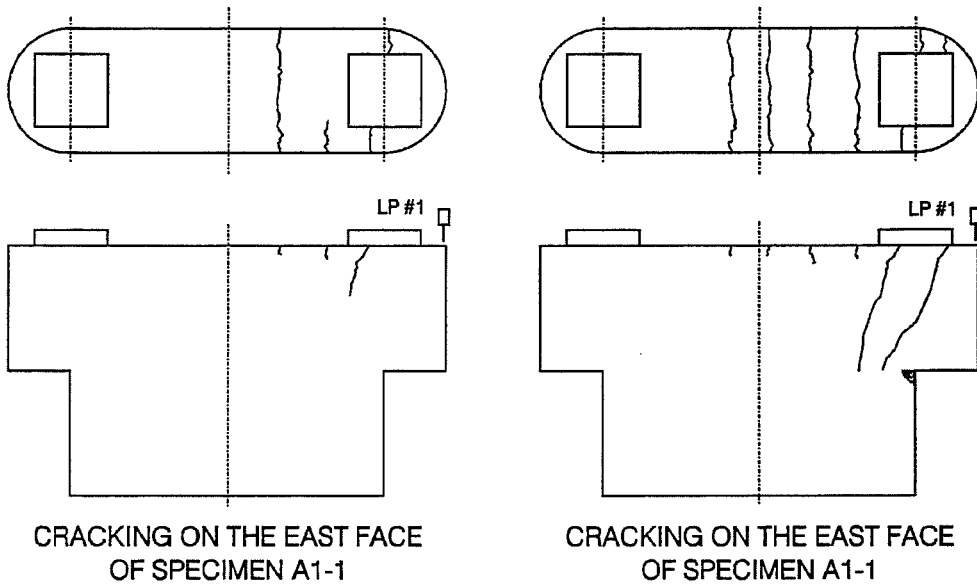
This smaller concrete strength at the time of testing specimen E was reflected in the capacities for both tests on specimen E. It was expected that Specimen E would have a strength very similar to Specimen C since the two piers are almost identical. Reinforcement patterns for the two piers differ only in that specimen C has a continuous loop in the top layer of the pier cap, while specimen E uses lapped hoops in the top layer as presented in Chapter 2. If the strength of specimen E is normalized to the effective concrete strength of specimen C by direct proportioning, its strength is 296 kips (multiply 269 kips by 4016 psi/3651 psi). The normalized strength for specimen E matches very well with the tested strength for specimens C, 299 kips.

3.4 LOAD-DEFLECTION BEHAVIOR

The load-deflection performance for all the specimens was very similar, so behavior of a typical specimen is first described. The static loading curve for Pier A1-1 is shown in Figure 3.3. The load is the resultant load on the tested end of the pier, and deflection is taken at linear pot #1, the "tip" deflection, whose location was presented in Chapter 2. The loading curve has been shifted so load is non-zero when deflection is zero. Under small net loads of only 25 to 50 kips, there was a large variability in tip deflections for the different tests. These deflections did not represent movement of the end of the pier cap with respect to the column, but were caused by seating of the specimens on the test floor. To remove this scatter and allow a better comparison of test results the loading curves were shifted so the first data point began at around 25 to 50 kips. The shift was made by subtracting the original deflection at the first data point on the new curve from all



CRACK DIAGRAMS ARE DRAWN TO SCALE



CRACKING ON THE EAST FACE OF SPECIMEN A1-1
POINT "B"
RESULTANT LOAD = 186 kips

CRACKING ON THE EAST FACE OF SPECIMEN A1-1
POINT "C"
RESULTANT LOAD = 269 kips

Figure 3.3 Load-Deflection Behavior for Pier A1-1

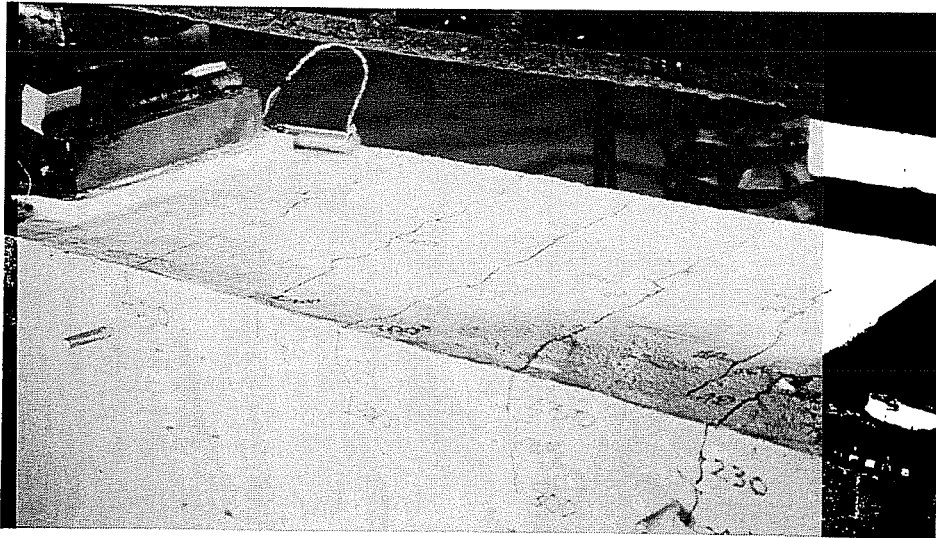


Figure 3.5 Crack Distribution at the Top of Pier A1-1 After Failure

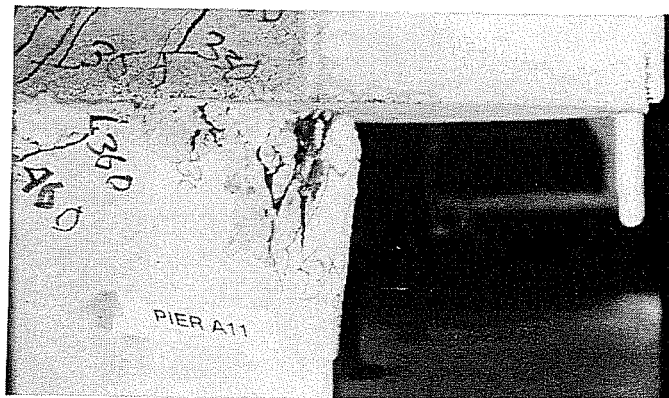


Figure 3.6 Crushing of Pier A1-1 After Failure

Plots of resultant load against the deflection at linear pot #1 for all specimens are shown in Figure 3.7. To reduce clutter, deflections for Pier A2-2 and A2-3 were omitted. Tip deflections in the elastic region were very similar, showing minimal effect from the different reinforcing patterns used in the pier cap. This similarity was expected, as the initial stiffness of the overhang

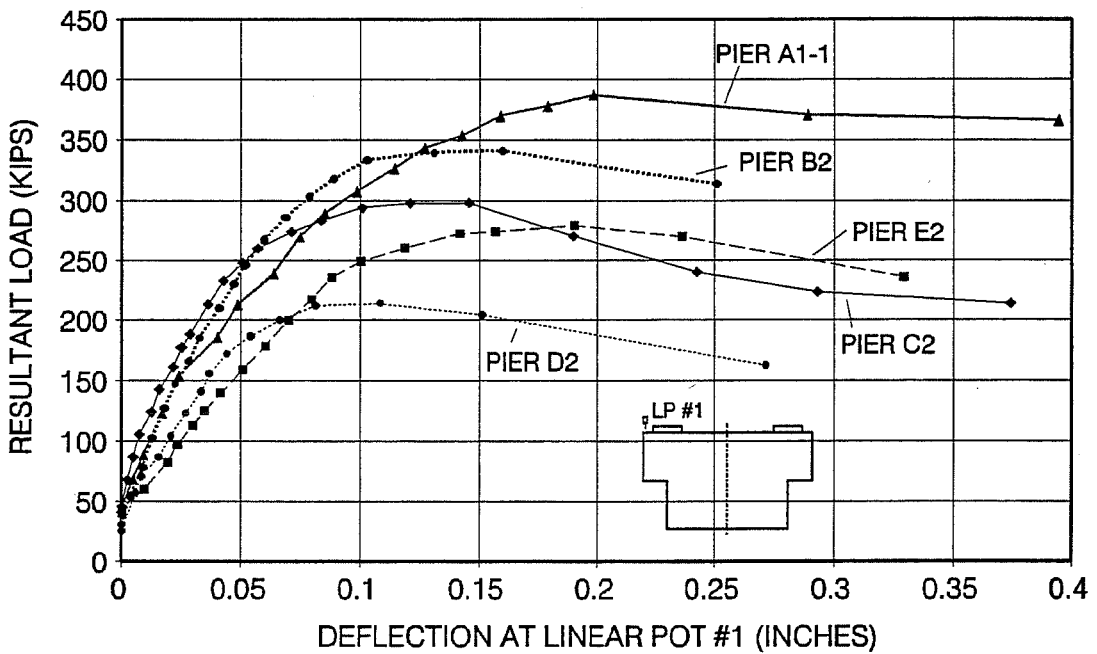
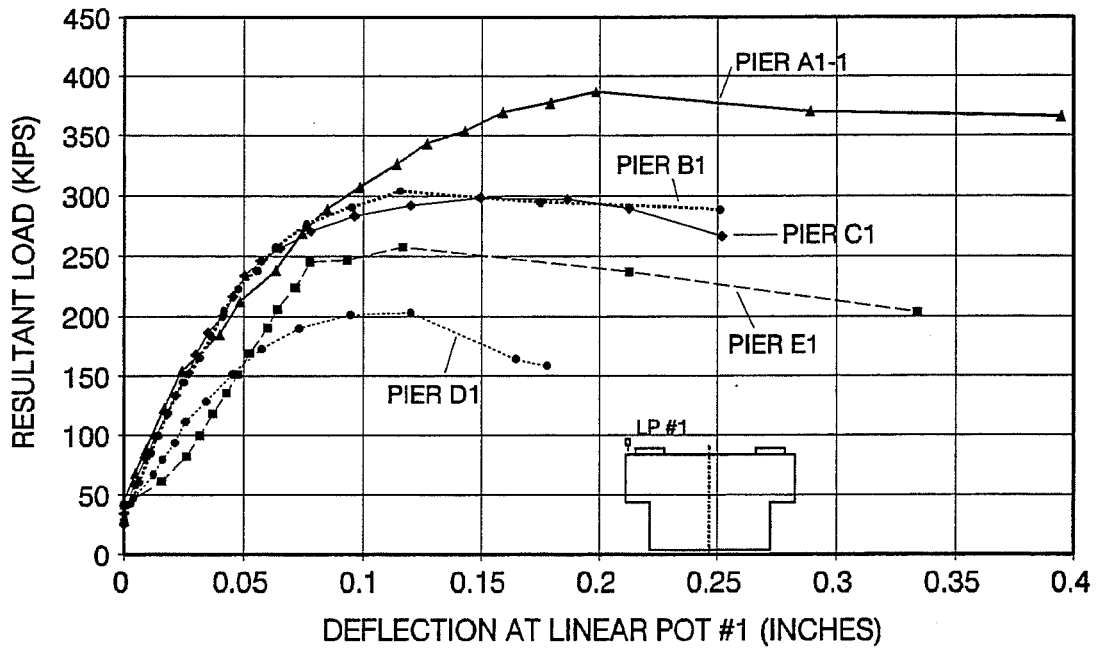


Figure 3.7 Comparison of Resultant Load vs. Deflection at Linear Pot #1

largely is produced by the small span to depth ratio. Somewhat less stiff than the other piers were specimens D and E. Since specimen E had a smaller effective concrete strength, this reduced stiffness was expected. Specimen D was the least stiff, reflecting the specimens minimal reinforcement, and the different behavior of Specimen D. Specimen D showed more of a flexural failure, with the bending action allowing more deformation than the compression struts formed in the other specimens. The deflections at linear pot #2 on the underside of the overhang were essentially the same as linear pot #1 as shown in Figure 3.8.

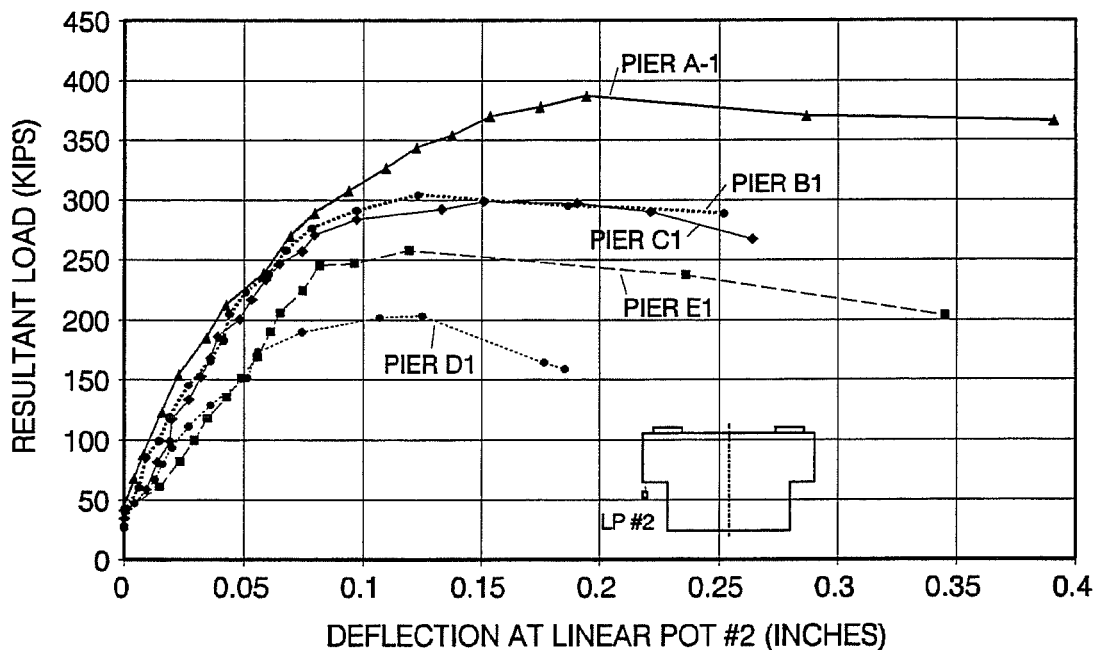


Figure 3.8 Comparison of Resultant Load vs. Deflection at Linear Pot #2

Plots of resultant load against the deflection at linear pot #3, the "column line" deflection, are shown in Figure 3.9. Again, elastic behavior for the specimens was very similar because deflection depends on shearing of the end of the cap relative to the pier, or compression of the entire specimen. Deflections at linear pot #4 were consistent with those at linear pot #3, and are left in the appendix.

For all specimens, plots of resultant load against deflection for linear pots 1 through 4 are shown in appendix B. Deflections at the far tip of the pier were negligible, and are not presented.

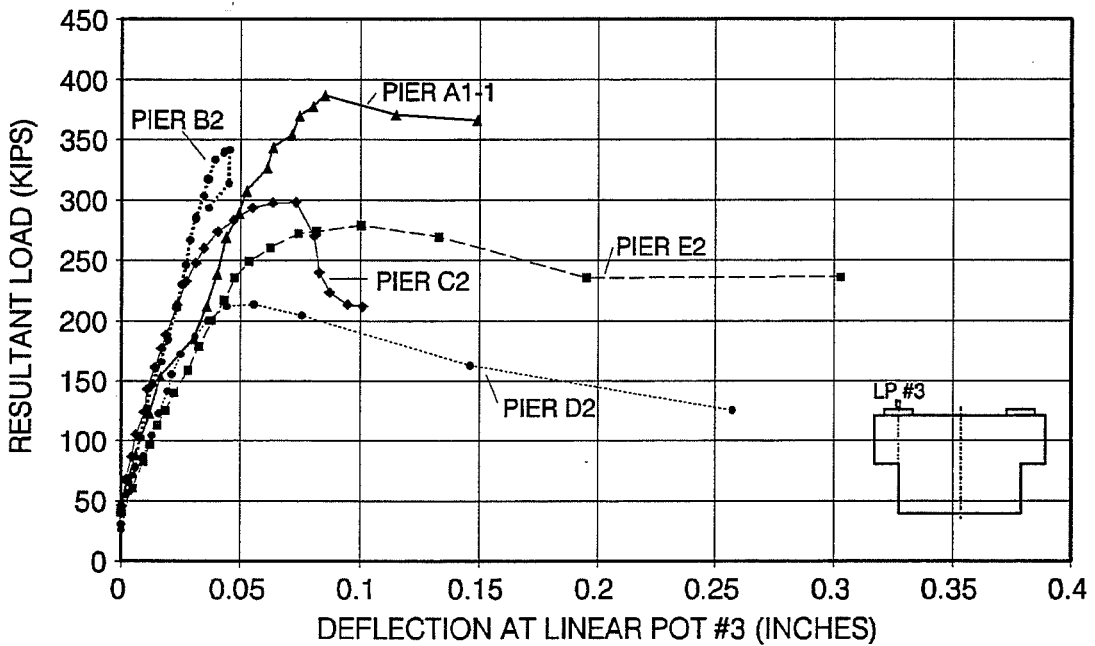
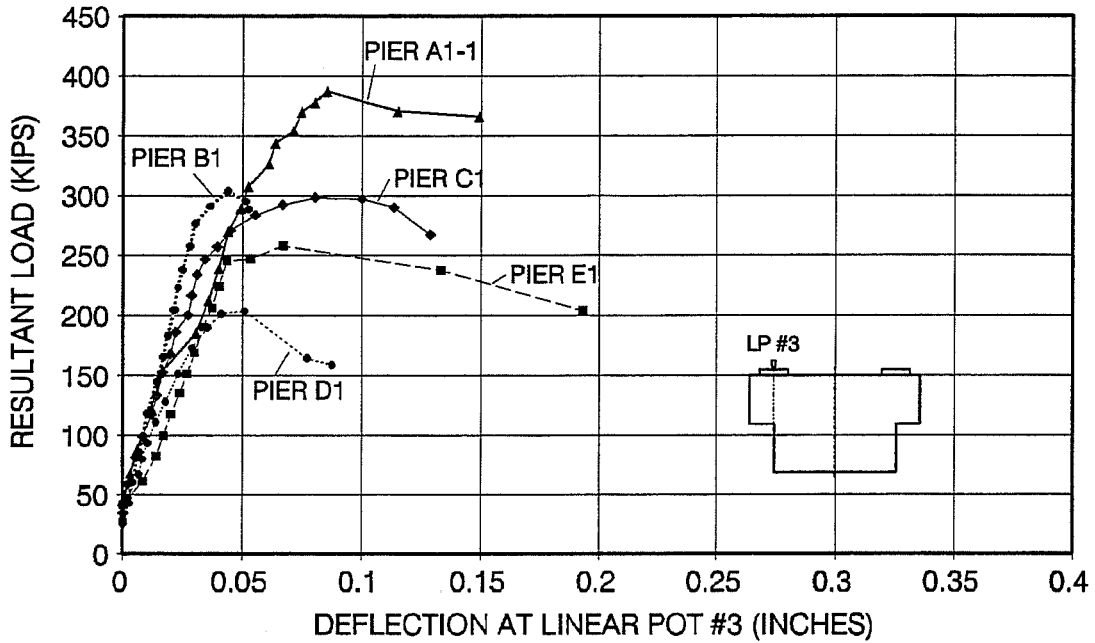


Figure 3.9 Comparison of Resultant Load vs. Deflection at Linear Pot #3

3.5 CRACKING LOADS

In general, cracking loads are subjective due to the variability in concrete tensile strength, and because cracks may not immediately be seen when they originate due to their minute size. Also, the load listed as the cracking load represents the range of load covered in the previous load step - 20 to 30 kips. Since load steps were not uniform for all specimens, there is additional variability.

The loads at which different crack types were first observed are listed in Table 3.3. The

Table 3.3 Specimen Cracking Loads

Test	Capacity	Cracking Loads (kips)			
		Flexure	Flexure Shear	Shear	Crushing
A1-1	387	186	154	154	269
A2-2	368	167	145	205	297
A2-3	430	174	150	112	205
B-1	304	166	166	276	291
C-1	299	99	153	168	257
D-1	203	67	none	152	203
E-1	258	118	152	224	258
B-2	341	127	166	147	341
C-2	298	124	124	105	283
D-2	214	87	212	214	214
E-2	279	159	140	125	261

table has been split into two groups to reflect the loading process. The first group in the table lists cracking loads from the virgin test on the pier, while the second group gives cracking loads for the second tests on specimens. For the virgin test on the pier, the true cracking loads are obtained. For the second test on the opposite end of the specimen, the flexural cracking loads could have been affected by previously formed cracks. During the first test on a specimen, flexural cracks sometimes propagated to the opposite end of the pier. Thus, for the second test of the specimen, the existing flexural cracks could absorb deformations, delaying the onset of additional flexural cracking. Although the rate of formation of flexural cracks may have been effected, specimen

failure modes were not altered. Cracking loads for Pier A2-2 and Pier A2-3 are grouped with the virgin test results since their cracking loads were obtained by examining results from Pier A2-1, which equally loaded the two ends of the pier cap.

Typically, flexural and flexure/shear cracks formed at about the same time, followed by the formation of shear cracks before crushing began. Specimens A1 and A2 with #6 bars in the top layer had the highest flexural cracking loads, indicating the larger bars could absorb tensile force with less strain than the #3 bars, reducing strain in the concrete. Specimen D allowed the earliest formation of flexural cracks, and also had the smallest stiffness as shown by the loading curves. Specimens C and D were identical except that Specimen D had no intermediate layers of horizontal stirrups. Thus, the layers of horizontal stirrups (bars B) in Specimen C help to reduce deflections, limiting the formation of flexural cracks. For specimens other than specimen D, flexure shear cracks formed at almost the same load, about 150 kips. This was expected, as all these specimens had the same distribution of horizontal stirrups (bars B). Crushing loads for specimens other than specimen D were reasonably close, indicating that the distribution of forces within the specimens was similar up until that point. After crushing began, specimens that could redistribute internal forces and put more tension in the top layer of steel could add load, while those that could not redistribute loads failed with the onset of crushing.

There was considerable variability in cracking loads for a given specimen, but the largest variability came in the comparison of shear cracking loads for a given specimen. For specimen B-1, the first shear crack was seen at 276 kips, while for specimen B-2 the first shear crack was seen at 147 kips, a difference of 129 kips. This scatter in shear cracking loads is related to the definitions used for classifying cracks. Since flexure/shear cracks often developed first and then added shear components, it sometimes took much more load to develop an independent shear crack.

3.6 FAILURE MODES

The test specimens showed three basic failure modes. The most common failure, seen in specimens A, C, and E, was caused by crushing of concrete in the compression strut and at the cap/column interface. Photos of Piers A1-1 and C-1 after failure are shown in Figure 3.10. Photos of all the failed specimens are shown in Appendix C. For specimens A, C, and E, flexure/shear and shear cracks propagated across the depth of the pier cap and began to open with increasing load, limiting the size of the compression strut. Eventually, the force in the strut caused crushing at the interface. With additional load, inclined cracks opened further and there was additional

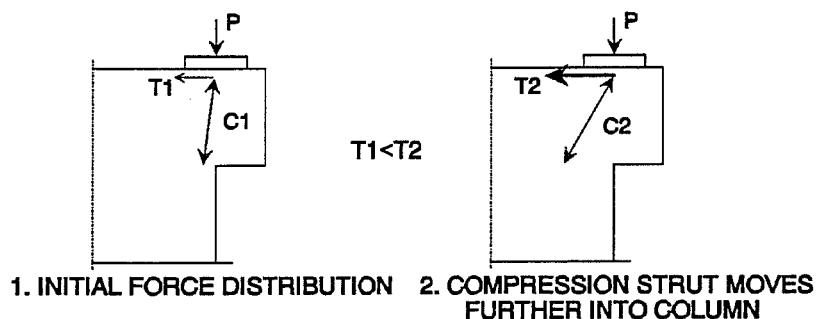


Figure 3.11 Redistribuition of Internal Forces in the Pier Cap

a much smaller lag between first crushing at the interface and the ultimate load. Since specimens C and E had much less reinforcing in the top layer than specimens A, redistribution of the strut after crushing began was limited.

Specimen B showed a second failure mode. Specimen B initially performed like specimens A1 and A2, developing inclined cracks on the face of the pier cap. These cracks continued to grow across the depth of the pier and widen as for the A series specimens. However, soon after the onset of crushing the failure load was reached, indicating as for specimens C and E that additional tensile force in the top layer of the pier cap could not be developed. The inability to develop additional tension in the top layer of reinforcing was the root cause of the failure. Without the continuous loop (bar T) around the end of the pier, the specimen had to develop tension solely through the straight bars which had very small development lengths as shown in Figure 3.12. The lack of development length became evident during testing, with bond distress in the top layer shown by the formation of splitting cracks on the top of the pier as shown in Figure 3.13. Aside from reducing the ability to develop tension in the top layer, removal of the continuous loop around the top layer caused two major problems. First, a flexure/shear crack opened very wide at the face of the pier without any reinforcement to limit its growth as shown in Figure 3.14.

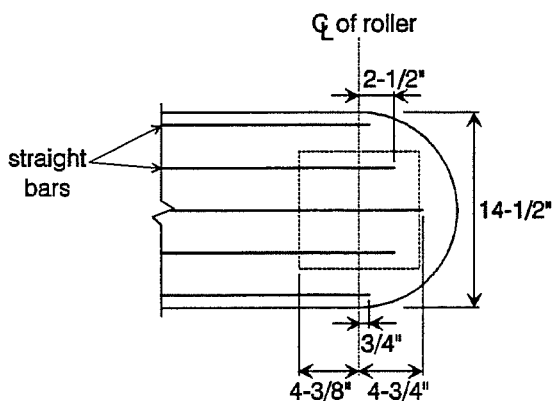


Figure 3.12 Development Lengths for Top Layer Reinforcing in Specimen B

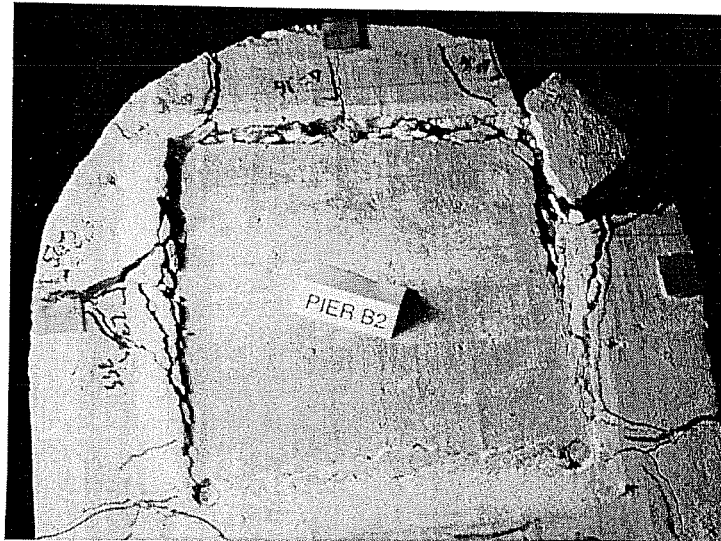


Figure 3.15 Punching of the Base Plate into Pier B2-2

Specimen D, with its minimal reinforcing behaved quite differently than the other specimens with a cracking pattern shown in Figure 3.16. Flexural cracks formed initially, with long

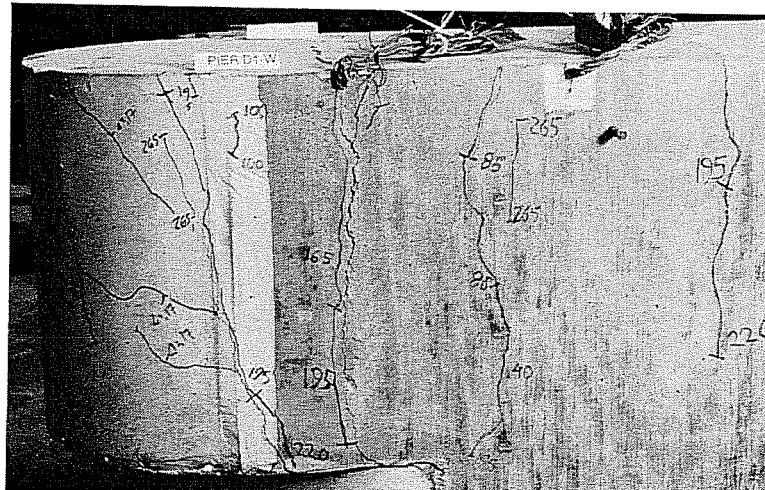


Figure 3.16 Crack Distribution on the Face of Pier D-1 After Failure

components on the faces of the pier. In particular, a flexural crack formed at the interior edge of

the base plate. For other specimens, inclined cracks formed near the point of load application, forming a defined compression strut. For specimen D, however, the cracks in this region were almost vertical indicating minimal compression strut formation. With increasing loads, the flexural crack at the interior edge of the base plate grew across the depth of the pier. This eliminated the area available for direct transfer of shear, but left a bearing surface at the top of the column to handle strut forces as shown in Figure 3.17. Therefore, in both tests on specimen D failure corresponded to the beginning of crushing at the cap/column interface since there was no possible redistribution of loads. Essentially, the specimen failed because flexural cracks opened so much that shear could not be directly transferred to the interior of the pier.

Inspection of specimens after testing showed two significant behavior patterns of concrete directly under the base plates. First, there was only extremely minor cracking under the base plates due to the confinement provided by the base plate. Flexural cracks that formed on the edge of the pier did not continue under the base plate, but stopped at the edge of the base plate as shown in Figure 3.18. Second, punching of the base plates into the top of the pier cap was seen to some extent for all specimens, with punching on Pier C-2 shown in Figure 3.18. The punching was magnified on the second tests on specimens, which were run to large deformations. Punching was greatest for specimen B, followed by specimens E, C, A, and D. While specimens A1 and A2 reached much greater loads than specimens B, E, and C, excellent confinement in the top layer for A series specimens was provided by the #6 continuous loop (bar T) which minimized punching. The punching seen in specimens B, E, and C was certainly enlarged due to the presence of a large flexural crack at the interior edge of the base plate. Formation of this crack eliminated the confinement available from the underlying concrete along this edge. While the beginning of punching was seen, punching did not contribute to the failure of specimens and became most notable only when damage to the specimens was forced.

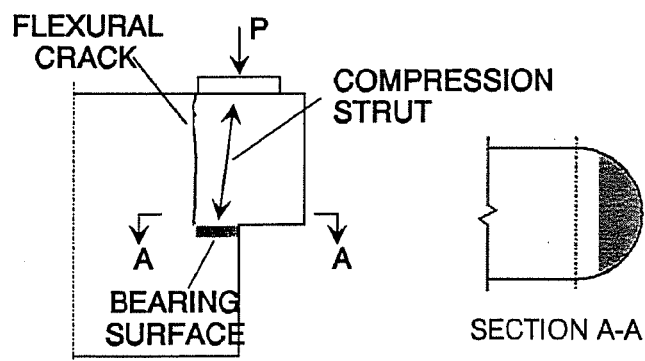


Figure 3.17 Force Distribution in Specimen D After Opening of the Flexural Crack

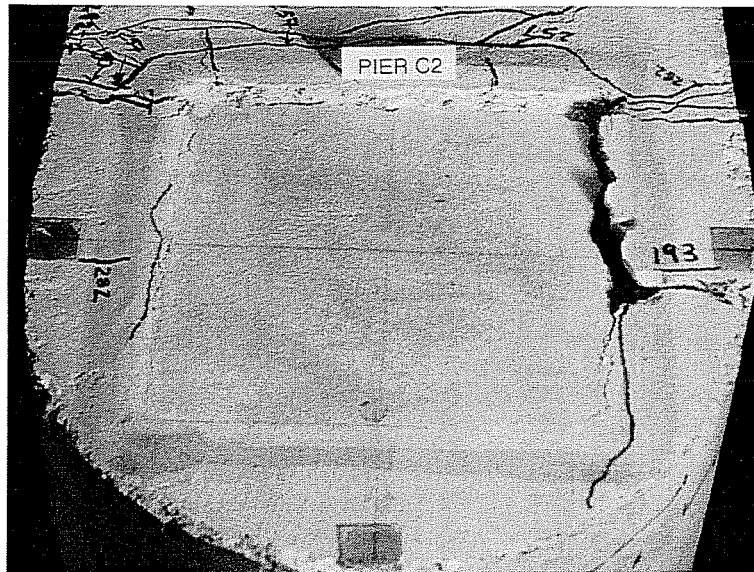


Figure 3.18 Cracking and Punching Under the Base Plate for Pier C-2

3.7 STRAIN GAGES

Strain gages were placed on the top layer reinforcing steel of specimens C and D as presented in Chapter 2 and shown in Figure 3.19. Since gages were not under the base plates, the strain readings describe a state of pure tension on the top of the pier cap. Because gages were

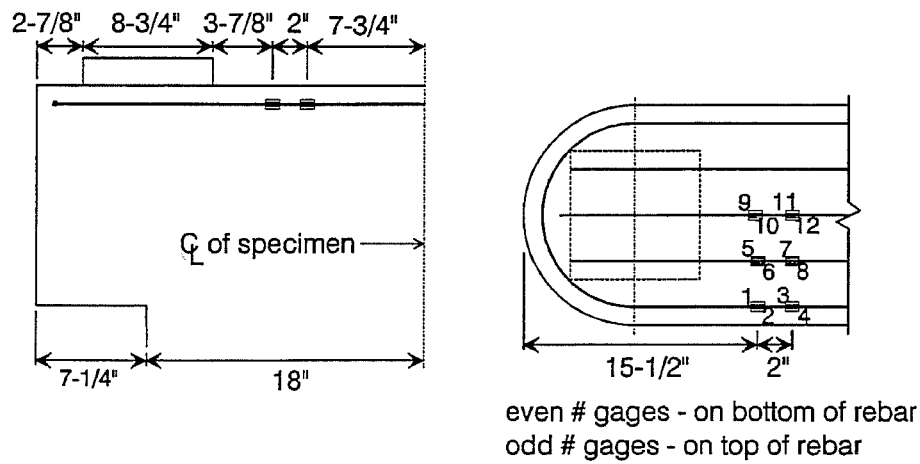


Figure 3.19 Strain Gage Locations in Specimens C and D

placed at only one end of the pier cap, the end of the pier with the strain gages was loaded first. For the second test on the specimen, the strain gages were at the far end of the pier which saw minimal load. All strain gages were operable at the beginning of testing and up to the yield strain of the rebar. After yielding, some of the gages failed so readings for the failed gages are omitted. For the second test on a specimen, the accuracy of strain gage readings may have been reduced since gages had undergone very large strains in the first test of the pier.

Pier C-1 Strains. A plot of the resultant load (the load at the tested end of the cap) against the strain on gages 1 through 4 for Pier C-1 is shown in Figure 3.20. The yield strain, 1,630

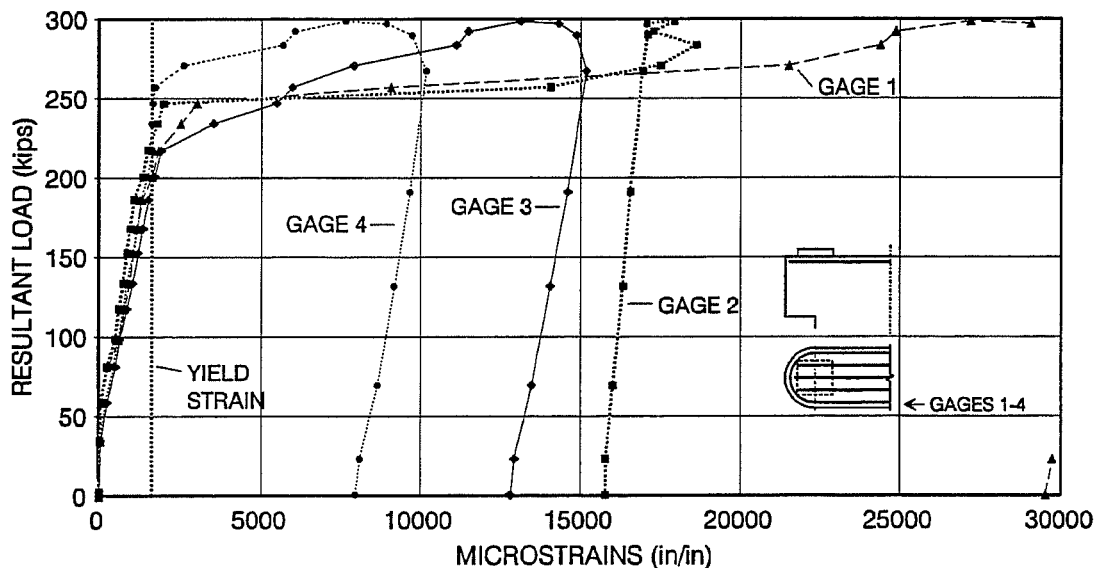


Figure 3.20 Resultant Load vs. Strain on Gages 1 - 4 for Pier C-1

microstrains, was obtained by dividing the experimentally obtained yield stress of 47.4 ksi by the modulus of elasticity, 29,000 ksi. The load-strain curve was linear up to the yield point, after which point a plateau was essentially reached. Analysis of data showed that bars 2 and 3 began yielding at a resultant load of 186 kips and that all bars had completely yielded by a resultant load of 234 kips, much less than the specimen capacity of 299 kips. During yielding of the bars, there was no change in specimen load-deflection behavior and no significant change in crack formation. Crack formation during yielding of the bars consisted of:

1. A 13 inch long shear crack on the east face of the cap.

2. Shear cracks with a combined length of 7 inches on the west face of the cap.
3. A flexural crack extending across the full width of the cap, about 6 inches south of the piers centerline.

Crushing at the pier cap and column interface did not occur until a load of 257 kips, after the top layer reinforcing had already yielded. Other strain gage data for Pier C-1 is given in appendix D.

Pier D-1 Strains. A plot of resultant load versus the strain in gages 9 through 12 for Pier D-1 is shown in Figure 3.21. Strain gages for Pier D-1 had a behavior similar to Pier C-1, with the

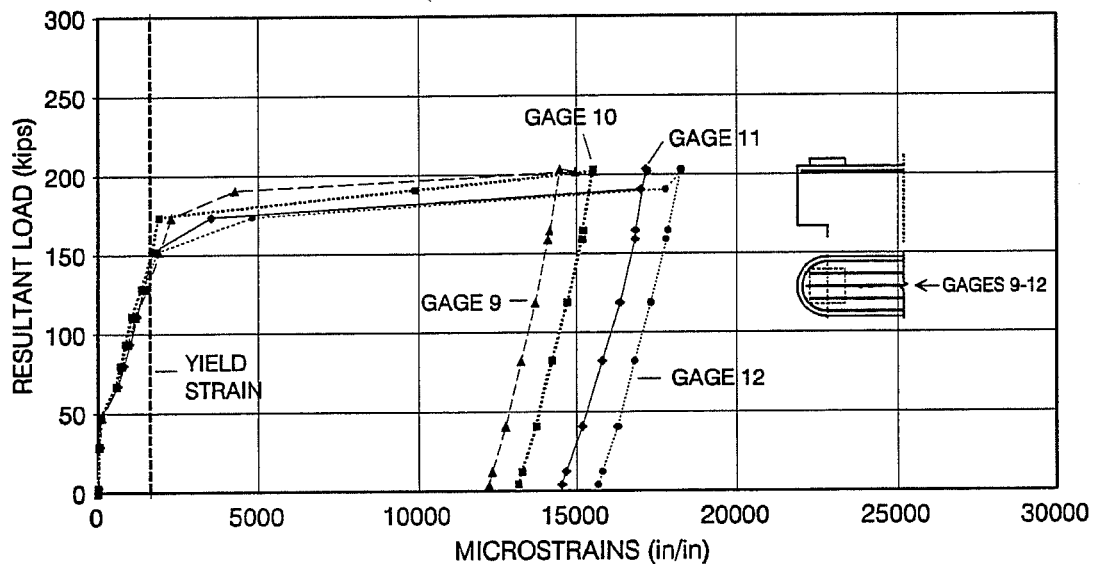


Figure 3.21 Resultant Load vs. Strain on Gages 9 - 12 for Pier D-1

load-strain curve linear up to yielding before reaching a plateau. There was a jump in strain between loads of 48 and 67 kips, corresponding to the formation of the first flexural crack across the top of the cap which ran between the sets of gages. Bar 1 yielded at a load of 129 kips, bar 3 yielded at 152 kips, and bar 2 yielded between 152 and 173 kips. Again, yield loads were significantly lower than the pier capacity of 203 kips. For Pier D-1, there was a good correlation between yield in the bars and crack formation. Cracking forming during yield of the bars is described below.

1. The flexural crack at the interior edge of the base plate grew to extend across the depth of the pier cap on both faces of the specimen. Prior to yielding, the flexural

component on the west face of the pier was 1 and 1/4 inches long, and there was no flexural component on the east face of the pier.

2. A flexural crack extending across the width of the pier formed at the center of the pier cap.
3. The first shear crack formed and extended across the full depth of the west face of the pier cap.

While significant cracking occurred during yielding of the bars, there was no change in load-deflection behavior as bars yielded. Crushing occurred after the bars had yielded, and corresponded to the specimen capacity of 203 kips. Other strain gage data for Pier D-1 is given in appendix D.

Pier C-2 and Pier D-2 Strains. Plots of resultant load versus strain on gages 5 through 8 for Pier C-2 and Pier D-2 are shown in Figure 3.22 and Figure 3.23, respectively. Strain gage

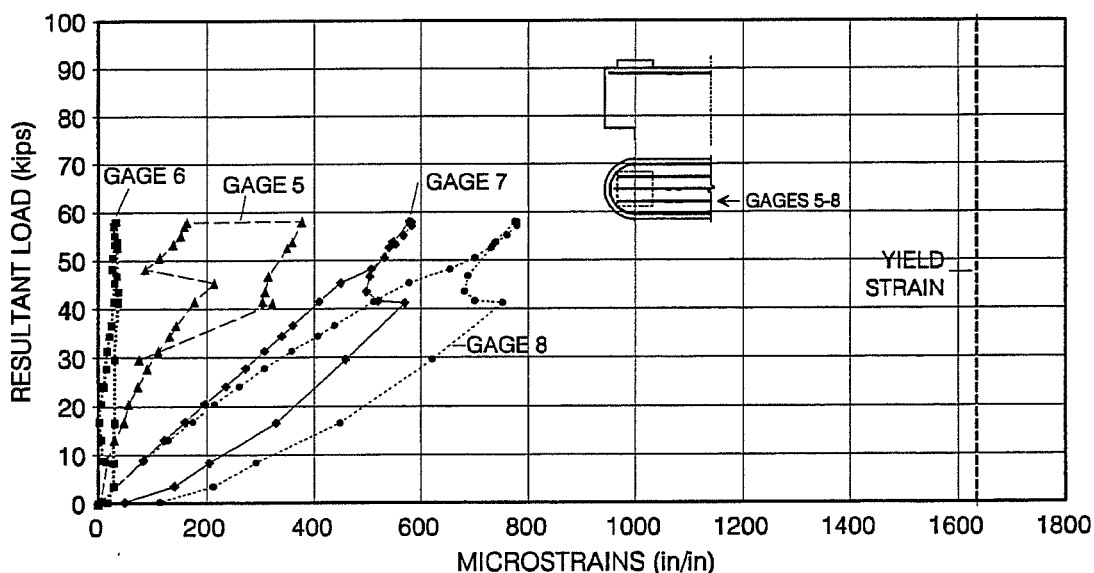


Figure 3.22 Resultant Load vs. Strain in Gages 5 - 8 for Pier C-2

readings for both tests were comparatively low, reaching a maximum of about one half the yield strain. Low strains were expected on the second test of a specimen since the resultant load nearest the strain gages was low, about 50 kips. However, at these small loads strains in the rebar were significantly higher than in the first test on a specimen as shown in Table 3.4 which compares the average strain on all gages at a given load for the two tests on a specimen. For the first test on a

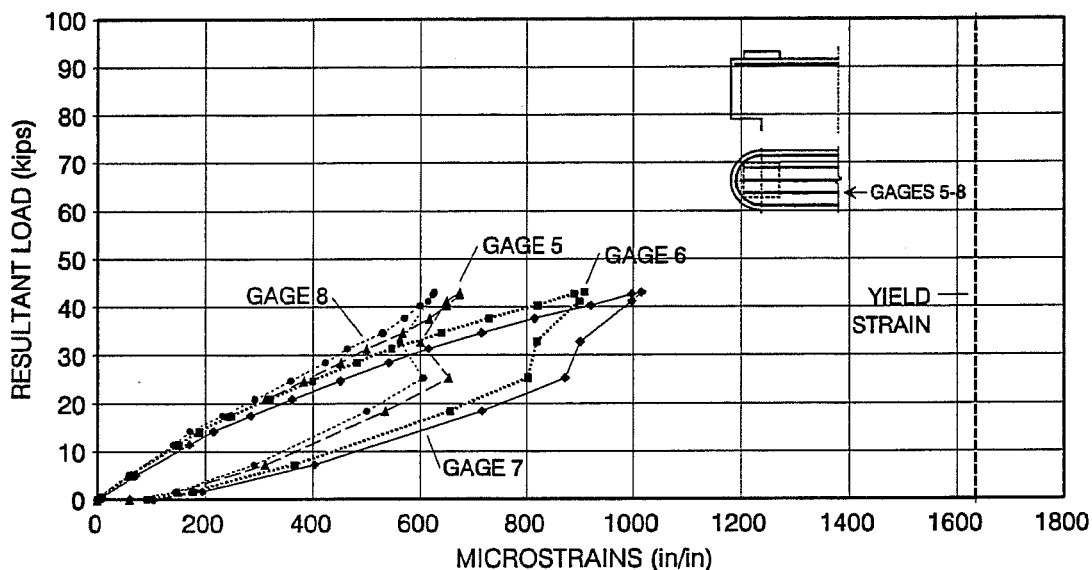


Figure 3.23 Resultant Load vs. Strain in Gages 5 - 8 for Pier D-2

specimen, the uncracked concrete carried tension at these small loads. However, for the second test on a specimen the concrete at the strain gage location was already cracked so the steel had to absorb all the tension, resulting in the larger strains at a given load. Again, complete strain gage data for Pier C-2 and Pier D-2 is given in appendix D.

Table 3.4 Comparison of Strain for the First and Second Tests on a Specimen

Specimen	Load (kips)	Average Microstrain
C-1	58.8	155
C-2	58.0	408
D-1	47.5	81
D-2	43.1	801

CHAPTER 4

ANALYSIS OF RESULTS

4.1 INTRODUCTION

In this chapter, test results are summarized and the specimen capacities predicted by different design methods are compared with test results. First, conventional design methods from the 1992 AASHTO provisions and ACI 318-89 (ACI 1989) code are examined. The two design methods most suited to the problem geometry are the corbel and deep beam provisions from AASHTO Section 8.16.6.8 and ACI 318-89 Chapter 11, respectively. Next, the strut and tie method is used to predict the pier cap strength using two strut and tie models. To demonstrate the use of the strut and tie method, a sample design of a full size pier cap using this method is presented. The strut and tie method is also used to predict the strength of a typical pier cap design. Finally, criteria for judging constructed pier caps through field inspection are given. It should be noted that the above approaches for sizing a pier cap and its reinforcing are all design methods. Thus, the use of these methods as analysis tools requires making some judgements to predict the specimen strength based on the actual reinforcement used. The analyses focused on specimens A and C because those two specimens are most representative of reinforcing that has been and would be used in the pier cap.

4.2 DISCUSSION OF TEST RESULTS

The ultimate strengths of the test specimens are shown in Table 4.1. Specimen capacity is directly related to the amount of horizontal reinforcing, which is needed to develop the action of a tied arch. The effect of the amount of steel in the top layer of the pier cap is shown by a comparison of specimens A and C. Specimen A, with #6 bars in the top layer had a capacity $P_u = 395$ kips, while specimen C with #3 bars in the top layer had a capacity of $P_u = 299$ kips. The only difference in reinforcing for specimens A and C is the size of the bars in the top

Table 4.1 Test Specimen Strengths

Specimen	Average Static Capacity (kips)
A	395
B	323
C	299
D	209
E	269

layer. The ability to *develop* the strength of the bars in the top layer of the cap is also critical. Specimen B is identical to specimens A, except that in the top layer of the pier cap only straight #6 bars are used, resulting in very small anchorage lengths. The small anchorage lengths provided for the top bars of Pier B are inadequate to develop the required bar force, as bond distress was observed during testing. The capacity of specimen B was 323 kips, much less than specimen A capacity.

The quantity and anchorage of steel in the top layer of the pier has a large influence on specimen strength, and the importance of the steel can be explained considering specimen failure modes. As load was increased on a specimen, crushing at the pier cap/column interface eventually occurred. To carry more load, the compression strut has to move further into the column, requiring a larger tie force to maintain equilibrium. In specimens B, C, D, and E, the capacity of the bars in the top layer of the pier cap was limited, so failure was reached soon after crushing at the pier cap/column interface began.

The placement of the intermediate hoops (bars B) also has a considerable effect on specimen strength as shown by a comparison of piers C and D. Piers C and D are identical except that bars B (and bars U) are removed from specimen D. Without the intermediate hoops, specimen D capacity was only 209 kips, as compared to 299 kips for specimen C. The mechanism by which bars B contribute to the specimen capacity is not as clear as for the bars in the top layer of the pier cap. The intermediate hoops closest to the top of the pier see the largest force, so those bars act mainly as tension ties. The intermediate hoops also can resist loads by dowel action.

Examination of the specimens shows that bearing failure did not limit the capacity of any of the specimens, although punching of the base plates was seen on all specimens. The conclusion that bearing strength did not limit pier cap strength comes from a comparison of the concrete damage seen in the first and second tests on a specimen. For the first test on a specimen very limited punching occurred, while for the second test of a specimen in which large deformations were forced, more significant punching occurred. Thus, most of the punching occurs after a specimens capacity has already been reached. For specimens A, which had the greatest capacity, the average bearing stress sustained was 5.16 ksi, or $1.27 f'_c$ ($f'_c = 4,050$ psi). The bearing strength on top of the pier cap is helped by the continuous rebar (bar T) around the perimeter of the cap, which provides confinement. The bearing stress, f_b , sustained can be compared to the load factor design provisions for bearing of AASHTO section 8.16 with the Φ factor removed.

From AASHTO (1992):

$$P_n = f_b A_1$$

where

$$f_b = 0.85 f'_c \sqrt{\frac{A_2}{A_1}} = \text{ultimate bearing stress} \quad (4.1)$$

$$f'_c = 4,050 \text{ psi}$$

$$A_1 = \text{base plate area} = 76.56 \text{ in}^2$$

$$A_2 = \text{surrounding concrete area} = 187.7 \text{ as a maximum}$$

so

$$f_b = 1.33 f'_c$$

When the Φ factor is not applied to code provisions, the code specified ultimate bearing stress and largest tested bearing stress agree, $1.33 f'_c$ and $1.27 f'_c$, respectively. Since the applied bearing stress was slightly less than the code value, and bearing failure did not occur, no conclusions can be reached regarding the maximum permissible bearing stress. Further testing needs to be conducted to determine the bearing strength at the top of the pier caps.

4.3 CORBEL ANALYSIS

The pier cap geometry studied looks quite similar to a corbel, so the corbel provisions were the first application of conventional analysis to predict specimen capacity. The action of a corbel as used in the 1992 AASHTO code is shown in Figure 4.1. The corbel design technique is intended for span to depth ratios less than one, where ordinary flexural theory is not applicable (Salmon 1985, ACI 1989). In the AASHTO (1992) corbel code provisions, the shear strength comes entirely from shear friction.

The AASHTO (1992) code procedure gives an area of steel in the

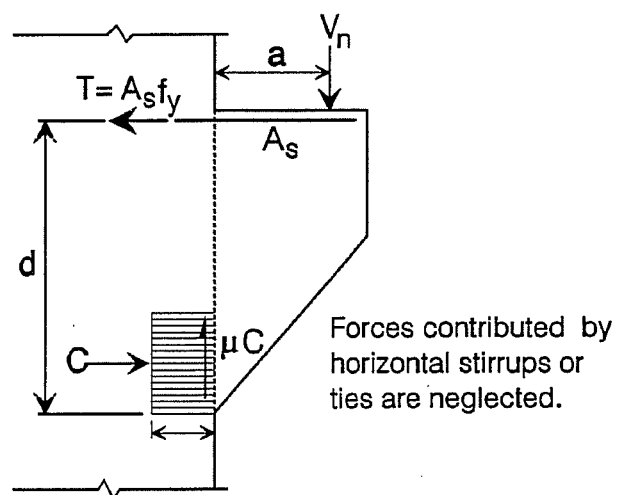


Figure 4.1 Force Distribution Assumed in Corbel Code Provisions (Salmon 1985)

top layer of the corbel based on two checks. The first check considers shear, while the second check considers moment. The intermediate stirrups are sized based on the amount of steel in the top layer of the corbel. For the pier cap geometry chosen, the check based on shear controls because the moment is extremely small. Using the AASHTO (1992) code as an analysis method gives:

$$V_n = 1.5A_v f_y u, \text{ the nominal shear strength } \leq 0.2f'_c b d \text{ and } [800 \text{ psi}] b d$$

where

$$A_v = \text{the area of steel in the top layer of the corbel} \quad (4.2)$$

[bars A and T in the specimen]

$$\mu = \text{coefficient of friction for normal weight concrete cast monolithically} = 1.4$$

$$b = \text{the corbel width}$$

$$d = \text{depth of reinforcing shown in Figure 4.1}$$

The multiplier of 1.5 reflects the benefit of the additional layers of stirrups. A comparison of corbel design strengths and the test results for specimens A and C is shown in Table 4.2. For specimen A, the limiting shear strength controlled the corbel design strength. As the results show, the corbel provisions are inadequate to predict pier cap strength because they only consider shear friction to resist applied loads and ignore the inclination of the compression block.

Table 4.2 Test Specimen Capacity Compared to the Strength Predicted by Conventional Design Methods

Specimen	Average Test Capacity (kips)	Corbel Design Strength (kips)	Deep Beam Strength (kips)	Corbel Parameters	
				A_v (in ²)	f_y (ksi)
A	395	151	95	2.2	60
C	299	55	95	0.55	47.4

4.4 DEEP BEAM ANALYSIS

The deep beam provisions in the ACI 318-89 code also appear applicable to the pier cap design. These provisions reflect the different behavior and capacity of beams with span to depth ratios less than five (Salmon 1985, ACI 1989). The deep beam provisions follow the same basic

approach used to find the shear strength of a regular beam, with the concrete and stirrups both contributing to the shear resistance as shown in Equation 4.3.

$$V_n = V_c + V_s \leq 8\sqrt{f'_c} b_w d$$

where

$$V_c = \text{shear strength from concrete}$$

$$V_s = \text{shear strength from steel stirrups}$$
(4.3)

For the deep beam provisions, the V_c term includes the effect of the ratio M_u/V_u at the critical section. Also, the V_s term considers the contribution of horizontal stirrups to the shear resistance. Using the deep beam provisions for specimens A and C, the upper limit on shear strength controlled. The design capacity for both specimens was 95 kips, much less than the test capacity given in Table 4.2. Thus, the deep beam provisions are also inadequate for the design of the pier cap region.

4.5 THE STRUT AND TIE DESIGN METHOD

4.5.1 Introduction

Obviously, traditional design procedures for shear in the 1992 AASHTO and ACI 318-89 codes are inadequate to realistically predict the strength of the pier caps tested. The load carrying capacity of the pier cap comes from direct compression of an inclined strut, and this action is not explicitly covered in the 1992 AASHTO provisions or the ACI 318-89 code. The inadequacy of normal design codes is not limited to the pier cap studied, but also to other abnormal regions of structures where plane strain conditions do not exist (Bergmeister et. al. 1990, Schlaich et. al. 1987). In contrast, the strut and tie method is well suited to the design of abnormal geometries because the method simplifies the behavior of an indeterminate region into discrete load carrying members (Schlaich 1987). Essentially, the strut and tie method is a more general application of the classical truss analogy used for beams. The method is also similar to the tension field concept for the shear strength of steel plate girders. The strut and tie method is used to break a structure into a static force system composed of three elements (Bergmeister 1990):

1. compression struts
2. tension ties
3. nodes

Some examples of strut and tie models are shown in Figure 4.2. The strut and tie model essentially forms a truss to resist loads applied to the structure. As in a truss, forces are uniaxial and change direction only at the nodes. One of the benefits of using a strut and tie model is a better understanding of the distribution of forces within the structure, allowing the engineer to more successfully detail reinforcing.

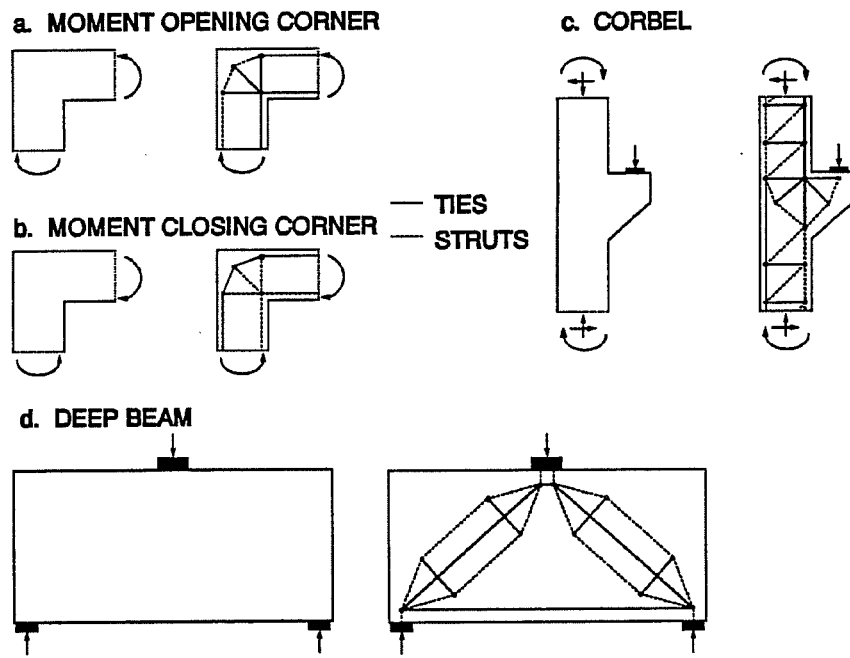


Figure 4.2 Examples of Strut and Tie Models (from Schlaich 1987)

A detailed discussion of the theory behind the strut and tie method is beyond the scope of this research. However, the most important concepts relevant to the pier cap design are covered. An excellent summary of the strut and tie method in general is given by Anderson (1988), and a thorough background of the design concept is given by Schlaich (1987). Finally, a summary of the state of the art of the strut and tie method and tests on strut and tie elements is given by Bergmeister et. al. (1990) from which stress limits for the concrete are chosen.

4.5.2 Major Assumptions of the Strut and Tie Method

Perhaps the most important consideration in examining the use of a strut and tie model for design is its adherence to the lower bound theorem. The lower bound theorem states that a load carrying system based on a statically allowable stress field which does not go beyond the yielded state is a lower bound to the limit load (Bergmeister 1990, Yura 1992). As a condition of this theorem, the statically allowable stress field must satisfy equilibrium and boundary conditions (Bergmeister 1990, Yura 1992). The use of a lower bound method is well suited to concrete, as concrete has little ability to undergo plastic deformations. Thus, the strut and tie model should be chosen so that the deformation capacity of the concrete is not exceeded before the structure reaches its assumed state (Schlaich 1987). To meet this condition, Schlaich (1987) suggests the strut and tie model should be oriented based on elastic stress fields. Therefore, a strut and tie model based on elastic stress fields represents a lower bound solution, and will give conservative results so long as sudden failures due to instability or localized crushing are prevented (Bergmeister 1990).

In applying the strut and tie model, five major assumptions are made (Bergmeister 1990, Anderson 1988):

1. Failure coincides with the formation of a mechanism caused by yielding of one or more of the ties.
2. Concrete does not crush prior to yielding of the ties. The crushing is prevented by limiting stress in the concrete.
3. Forces in the struts and ties are uniaxial.
4. All external loads are applied to nodes of the strut and tie model. When distributed loads exist, the model must realistically fit the applied loading.
5. Reinforcement is detailed so bond and anchorage failures are prevented.

4.5.3 Creation of a Strut and Tie Model

To apply the strut and tie model to a structure, Schlaich (1987) proposed breaking a structure up into "B" and "D" regions as shown in Figure 4.3. The B regions adhere to Bernoulli's assumption of plane strain, so internal forces for these regions are known. The D regions consider discontinuities in the structure where the distribution of strain is extremely non-linear (Schlaich 1987) such as the pier cap studied. The design of B regions is very well documented, so the use of the strut and tie model is typically applied to D region design.

Once the B and D regions are identified, the strut and tie models for the D regions can be formulated. Schlaich (1987) gives two main techniques for finding the layout of struts and ties in a model. In the first method, a finite element analysis of the D region can be made to determine the distribution and orientation of principal stresses in the region. The struts and ties can then be aligned with the axes of the corresponding principal stress fields (Schlaich 1987). The second method, the "load path method", can be used to determine the strut and tie model if an elastic analysis is not possible, or if the internal distribution of forces is evident. For the load path method, all sectional forces, loads, and reactions acting on the boundaries of the D region are found. Using the stresses on the cross section as boundary conditions, stress distributions on one side of the D region are connected with their corresponding boundary conditions on the other side of the D region as shown in Figure 4.4.

The struts and ties should be oriented at the centroids of the respective stress diagrams. With the main load paths arranged, additional struts and ties are added to allow equilibrium at the nodes (Schlaich 1987).

Finally, the quality of the strut and tie model can be judged realizing that loads in a structure follow the path of least resistance. As Schlaich notes (1987), the ties are much more

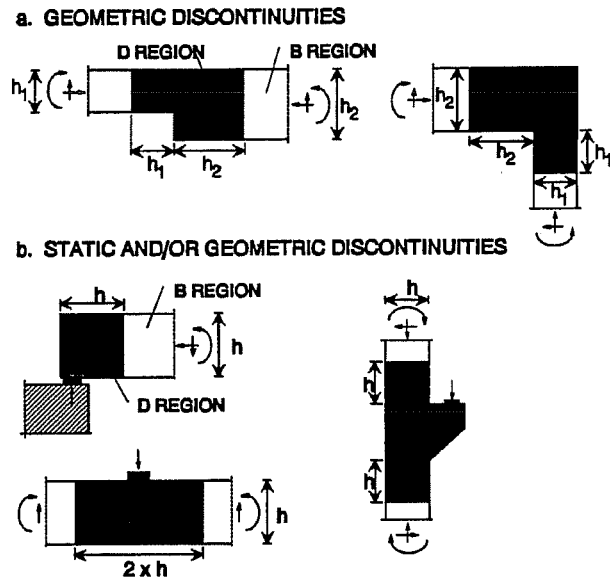


Figure 4.3 B and D Regions (Shaded) of a Structure (from Schlaich 1987)

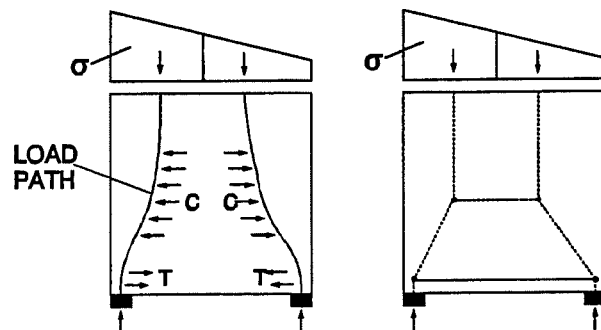


Figure 4.4 Use of the Load Path Method to form a Strut and Tie Model (from Schlaich 1987)

deformable than the struts, so the model with the least ties is best by an energy criterion. An example of this concept is shown in Figure 4.5.

4.5.4 Individual Elements of the Strut and Tie Model

4.5.4.1 Ties. Ties are tension carrying elements and in the pier cap can consist of reinforcing steel or concrete carrying tension. In this research, only reinforcing steel was considered. The strength available to a tie is taken as the yield capacity of the bars:

$$T = A_s f_y$$

where

$$A_s = \text{the area of steel in the tension tie}$$

$$f_y = \text{the yield stress of the steel}$$
(4.4)

The strength check for the tension ties is very straightforward, but there are several other concerns. First, following the major assumptions of the strut and tie method, the main reinforcement should yield at the ultimate load. To allow a ductile failure, the bars must be able to undergo plastic deformations before crushing of the concrete begins (Bergmeister 1990). Second, the bars must be able to develop the required strength at the node location. This condition means that the bars must have adequate anchorage behind the node. Also, tension steel should be evenly distributed over the full width of the tension tie. Finally, consideration should be given to crack control under service loads.

4.5.4.2 Struts. Struts are compression carrying elements and consist of concrete and compression steel that does not buckle. Three basic concrete compression struts are available as shown in Figure 4.6 (Schlaich 1987). The models proposed for the pier cap use only the prismatic compression strut (Figure 4.6.c).

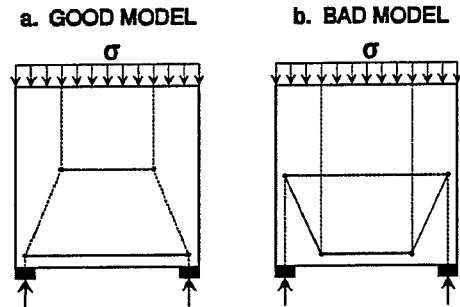


Figure 4.5 The Good Strut and Tie Model has Shorter Ties Than the Bad Model (from Schlaich 1987)

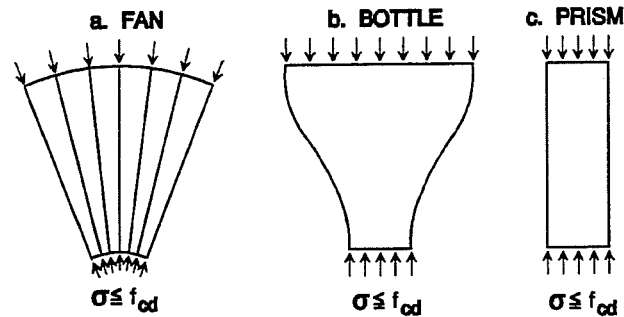


Figure 4.6 The Three Compression Struts (a) The Fan (b) The Bottle (c) The Prism (from Schlaich 1987)

The allowable load in the strut is the sum of the contributions from the steel and concrete:

$$C = C_s + C_c$$

where

$$C_c = A_c f_{cd} = \text{compression in the concrete}$$

$$C_s = A_s f_s = \text{compression in the steel}$$

where

$$A_c = \text{area of the strut}$$

$$f_{cd} = \text{design stress in concrete} = \nu f'_c$$

$$\nu = \text{concrete efficiency factor}$$

$$f_s = \text{stress in steel}$$
(4.5)

The concrete efficiency factor accounts for the different strength of concrete in the structure as compared to the strength measured by cylinder compression tests. As presented by Bergmeister (1990), the efficiency factor accounts for conditions in the structure such as:

- a multiaxial state of stress
- cracking
- disturbances caused by reinforcing steel
- aggregate interlock

The efficiency factors are different for different types of struts. For undisturbed struts a larger efficiency factor is used, while if cracks interrupt the strut, a smaller efficiency factor is used (Schlaich 1987). Essentially, all struts in the proposed model are not interrupted by skew cracking. Thus, for the prismatic compression fields used, Bergmeister (1990) suggests using the following concrete efficiency factors:

$$\begin{aligned}
 v &= 0.8 \text{ for } f'_c \leq 4,000 \text{ psi} \\
 v &= 0.9 - 0.25 \frac{f'_c}{10,000} \text{ for } 4,000 < f'_c < 10,000 \text{ psi} \\
 v &= 0.65 \text{ for } f'_c \geq 10,000 \text{ psi}
 \end{aligned}
 \tag{4.6}$$

Since concrete strength was 4,000 psi for specimens A and C, v is taken as 0.8 for the strut and tie models considered.

It is important to consider compatibility when examining concrete struts. Large compressive stresses in concrete struts give rise to transverse tensile stresses which can cause cracking and loss of capacity. Thus, it may be necessary to refine a model so transverse tensile forces are considered as shown in Figure 4.7 (Schlaich 1987).

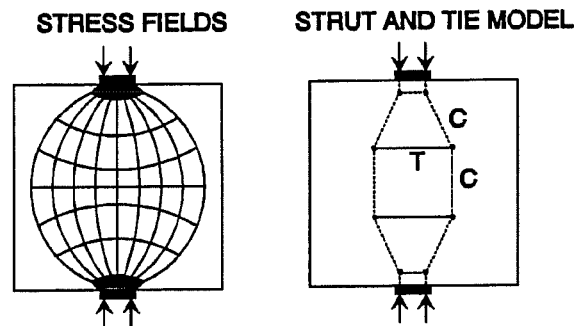


Figure 4.7 Strut and Tie Model Considering Transverse Tensile Stresses (from Schlaich 1987)

4.5.4.3 Nodes. Nodes are the points in a strut and tie model where truss forces change direction. Nodes combine three truss elements, so they are classified as either CCC, CCT, CTT, or TTT nodes based on the forces in the truss members they connect (Schlaich 1987). For example, a CCT node is the intersection of two compression struts and a tension tie. Nodes can be further classified as singular or smeared (Schlaich 1987). The models presented consider singular nodes, where the intersection of forces occurs in a small area around the theoretical node location (Schlaich 1987). Bergmeister (1990) gives two considerations for dimensioning the nodes:

1. The lines of action at the centroid of the ties, struts, and external loads must coincide.
2. The widths and relative angles of the struts and ties limit the dimensions of the sides of the nodes.

Obviously, the dimensions chosen for the nodes will affect the strength check for the nodes. Since the strength checks for nodes are not well defined, adherence to the above two recommendations to dimension nodes is probably adequate. The two node types used in the proposed strut and tie models are CCC and CCT nodes.

CCC Nodes. An example of a CCC node is shown in Figure 4.8. The ideal condition for a CCC node is a "hydrostatic" state of stress (Schlaich 1987). In a CCC node, a hydrostatic stress state is achieved when all stresses on the faces of the node are equal, and when node faces are perpendicular to their corresponding stress fields (Bergmeister 1990). An example of a CCC node in a hydrostatic state of stress is shown in Figure 4.9. In a hydrostatic stress state, both principal stresses in the node are equal to the boundary stress (Bergmeister 1990). Thus, since all boundary stresses must be within allowable limits, the stresses in the node are also within allowed limits. If a hydrostatic stress state at the node does not exist, Schlaich (1987) suggests two conditions that should be met for the node strength to be considered satisfactory. First, nodes that have a ratio of stress on adjacent sides not less than 0.5 are probably satisfactory. Second, boundary stresses on the faces of a node should all be within their respective limits.

CCT Nodes. The geometry of a CCT node which will be used in the proposed strut and tie models (sections 4.6 and 4.7) is shown in Figure 4.10. For the CCT node shown in Figure 4.10, the geometric constraints of the base plate width and the tension tie width define the strut width. For this CCT node model, the tie width (wT) is taken as the out to out dimensions of the rebar as shown in Figure 4.10. When there is only one layer of tension steel, the tie width is taken as the bar diameter. A summary of other techniques to find the width of the tie based on stress fields is presented by Anderson (1988). At this node, bearing stress, stress in the strut, and anchorage are checked independently using the

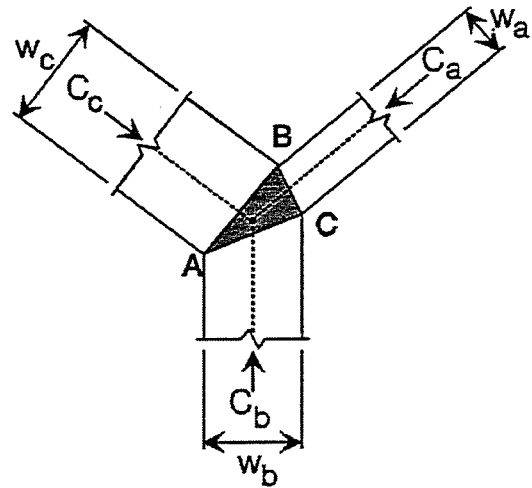


Figure 4.8 CCC Node with Unequal Pressure (from Barton 1988)

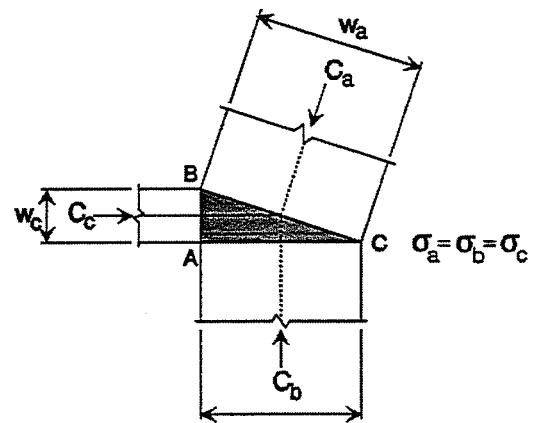


Figure 4.9 CCC Node Under Hydrostatic Stress (adapted from Anderson 1988)

geometry of Figure 4.10. Bearing and anchorage can both be checked using the 1992 AASHTO provisions. For the CCT node, anchorage of the bars is essential and may require hooks or loop anchorage. Bergmeister (1990) states that anchorage begins where the compression struts meet the bar as shown in Figure 4.10. Conservatively, development length can be taken as beginning at the interior edge of the base plate. For the compression strut at the CCT node, Bergmeister (1990) suggests using a concrete efficiency factor based on tests of CCT nodes by Bouadi (1989). For the strut at the CCT node shown in Figure 4.10, the recommended efficiency factor is the same as that presented earlier for prismatic compression struts ($\nu=0.8$). As a final note, Bouadi's tests on CCT nodes showed that the use of vertical hooks crossing the compression strut may decrease the overall capacity of the strut by about five percent. This possible loss of strength is very small compared to the overall uncertainty of the node and model design (Bergmeister 1990, Bouadi 1989).

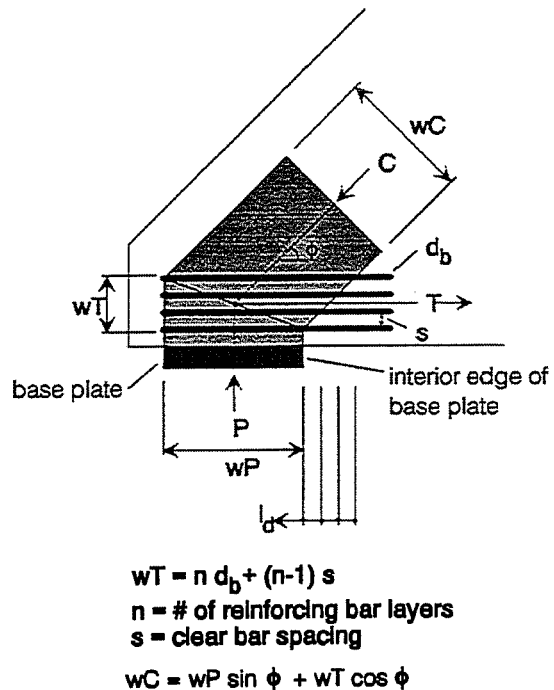
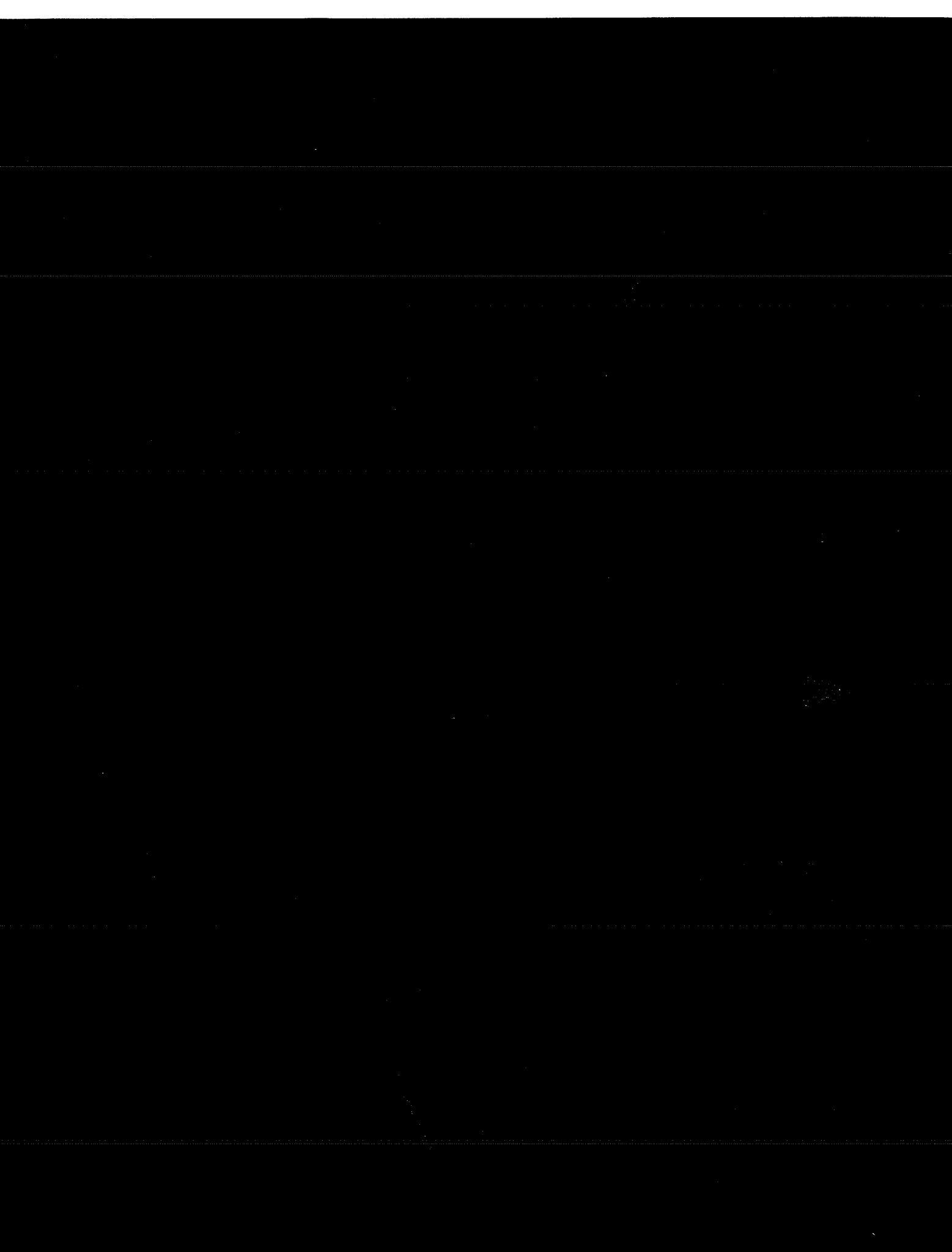


Figure 4.10 CCT Node With Multiple Layers of Reinforcing (from Bergmeister 1990)

4.6 STRUT AND TIE MODEL 1

4.6.1 Geometry and Assumptions of Model 1

The layout of the first strut and tie model for the piers was determined using the results of a plane stress finite element analysis and the cracking patterns observed during testing. The finite element program used was ANSYS. The finite element mesh is shown in Figure 4.11. Eight node elements were used for the pier cap and column, while four node elements were used for the base plate. To simulate loads from the roller, a pressure loading of 10 ksi was applied on two of the base plate elements (total width = 1.46") as shown in Figure 4.12. Contour plots of principal tensile and compressive stresses in the pier from the finite element analysis are shown in Figures



Inspection of the contour plots shows that the load on the finite element model was applied at a small eccentricity relative to the edge of the column. This eccentricity of the load is not apparent when examining a profile view of the pier cap. However, by taking a slice through the piers longitudinal axis the shear span can be observed as shown in Figure 4.16. Slice "A" represents

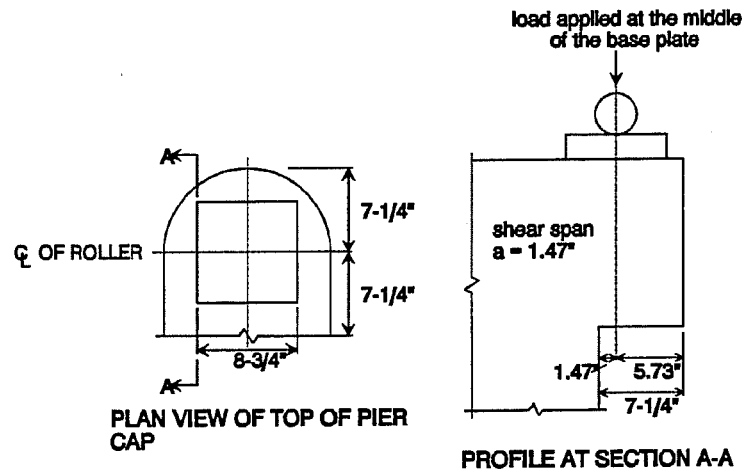


Figure 4.16 Shear Span Modelled in the Finite Element Analysis

the largest shear span for the applied loading, so this shear span was used for the finite element analysis to examine the greatest inclination of the load path.

The layout of members and nodes of strut and tie Model 1 is shown in Figure 4.17. The heavy compression strut is modelled with a "bottle" strut which provides an indication of transverse tensile forces. The net compression load carried by the bottle strut is C_1 , and the angle of inclination of this strut is θ . At nodes 1 and 2 struts C_2 are separated by an angle 2ϕ , with the angle ϕ termed the "diffusion" angle for the strut. The strut diffusion angle defines the slope at which compression forces spread from under the base plate (Bergmeister 1990). Bergmeister (1990) suggests that the diffusion angle can be found using Equation 4.7. The *compression field width* in

$$\text{diffusion angle } \phi = 12 \frac{3}{\sqrt{\frac{w}{h}}} \quad (4.7)$$

where

w = bearing plate width

h = compression field width

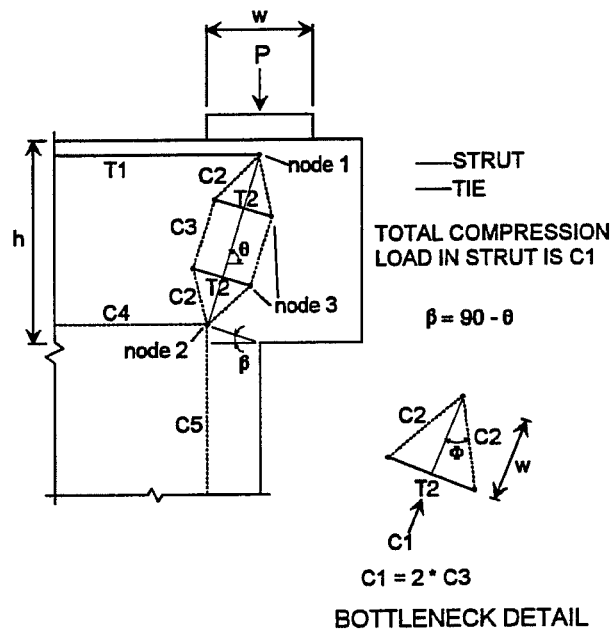


Figure 4.17 Configuration of Strut and Tie Model 1

Equation 4.7 is not the same as a strut width, but represents an outer boundary to the compressive stress field under the base plate. The value for 'h' is determined considering the physical boundaries of the structure as shown in Figure 4.18. The limit on the distance 'n' in Figure 4.18 is found where a 45° line starting at the centerline of the base plate intersects the edge of the structure. The value of 'h' is the smaller of m and 2*n. For the pier studied, the compression field width, h, is the depth of the pier cap (14.5") as shown in Figure 4.17.

Several analyses of Specimens A and C were made using Model 1 (reinforcing is described in section 2.2.2). The steps for conducting the analyses are given below.

1. Beginning at node 1, the force in the main tension tie (T1) was assumed.

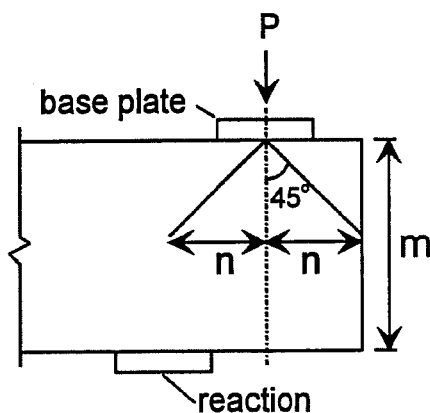


Figure 4.18 Determination of the Compression Field Width

2. The angle of inclination, θ , of the main compression strut (C1) was assumed.
3. Using the force T1 and angle of inclination from steps 1 and 2, all forces in the strut and tie members were calculated.
4. The centroid of compression strut C5 was then found, considering that the maximum concrete strain is located at the edge of the column. The centroid location is shown in Figure 4.19.
5. The centroid location computed in step 4 was then compared to the centroid location predicted by the angle of inclination assumed in step 2. If the two locations agreed, the system was in equilibrium. If the centroids did not match, the procedure returned to step 2, and further iterations were made as needed.

When choosing the force in T1 in step 1 above, the tie forces were always assumed less than or equal to the yield capacity of the existing steel. For T1, the corresponding rebar in the specimen is bars A and T. For Piers A the tie capacity was 132 kips, while for Pier C the tie capacity was only 26.1. Both tie capacities are based on using the full yield strength of the bar as determined by tensile tests.

To find the centroid of compression strut C5 in step 4 above, compression carried by the column steel was considered. The inclusion of compression steel to the force in C5 meant that a transformed area approach had to be used to find the centroid of strut C5. Since column steel compression strains were not measured during tests, three compression forces from the steel, C_s , were considered:

1. $C_s = 0$.
2. $C_s = 58$ kips. This force was determined using compatibility between the steel and concrete. The concrete deforms under load, so the compression steel is subjected to the same strains as the concrete. Knowing the maximum stress allowed in the concrete, the steel stress was computed as shown below:

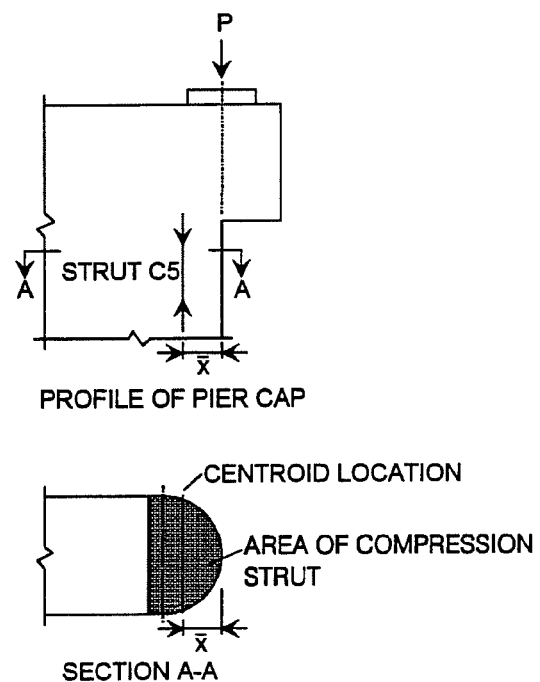


Figure 4.19 Centroid Location for the Column Compression Strut

given

$$\sigma_{cmax} = \sqrt{f'_c} \text{ allowable concrete stress} = 3.2 \text{ ksi}$$

$$E_c = 57\sqrt{f'_c} \text{ [ksi]} \text{ by ACI 318-89, concrete modulus} \quad (4.8)$$

$$\epsilon_c = \frac{\sigma_{cmax}}{E_c}, \text{ strain in concrete}$$

$$\epsilon_s = \epsilon_c \text{ strain in steel}$$

$$\text{so } f_s = E \epsilon_s = 25 \text{ ksi} = \text{stress in steel}$$

Only the column steel around the periphery of the circular end of the column as shown in Figure 4.20, was considered to contribute to the strength of strut C5. All six bars in Figure 4.20 were used to find the force in the compression steel, as the bars fell within the main stress field for strut C5. Thus, the force in the compression steel is:

$$C_s = 6A_b[f_s - \sigma_{cmax}] = 58 \text{ kips} \quad (4.9)$$

3. $C_s = 119$ kips. This force was determined considering the design of columns under pure axial load. Under pure axial load, the full yield capacity of the compression steel is used to find the column capacity (Salmon 1985, ACI 1989). Considering that the main compression field of the finite element analysis is concentrated close to the edge of the column, only bars 2 through 5 of Figure 4.20 were assumed to yield. Bars 1 and 6 were assumed to have a compatibility force as assumed in part 2 above. Thus, the total compression is:

$$C_s = 4A_b[f_y - \sigma_{cmax}] + 2A_b[25\text{ksi} - \sigma_{cmax}] = 119 \text{ kips} \quad (4.10)$$

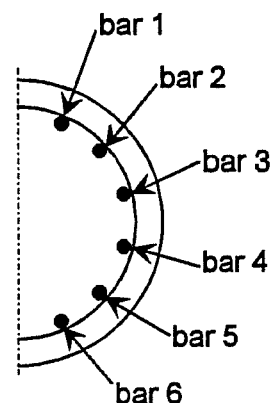


Figure 4.20 Layout of Compression Steel at the Edge of the Column

Both of the compression forces used above are arbitrary, but allow a reasonable approach to account for the column compression steel.

When examining results from the strut and tie analyses, the force in strut C1 was checked to insure the validity of the model. The force allowed in C1 was calculated in accordance with the CCT node geometry of Figure 4.10, with the concrete efficiency factor as presented earlier. Thus, the limit on C1 is shown in Equation 4.11. Since concrete strength was very close for specimens A and C, a value of 4,000 psi was used for f'_c .

$$C = A_c F_c$$

where

$$f_c = \text{allowable stress} = 0.8f'_c \quad (4.11)$$

$$A_c = bw$$

b = thickness of pier cap, 14.5"
 w = strut width based on Figure 4.10

4.6.2 Analysis Results from Strut and Tie Model 1

The analysis results using Model 1 with several different combinations of T1 and C_s are shown in Table 4.3. Only the analyses satisfying allowable stresses for C1 and T1 are presented.

Table 4.3 Specimen Capacity and Member Forces for Strut and Tie Model 1

		Pier A			Pier C	
Analysis		1-1	1-2	1-3	1-4	1-5
Capacity, P		311	344	373	132	159
ratio of theory/test		0.79	0.87	0.94	0.44	0.53
Inclination, θ_1		67.0	69.0	70.5	78.8	80.7
Compression in Steel		0	58	119	0	58
Forces (kips)	T1	132	132	132	26.1	26.1
	T2, horizontal	44.3	49.0	53.1	18.8	22.7
	T2, vertical	18.8	18.8	18.8	3.7	3.7
	C1	338	368	395	134	162
	C2	176	191	206	69.9	84.0
	C3	169	184	198	67.2	80.8
	C4	132	132	132	26.1	26.1
	C5	311	344	373	132	159
Centroid		4.68	4.35	4.09	2.52	2.11

For specimen C, the model with $C_s = 119$ kips is not listed as the column bars that were assumed to have yielded did not fit within the calculated compression field. The results from tests on Specimens A and C are summarized in Table 4.4. Physically, the analysis models agree with the test results as the angles of strut C1 inclination for the strut and tie models are close to the observed cracking patterns. For Pier A, the loads predicted by the strut and tie analyses agreed

very well with test results. For Pier C, however, the strut and tie model was extremely conservative, predicting less than half the tested capacity. The strut and tie results for Pier C showed better correlation to the load at which reinforcing in the top layer yielded during testing, about 200 to 217 kips. It is reasonable that the strut and tie model is more accurate in predicting the specimen yield load, because the strut and tie method assumes

failure occurs with yielding in the ties as discussed in section 4.5.2. The discrepancy between Model 1 strength predictions and the tested specimen capacities can be accounted for by load carrying components other than the tie/arch action accounted for in the strut and tie model. Additional strength may come from dowel action, aggregate interlock, and shear transfer in the uncracked concrete (Salmon 1985).

The compression steel force assumed in strut C5 had a significant impact on results of the strut and tie analyses. There was a direct correlation between C_c and the predicted pier capacity, with the pier capacity rising with larger C_c values. This trend can be explained by looking at the inclination of strut C1. As the force in the compression steel rises, the centroid of C5 moves closer to the edge of the column, increasing the angle of inclination of strut C1. For a larger angle of inclination, the vertical component of the main strut increases, enlarging the predicted specimen capacity. The extent of this increase in capacity is limited by the allowable compression stress in the main compression strut, and the capacity of the tension tie T1.

The difficulty of using a strut and tie model as an analysis tool can be seen by considering tie T2. The horizontal and vertical components of T2 are listed in Table 4.3 because those components match the orientation of stirrups (bars B and S) in the pier cap. Considering the layout of reinforcing in the test specimens, the limits for the components of T2 are given in Table 4.5. For

Table 4.4 Tested Capacities for Pier A and Pier C

	Pier A	Pier C
Average Capacity	395	299
Average Inclination of Main Strut Cracks	66°	75°
Test 1 Capacity (kips)	368	298
Test 2 Capacity (kips)	387	299
Test 3 Capacity (kips)	430	-

Table 4.5 Limitations on the Components of T2 Based on Reinforcing in the Test Specimens

	Pier A	Pier C
Maximum T2 Horizontal	19.8 kips	15.6 kips
Maximum T2 Vertical	6.6 kips	5.2 kips

both Piers A and C, the strut and tie analysis predicts larger forces than the stirrups can handle. However, the magnitude of T2 depends greatly on the diffusion angle, which is only generally known. Also, tension in the concrete has not been considered. Because of the uncertainty of the magnitude of transverse tensile forces, the inadequacy of stirrups as predicted by the strut and tie model was ignored because all the analysis results were conservative. When examining member forces from an assumed model, the allowed stresses on T1 and C1 were used to judge the validity of the analysis as T1 and C1 are the most critical load carrying components of the model.

4.7 STRUT AND TIE MODEL 2

The second strut and tie model was created to increase the predicted capacity for Pier C, and is shown in Figure 4.21. Model 2 follows the main stress fields of the finite element analysis,

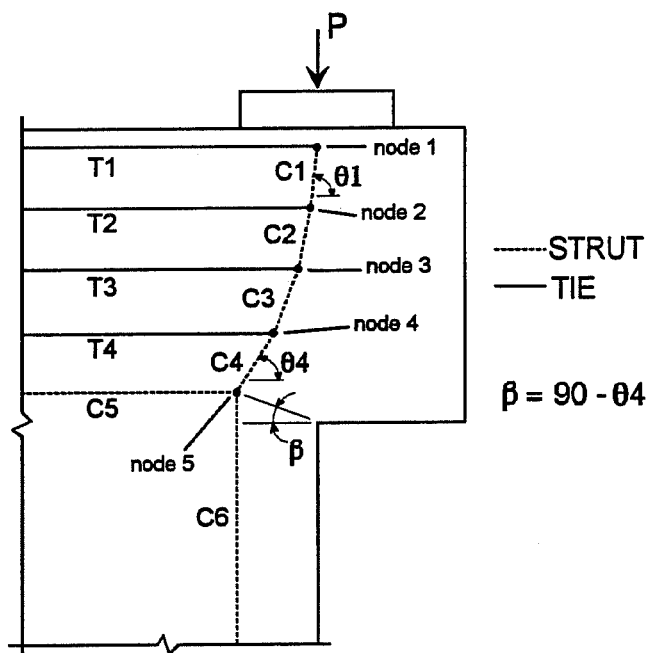


Figure 4.21 Configuration of Strut and Tie Model 2

but considers the restraint of the horizontal stirrups individually. For Pier C, the forces in the intermediate stirrups (T2-T4) were chosen as the yield capacity of the bars to give the maximum benefit of each tie. While this assumption gave the best results for the model, it is not certain that

all of the ties across the pier cap depth yielded. The assumption that all the intermediate stirrups yielded is consistent with a linear distribution of strain across the depth of the pier cap. At the ultimate load for specimen C, the maximum crack size at the top of the pier was approximately 1/16", and the average strain in the top layer reinforcing steel was about 12,000 microstrains. Since cracking extended across the full depth of the pier at the peak load and strain at the top layer was very large, it is probable that at least two layers of the intermediate stirrups yielded in specimen C. For Pier A, the force was found by assuming a linear distribution of strain across the pier cap height, with the maximum strain found in the top layer of reinforcing.

The capacities and member forces for Specimens A and C as predicted by Model 2 are given in Table 4.6. The second model did predict a greater capacity for Pier C, but the analysis

Table 4.6 Specimen Capacity and Member Forces for Strut and Tie Model 2

		Pier A		Pier C		
Analysis		2-1	2-2	2-3	2-4	2-5
Capacity, P		319	353	171	198	236
ratio of theory/test		0.81	0.89	0.57	0.66	0.79
Theta 1		67.5	69.5	81.3	82.5	83.7
Compression in Steel		0	58	0	58	119
Forces (kips)	T1	132	132	26.1	26.1	26.1
	T2	10.2	10.2	10.4	10.4	10.4
	T3	7.3	7.3	10.4	10.4	10.4
	T4	4.3	4.3	10.4	10.4	10.4
	C1	345	377	173	200	238
	C2	349	381	174	202	239
	C3	352	383	177	204	241
	C4	354	385	180	206	243
	C5	154	154	57.3	57.3	57.3
C6	319	353	171	198	236	
Centroid		4.81	4.50	3.01	2.66	2.28

results were still much less than the tested capacity. Model 2 predicts a greater load than Model

1 for an assumed T1 and C_s. This increased strength occurs because the second model has a larger angle of inclination at node 1, increasing the vertical component of strut C1. In Model 2, the centroid of the compression strut was located further in the column than for Model 1 because the compression strut changes inclination at each horizontal stirrup.

4.8 SUMMARY OF STRUT AND TIE RESULTS

While both strut and tie models did not accurately predict Pier C capacity, strength predictions from the models agreed quite well with Specimen A test results. The poor results for specimen C can be partially explained considering the assumption of the strut and tie model that load is carried only through the action of a tied arch. If the size of T1 is reduced to zero kips, the strut and tie model predicts that the specimen capacity is zero. However, the specimen will have as a minimum capacity the concrete strength in shear.

Specimen C could not reach the available capacity of the inclined compression strut because the restraining tie at the top of the pier cap was too small. Since the compression strut for pier C is not fully used, the contribution of shear carrying mechanisms such as aggregate interlock make up a larger proportion of the total load in specimen C. Because the strut and tie model only considers the capacity provided by direct strut action, there will be less accuracy for Pier C as the compression strut capacity was not reached. For specimen A, the other shear carrying mechanisms carry a smaller portion of the load, so the strut and tie model had more accuracy.

To account for the load carried by shear in the concrete, a concrete shear strength term, V_c can be added to the strut and tie strength. Using the upper limit on V_c from the ACI 318-89 deep beam provisions, the shear contribution is:

$$V_c = 6 \sqrt{f'_c} b_w d = 72 \text{ kips}$$

where

$$f'_c = 4,000 \text{ psi}$$

$$b_w = 14.5 \text{ inches}$$

$$d = 13.0 \text{ inches}$$
(4.12)

The specimen capacities resulting when the concrete shear strength term is added to the strength of strut and tie Model 1 are shown in Table 4.7. The addition of the V_c term to the strength from strut and tie Model 1 greatly improves results for specimen C. For Piers A, the addition of the V_c term gives results that are slightly unconservative when the effect of compression steel is considered.

Table 4.7 Predicted Specimen Capacities when a V_c Term is Added to Strengths from Strut and Tie Model 1

Analysis	Pier A			Pier C	
	1-1	1-2	1-3	1-4	1-5
Capacity from Strut and Tie Model 1 (kips)	311	344	373	132	159
Old Ratio of Theory/Test	0.79	0.87	0.94	0.44	0.53
V_c Term (kips)	72	72	72	72	72
Strength from Model 1 and V_c Term (kips)	383	416	445	204	231
New Ratio of Theory/Test	0.97	1.05	1.13	0.68	0.77

However, compression steel is not typically used in strut and tie designs, so the inclusion of the V_c term for Piers A would be acceptable. Further consideration of a concrete shear strength term, V_c , in addition to the strut and tie strength should be developed in future reports.

For the strut and tie analyses, the force in T1 was assumed. This assumption is critical, because the tie capacity used in the strut and tie analysis limits the specimen capacity by equilibrium at node 1. For specimen C, strain gages on the bars showed that all bars in the top layer of the pier had yielded before the peak load was reached, so the yield capacity of the bars was used for the strut and tie model. Since bars in the top layer of specimen A did not have strain gages, the force in the bars had to be assumed. For specimen A, the force for T1 was assumed as the full yield capacity of the bars in the top layer, 132 kips. This assumption gave strut and tie strength predictions that agreed well with tested results. However, it is very unlikely that the full yield strength of all bars in the top layer of pier A was reached. For specimen C, the #3 bars in the top layer of the pier yielded at a load of around 200 kips. Since the area of a #3 bar is 1/4 that of a #6 bar, the force in the #6 top layer bars of specimen A was probably 1/4 the yield capacity of the #6 bars at a load of 200 kips. Extrapolating to the capacity of specimen A, the #6 bars would probably see a load of about 1/2 their yield capacity at a load of 400 kips.

The anchorage of the bars can also be considered in predicting the actual force in tie T1. For specimen A, inspection of the failed specimen showed no signs of bond distress. However, for the straight bars in specimen A, the available development length for the bars was very small and inadequate to develop the yield strength of the bar. If the straight bars in specimen A had to

develop a large portion of their capacity, bond distress would have been observed as for specimen B. This discrepancy between the assumed force and observed behavior can partially be explained by considering tension in the concrete. Also, the strut and tie model only considers the action of the tied arch to carry loads. However, other shear carrying mechanisms carry load, so the strut and tie model will overestimate the required steel in the top layer.

For strut and tie Models 1 and 2, the analyses considered the effect of compression in the column steel. The inclusion of the steel increased the angle of strut inclination, enlarging the predicted capacity of the pier. Since no strain gages were located on the column steel, the magnitude of C_s assumed was very arbitrary. Still, the inclusion of compression steel in the strut and tie model reflects the behavior of the specimen and increased the strut and tie model accuracy. However, the effect of compression steel has not been considered in the general strut and tie theory at this point. One of the problems of using compression steel is an inability to check the stress at a CCC node. Because the strut and tie theory has not yet developed procedures for considering compression steel, the effect of compression steel was ignored in the design example.

While the strut and tie model results give conservative estimates of the specimen strength, either model predicted strength much more accurately than a conventional analysis. To increase the strength predicted by a strut and tie model, a concrete shear strength term may be added to the strut and tie capacity. The average ratios of the theoretical load to tested specimen capacity for all design methods are summarized in Table 4.8. Additionally, all strengths predicted by the strut and tie models that met limit stresses in the main strut and tie were conservative. The author feels that Model 1 is a better model for design than Model 2. Model 2 ends up assuming forces in the horizontal stirrups that were not verified by strain gages. Additionally, Model 2 does not consider transverse tensile strains in the main compression struts. Thus, Model 1 is used in the design example.

Table 4.8 Comparison of Average Ratio of Theory/Test Capacity for Different Design Methods

Average Ratio of Theoretical Capacity to Tested Strength	Pier A	Pier C
Strut and Tie Model 1 Plus a V_c Term	1.05	0.73
Strut and Tie Model 1	0.87	0.49
Strut and Tie Model 2	0.85	0.67
Corbel Analysis	0.38	0.18
Deep Beam Analysis	0.24	0.32

4.9 DESIGN EXAMPLE USING STRUT AND TIE MODEL 1

A design example using the strut and tie method for a typical pier cap geometry is presented. Strut and tie Model 1 is used, with the calculations presented identical to those used to analyze the scale specimens. For the design example, the benefit of compression steel in the column was not considered as explained previously. The example is based on ultimate strength design, which is the accepted procedure for use with the strut and tie method. For ultimate strength design, the criteria for specimen nominal strength is shown in Equation 4.13.

$$\phi P_n = P_u \quad (4.13)$$

$P_u = \text{factored load}$
 $P_n = \text{nominal strength}$
 $\phi = \text{strength reduction factor}$

PROBLEM STATEMENT

Determine the base plate size and pier cap reinforcing for the pier cap geometry shown in Figure 4.22 using the strut and tie model shown in Figure 4.23.

LOAD, DIMENSIONS, AND MATERIALS

$P = 1,200$ kips, a service load

$L1 = 12'-0''$

$L2 = 12'-0''$

$L3 = 8'-6''$

$B1 = 4'-0''$

$B2 = 3'-6''$

$h = 4'-0''$

$f'_c = 3,600$ psi

$f_y = 60$ ksi

cover = 2 1/4"

The given load is a service load, so this must be transformed to a factored load. A load

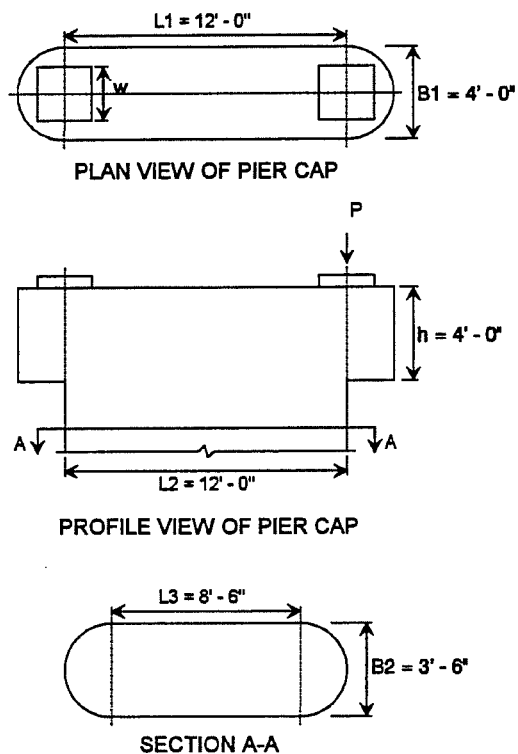


Figure 4.22 Pier Cap Geometry for the Example Problem

factor of 1.6 was used since individual load components were not known.

$$P_u = (\text{load factor})P = 1.6 * 1,200$$

$$P_u = 1,920 \text{ kips}$$

SIZE THE BASE PLATES

Base plates are sized using the 1992 AASHTO provisions, section 8.16.7.

$$P_u = 1,920 \text{ kips}$$

$$\Phi = 0.7 \text{ for bearing}$$

P_n = nominal bearing strength

$$P_n \text{ required} = P_u / \Phi = 2,743 \text{ kips}$$

$$P_n = 0.85 f_c' A_1 (A_2 / A_1)^{0.5}$$

where

A_1 = base plate area

A_2 = surrounding area of concrete, taken as

the area of a circle with a 4'-0" diameter = 1,810 in²

Try a base plate with $w = 25"$

$$\text{so } P_n = 0.85 * 3.6 * 625 * (1810 / 625)^{0.5} = P_n = 3,250 \text{ kips} > P_n \text{ required}$$

Obviously, a smaller base plate could be used. However, too small a plate will not adequately distribute load across the full pier cap width. For tested specimens, the ratio of base plate size to strut width (w/B) was 0.6 (8.75"/14.5"). Using a 25 inch base plate gives a ratio of plate width to strut width $w/B = 0.6$ (25"/42") to conform with the tested specimens. The strut width is chosen as the column width, 42", which is smaller than the pier cap width, 48". The column width is used for the w/B ratio as the smaller width will control strut widths.

SIZE C5 AND FIND THE LOCATION OF ITS RESULTANT

To find forces in the struts and ties, the angle of inclination, θ , is needed. Since $C5 = P_n$, the centroid of C5 can be found knowing the applied load. The inclination angle, θ , can then be determined based on the location of the centroid of C5. To find the required P_n for the pier cap, a Φ factor is needed. One Φ factor is used for the entire pier cap design, instead of different Φ factors for the different elements of the strut and tie model. Since the strut and tie method is

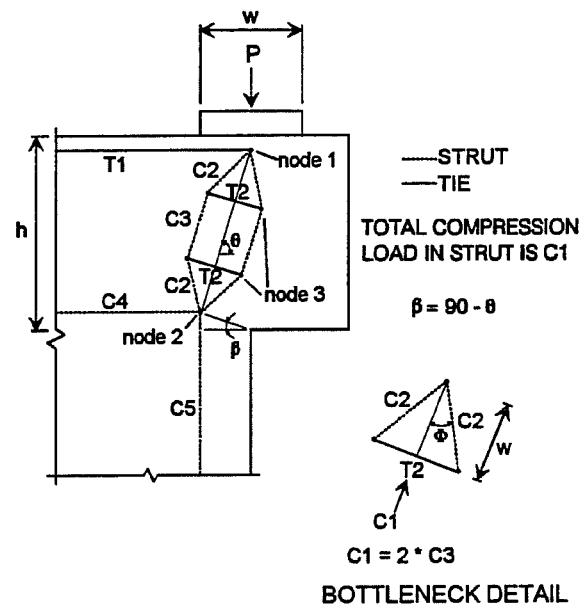


Figure 4.23 Strut and Tie Model for the Example Problem

KNOWING θ , CHECK T1 AND ASSUMED d

$$T1 = P_n / \tan \theta = 2,130 / \tan 72.8 = 659 \text{ kips}$$

$$AT1 = \text{area of steel for } T1 = T1 / f_y = 11.0 \text{ in}^2$$

use 8 #11 bars, with $A_s = 12.48 \text{ in}^2$

⇒ this implies that 2 layers of steel will be needed

RECALCULATE θ USING TWO LAYERS OF STEEL FOR T1

for 2 layers of steel, use clear spacing of $2d_b = 2.82''$

for a #11 bar

$$d = h - \text{cover} - d_b - \text{clear spacing}/2 = 42.9''$$

$$\text{so new } \theta = 0.5 \text{ asin } [2x_{cg}/d] = 71.8$$

Check T1 using the new θ

$$T1 = P_n / \tan \theta = 2,130 / \tan 71.8 = 700 \text{ kips}$$

$$AT1 = T1 / f_y = 11.7 \text{ in}^2 < 12.48 \text{ in}^2 \text{ provided, OK}$$

FIND ALL MEMBER FORCES

Compute the diffusion angle:

$$\Phi = 12 + 3 / [(w/h)^{0.5}] = 16.2^\circ$$

$$P_n = 2,130 \text{ kips}$$

$$T1 = 700 \text{ kips}$$

$$\theta = 71.8^\circ$$

$$C1 = P_n / \sin \theta = 2,242 \text{ kips}$$

$$C2 = 0.5 C1 / \cos \Phi = 1,167 \text{ kips}$$

$$C3 = C1 / 2 = 1,121 \text{ kips}$$

$$C4 = T1 = 700 \text{ kips}$$

$$C5 = P_n = 2,130 \text{ kips}$$

$$T2 = 0.5 C1 \tan \Phi = 326 \text{ kips}$$

$$T2_{\text{horiz}} = T2 \sin \theta = 310 \text{ kips} = \text{horizontal component of } T2$$

$$T2_{\text{vert}} = T2 \cos \theta = 101 \text{ kips} = \text{vertical component of } T2$$

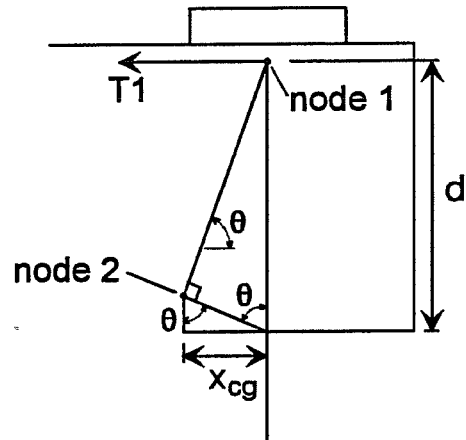


Figure 4.25 Location of Node 2 in the Strut and Tie Model

conservative, and its strength predictions for the tested piers were conservative, Φ was chosen as 0.9.

$$P_u = 1,920 \text{ kips}$$

$$\Phi = 0.9$$

$$P_n = P_u/\Phi = 2,130 \text{ kips} = \text{required pier cap strength}$$

Knowing P_n , the centroid of C5 can be found because $C5 = P_n$.

f_{cd} = concrete design strength = $\nu f_c'$ for all struts in the model

where $\nu = 0.8$ from section 4.4.4.2

$$f_{cd} = \nu f_c' = 2.88 \text{ ksi}$$

$$AC5 = \text{area of strut C5} = C5/f_{cd} = 740 \text{ in}^2$$

Consider the total area of strut C5 as two pieces, A1 and A2, as shown in Figure 4.24

$$AC5 = A1 + A2$$

$A1 = 693 \text{ in}^2$ so strut C5 must extend into the rectangular section of the column

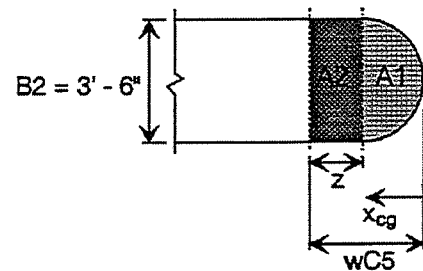
$$A2 = AC5 - AC1 = 47 \text{ in}^2$$

$$z = A2/B2 = 1.1 \text{ in}$$

$$wC5 = z + B2/2 = 22.1" = \text{the width of strut C5.}$$

The centroid of AC5 is then found,

$$x_{cg} = 12.7"$$



COLUMN CROSS SECTION

Figure 4.24 Cross Section of Strut C5

FIND THE INCLINATION ANGLE OF THE BOTTLE STRUT, θ

The location of node 2 is the intersection of struts C1, C4, and C5, and is defined by x_{cg} and θ , the angle of inclination, as shown in Figure 4.25. The inclination angle, θ , can be found knowing the centroid of strut C5, x_{cg} , and the depth of reinforcing, d .

$$d = h - \text{cover} - d_b/2$$

Assuming a #11 bar in the top layer, $d_b = 1.41"$

$$\text{so } d = 48 - 2.25 - 1.41/2 = 45.0"$$

$$\theta = 0.5 \text{ asin } [2x_{cg}/d] = 72.8^\circ$$

CHECK STRESS AT THE CCC NODE, NODE 2

The layout of the CCC node is shown in Figure 4.26. AC1 is the area of compression strut C1 at this node. Since AC5 is a combination of a circular and a rectangular section, AC1 is found by projecting from AC5.

$$AC1 = AC5 / \sin \theta = 740 / \sin 71.8 = 779 \text{ in}^2$$

wC4 = the width of strut C4

$$0.5 wC4 = c / \tan \theta = 3.09"$$

$$wC4 = 6.18"$$

The column width is used to find AC4 as the column width limits the strut width.

$$AC4 = B2 wC4 = 260 \text{ in}^2$$

$$\sigma_{C5} = \text{the stress on strut C5} = C5 / AC5$$

$$\sigma_{C5} = 2.88 \text{ ksi} = f_{cd} \text{ OK}$$

$$\sigma_{C1} = C1 / AC1 = 2.88 \text{ ksi} = f_{cd} \text{ OK}$$

$$\sigma_{C4} = C4 / AC4 = 2.67 \text{ ksi} < f_{cd} \text{ OK}$$

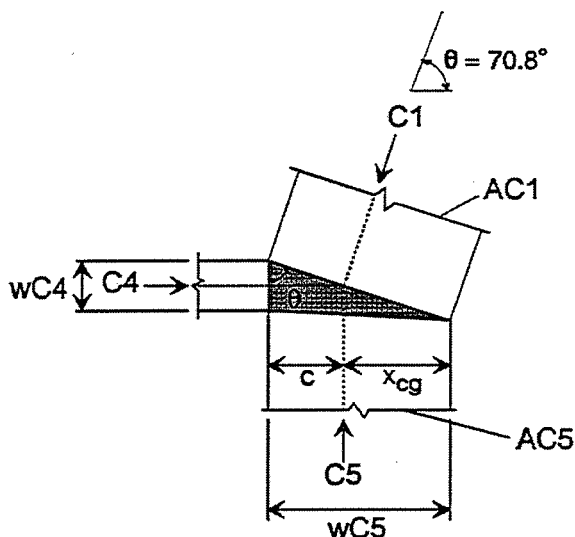


Figure 4.26 Geometry of the CCC Node
(Node 2 in the Strut and Tie Model)

All strut stresses at the node are less than or equal to the limiting concrete design stress, but a hydrostatic state of stress does not exist as all three stresses are not equal. Since the stress at the node is not hydrostatic, the checks suggested by Schlaich (1987) are used:

1. All strut stresses at the node are within design limits.
2. The smallest stress ratio between faces of the node is greater than 0.5.

$$\text{Check: } 2.67 / 2.88 = 0.93 > 0.5 \text{ OK.}$$

Since both checks are met, this node is satisfactory.

DESIGN STEEL FOR T1 AND THE COMPONENTS OF T2

$$T1 = 700 \text{ kips}$$

$$AT1 = T1 / f_y = 11.67 \text{ in}^2 = \text{area of steel required for T1}$$

$$\text{For T1, use 5 \#11 bars and 4 \#10 bars, } A_s = 12.88 \text{ in}^2$$

The layout of T1 steel at the top of the cap is shown in Figure 4.27.

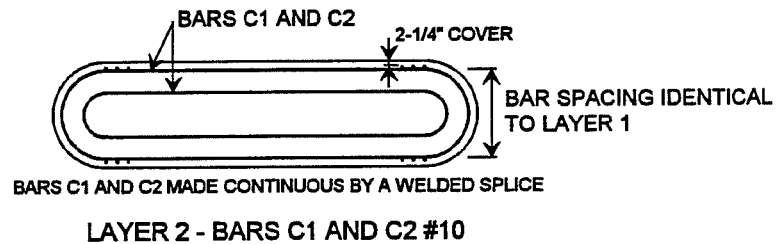
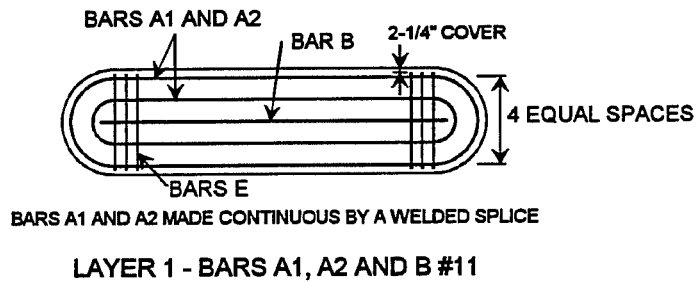
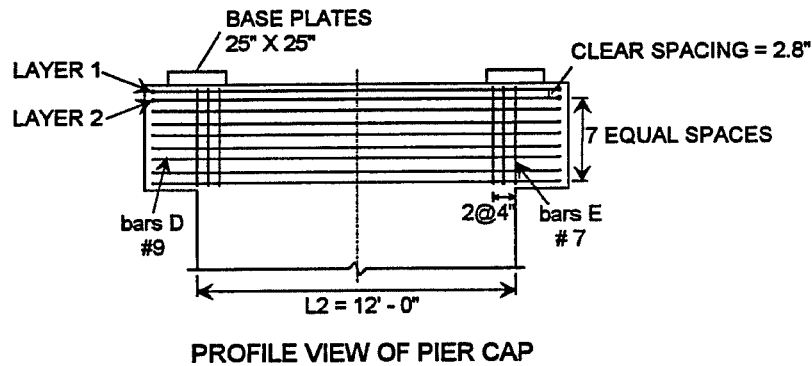


Figure 4.27 Steel Reinforcing Pattern from the Example Problem

For the components of T_2 , horizontal and vertical stirrups are used. Since there are two ties T_2 in the bottle strut, steel must be provided to resist $2 \cdot T_2$. Since steel will be distributed on each face of the pier, the steel required for T_2 is provided on each face of the pier cap.

$$T_{2_{\text{horiz}}} = 310 \text{ kips}$$

$$AT_{2_{\text{horiz}}} = T_{2_{\text{horiz}}} / f_y = 5.17 \text{ in}^2 \text{ on one face of the cap}$$

for $T_{2_{\text{horiz}}}$ use 6 #9 bars, $A_s = 6.0 \text{ in}^2$

The horizontal stirrups for T2 are evenly spaced across the depth of the pier cap as shown in Figure 4.27.

$$T2_{\text{vert}} = 101 \text{ kips}$$

$$AT2_{\text{vert}} = T2_{\text{vert}}/f_y = 1.68 \text{ in}^2 \text{ on one face of the cap}$$

for $T2_{\text{vert}}$ use 3 #7 bars, $A_s = 1.8 \text{ in}^2$

The vertical stirrups for T2 are spaced across the width of the compression strut as shown in Figure 4.27.

CHECK STRESSES AT THE CCT NODE

The geometry of the CCT node, node 1, is shown in Figure 4.28. Since the bearing stress is within its limit and T1 can be provided, only the stress in C1 needs to be checked.

To compute the area of C1 at this node the column width, B2, is used as the strut width instead of the pier cap width, B1. The smaller width is used because loads from the base plate can only be distributed over a limited concrete area.

$$wT1 = d_{b\#11} + d_{b\#10} + s = 1.41 + 1.27 + 2.82 = 5.5''$$

$$wC1 = w \sin \theta + wT1 \cos \theta = 25.5''$$

$$C1 = 2,242 \text{ kips}$$

$$AC1 = B2 wC1 = 1,071 \text{ in}^2$$

$$\sigma C1 = C1/AC1 = 2.09 \text{ ksi} < f_{cd} \text{ OK}$$

CHECK STRESSES IN C2, C3, AND NODE 3

Since the stress in C1 has been checked at both nodes 1 and 2 and is satisfactory there, both $\sigma C2$ and $\sigma C3$ will meet allowable stresses. The stresses at the nodes are most critical, because the area at the nodes is smallest. For struts C2 and C3 the load can distribute over a larger area,

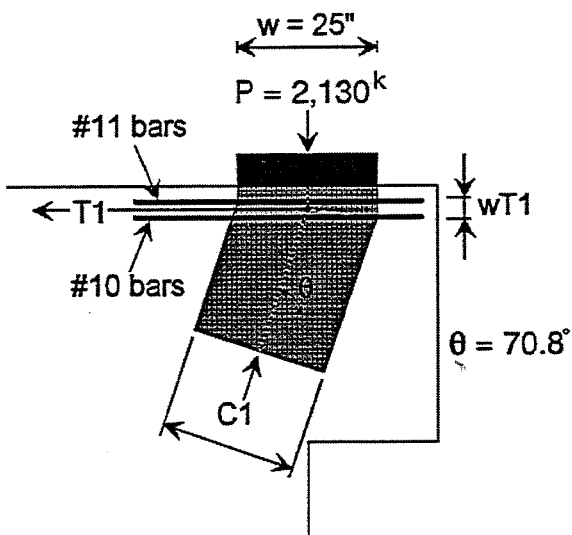


Figure 4.28 Geometry of the CCT Node (Node 1 in the Strut and Tie Model)

reducing stress. Using a similar argument, nodes 3 do not need to be checked. Also, node 3 does not need to be checked as T2 is spread over several stirrups.

CHECK ANCHORAGE REQUIREMENTS FOR T1 TIE

At the CCT node, the strut and tie method requires the full tensile strength of the bars to be provided. The development length is calculated using the 1992 AASHTO provisions, section 8.25.

$l_d = \{A B \dots\} l_{db}$ = the development length of a bar

A, B are multipliers based on rebar placement

$$l_{db} = 0.04 A_b f_y / (f'_c)^{0.5} = 62.4"$$

A = 1.4 = multiplier for top bars

B = 0.8 = multiplier for large lateral spacing

$$l_d = A B l_{db} = 70"$$

Since the development length is extremely large, straight bars can not be used to provide the full strength of T1. Therefore, continuous loops are used to provide anchorage as shown in Figure 4.27. The AASHTO provisions do not specify a development length for a full U, so the 1992 AASHTO provisions for a standard 180° hook, section 8.28, are examined.

$l_{hb} = \{A B \dots\} l_{hb}$ = development length of the hook

$$l_{hb} = 1,200 d_c / (f'_c)^{0.5} = 28.2"$$

A = 0.7 = multiplier for cover

$$l_{db} = A l_{hb} = 20.0"$$

This length can be provided under the base plate, so the development of the U hoops is considered adequate.

The area of steel that can be developed at the CCT node is thus the full strength of the U shaped hoops, and the developed strength of the straight bar. As suggested by Bergmeister (1990), the development length begins at the edge of the base plate.

$$AT1 = 4 A\#11 + 4 A\#10 + A\#11 (l_{d \text{ provided}} / l_{d \text{ available}})$$

$l_{d \text{ provided}} = 20"$ based on the bar layout shown in Figure 4.27.

$$AT1 = 4(1.56) + 4(1.27) + 1.56(20/70) = 11.77 \text{ in}^2 > 11.67 \text{ in}^2 \text{ reqd.}$$

Thus, tie T1 can provide the full capacity needed at the CCT node.

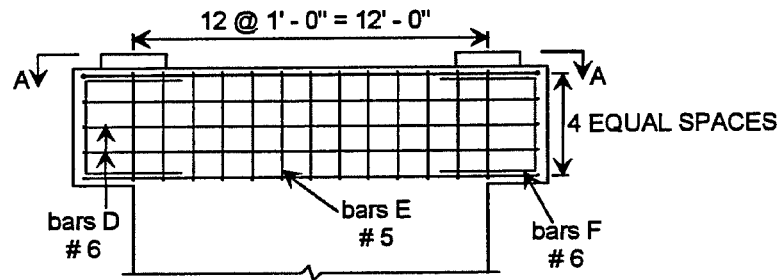
SUMMARY OF THE EXAMPLE PROBLEM

The reinforcing design for the example problem pier cap is shown in Figure 4.27. Using the strut and tie method, steel reinforcing for the pier cap can readily be designed. The main considerations in the strut and tie analysis shown were checks of the nodes, selection of reinforcement, and anchorage of reinforcing. Since the column width is less than the pier cap width, the column width was used to limit strut widths. Also, the base plate width is kept larger than required to allow distribution of loads across the pier. The tested specimens had a ratio of base plate width to strut width of 0.60, so this ratio was used for the full size pier. The calculations in the design example are lengthy, so a simplified procedure to predict the pier cap strength will be developed in future research.

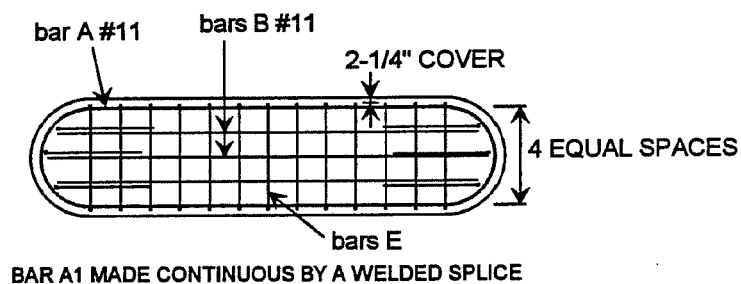
4.10 COMPARISON OF EXAMPLE PROBLEM REINFORCING STEEL TO A TYPICAL TxDOT DETAIL

The amount of reinforcing required for the strut and tie design example is much greater than that typically used by TxDOT. For the given geometry, a pattern of reinforcing often used by TxDOT is shown in Figure 4.29. The TxDOT steel detail has only one layer of #11 bars in the top of the pier cap for the main tension tie, T1, as opposed to two layers in the strut and tie design - #11 and #10 bars. Also, the TxDOT detail uses 3 layers of #6 bars for the horizontal stirrups as opposed to 6 layers of #9 bars for the strut and tie design.

To judge whether the difference in the two steel reinforcing details represents an understrength of the TxDOT design or the conservatism of the strut and tie method, a strut and tie analysis was made of the typical TxDOT design shown in Figure 4.29. The analysis used no compression steel, the full yield capacity of the of the bars in the top layer of the pier cap, and the column width as the strut width (the same parameters used for analysis 1-1 of Table 4.3). Using these parameters the strut and tie analysis predicts a capacity of the TxDOT design as $P_n = 1,747$ kips which was less than the $P_n = 2,130$ kips used in the strut and tie design. Member forces and the inclination angle from the strut and tie analysis are shown in Table 4.9. However, for the strut and tie analysis of the tested specimens using the same assumptions (no C_s and full f_y), the *average* tested specimen capacity was 27% greater than the strength from the strut and tie analysis ($395/311 = 1.27$). Thus, the true *average* capacity of the full size detail is probably closer to $1.27 \cdot 1,747 = 2,220$ kips. If the *minimum* tested strength for test specimen A is used, the tested pier capacity is only 18% larger than that predicted by the strut and tie analysis ($365/311$). Thus, the *least* capacity



PROFILE VIEW OF PIER CAP



SECTION A-A - BARS A AND B #11

Figure 4.29 Typical Steel Reinforcing Pattern Used by TxDOT

of the full size pier is likely $1.18 \times 1,747 = 2,070$ kips which is slightly less than the required design strength $P_n = 2,130$ kips. This indicates that existing piers may have a factor of safety less than expected for bearing loads.

The above strut and tie analysis of a full size pier, and extrapolation of analysis results based on tested scale specimen capacity may be slightly inaccurate because there are several differences between the test specimens and full size piers. For the tested specimens, $f'_c = 4,000$ psi as compared to 3,600 psi for the full size piers. The different concrete strength will change the concrete tensile strength, which may result in a different strut inclination. A different strut inclination will change the contribution to the pier cap strength of other shear carrying mechanisms such as aggregate interlock. The different concrete strength will also affect the development length of the reinforcing. For a larger concrete strength, the required anchorage length is smaller. Finally, for the scale specimens, the column width was the same as the pier cap width. For the full size pier

caps, the column width is less than the pier cap width. This reduced column size will increase the concentration of stress on the end of the column, resulting in earlier spalling.

A determination of the adequacy of existing full size pier caps is difficult, and can only be made on a case by case basis considering both the load and geometry. As a further consideration of the adequacy of current designs, the performance of existing piers can be considered. To the authors knowledge, details as shown in Figure 4.28 have performed adequately. However, it is difficult to quantify the loads that existing piers have actually sustained. The calculated bearing loads are typically conservative, so the smaller magnitude of true bearing loads must be considered if the performance of existing pier caps is to be projected to new designs. Improved analysis techniques to more accurately calculate bearing loads are currently being developed in a related study concerning the behavior of the steel bent to pier cap connection.

To give criteria for evaluating the adequacy of pier caps from field inspections, cracking patterns on test specimens A at a service level are considered. For the A series specimens, the average service load is $395 \text{ kips}/1.6 = 245 \text{ kips}$. At this service load, flexure/shear cracks extended about half way across the depth of the pier cap. Under a service load, cracks on full size piers should have a maximum size of 0.016" based on crack sizes observed on the scale specimens. Signs of concrete distress on the pier cap that would indicate overloads on the bridge or pier cap inadequacy are:

1. Significant crushing at the pier/cap column interface. If spalling of the concrete occurs, the pier cap has seen severe loadings.
2. Splitting cracks on the top of the pier indicating bond failure for the straight bars in the top layer of the pier cap.

Table 4.9 Strut and Tie Capacity and Member Forces for a Typical TxDOT Steel Detail (Figure 4.29)

Strut and tie analysis of existing TxDOT detail		
Capacity, P		1,747
$\theta 1$		75.0
Compression in Steel		0
Forces (kips)	T1	468
	T2 horizontal	249
	T2 vertical	66.7
	C1	1,808
	C2	940
	C3	904
	C4	468
	C5	1,747
Centroid		11.1"

3. Maximum crack openings on the pier significantly larger than 1/16".
4. Cracks extending across the full depth of the pier cap that have a significant width for the full length.

If any of the patterns of concrete distress listed above are observed, rehabilitation of the pier cap may be desirable.

Because there is some uncertainty as to the adequacy of the current steel reinforcing pattern, the strut and tie method is suggested for future designs. The strut and tie method is superior to conventional design techniques that could be used for the pier cap. The strut and tie method allows a logical design of reinforcing, and is a conservative design technique. To improve the efficiency of the strut and tie method, further research should be conducted into the addition of a concrete shear strength term to the strut and tie capacity.

CHAPTER 5

SUMMARY AND CONCLUSIONS

5.1 OBJECTIVES AND SCOPE

The objective of this research was to determine the strength and behavior of typical TxDOT bridge pier caps under compression loads. The pier caps typically used by TxDOT have a geometry whose design and behavior is not explicitly covered in current code procedures. Since no formal design procedure currently exists for determining the required amount and distribution of reinforcing steel in a pier cap, this research also had the purpose of providing design guidelines for the pier cap. To investigate the behavior of the pier caps, six test specimens were constructed at a 30% scale. Five different reinforcing steel patterns were used in the six specimens to examine the contributions of different reinforcing types to the pier cap strength.

5.2 OBSERVED BEHAVIOR

Eleven static load tests were conducted to failure on the six pier caps. For all specimens, load on the pier cap was primarily carried by the action of a tied arch which transferred load from the base plates into the column. Concrete distress associated with the arch action included flexural/shear and shear cracks on the faces of the pier cap which limited the size of the compression arch. Additionally, flexural cracks were seen on the top of the pier cap indicating a state of pure tension there. As load was applied to a specimen, flexure, flexure/shear, and shear cracks formed. As loading continued, crushing was eventually observed at the pier cap/column interface. The crushing at the interface limited the area at the base of the arch, so the compression arch had to rotate further into the interior of the pier for the specimen to carry additional load. The new orientation of the arch required additional tension in the reinforcement at the top layer of the pier cap to maintain equilibrium. Thus, if a specimen had sufficient reinforcement in the top layer of the pier cap, additional load could be carried. However, if the development of tension force was limited, failure of the pier cap coincided with the initiation of crushing at the cap/column juncture. Overall, specimens that had a greater quantity of horizontal reinforcing steel and adequate development of horizontal reinforcing had a greater capacity.

To investigate the necessity of the continuous steel loop around the perimeter of the pier cap (bar T) a specimen was constructed with only straight bars in the top layer of the pier cap.

Three problems arose when the continuous loop was not included in the top layer of the pier cap reinforcement:

1. Shear cracks on the face of the pier opened extremely wide because there was no reinforcement at the top of the pier to limit their growth.
2. Bond distress was seen for the straight bars in the top layer of the pier cap. The removal of the continuous loop left only straight bar anchorage as a means of developing the required force in the steel. Since development lengths for the straight bars were extremely short, the tension force at the top of the pier was limited, reducing the pier cap strength.
3. The base plate punched further into the top of the pier. Without the continuous loop, concrete at the end of the pier cap was not confined and additional punching could occur.

Punching of the base plates into the top of the pier cap was seen to some extent for all specimens. However, punching of the base plates was not the cause of failure because most of the punching occurred after the failure load had been reached. The bearing capacity of the pier cap was reduced by the formation of a flexural crack at the interior edge of the base plate. The formation of the flexural crack removed the confinement provided by the concrete in the interior of the pier. Bearing capacity of the pier cap was increased by the confinement provided by the continuous loop around the end of the pier cap.

5.3 COMPARISON OF DESIGN METHODS

Three design methods were used to analyze the strength of the pier caps tested:

1. AASHTO (1992) Corbel Provisions.
2. ACI 318-89 Deep Beam Provisions.
3. Strut and Tie Method.

The corbel and deep beam provisions were entirely inadequate to predict the capacity of the pier cap because they only consider concrete capacity in shear. Testing showed that the pier cap resisted loads through a tied arch, which is a much stronger load carrying mechanism than concrete in shear. The strut and tie models used were much more accurate than conventional design methods in predicting the capacity of the pier caps because they model the compression arch action observed during testing. The strut and tie method is suggested for design because strut and tie analyses gave the best correlation with test results, modelled true behavior, and were conservative. The strut and

tie method allows a logical design of reinforcing steel for a given load and specimen geometry, and is a conservative design method. To detail the use of the strut and tie method, a design example using a proposed strut and tie model was presented. Since the design calculations are lengthy, a simplified procedure to predict the pier cap strength should be developed. Also, recommendations for evaluating existing pier caps through field inspection are given.

5.4 AREAS FOR ADDITIONAL RESEARCH

Several possible areas of further research were identified during this study. The strut and tie models presented predicted strengths that were 20 to 50 percent less than the tested specimen capacities. Closer correlation to the tested pier cap strength was achieved by adding a concrete shear strength term to the strength predicted by the strut and tie model. Additional research should be conducted to refine the strut and tie model by adding a concrete shear strength term. Second, development of the strut and tie theory to allow consideration of compression steel is desirable. Consideration of compression steel would more accurately model specimen behavior, and would improve the accuracy and efficiency of strut and tie designs. Third, the development length required for U shaped, continuous stirrups is not detailed in any code provisions. The U shape allows much shorter anchorage lengths than straight bars. The continuous U stirrup will behave differently than a standard 180° hook as both ends of the continuous stirrup are being loaded. Finally, further study to determine the bearing capacity of the concrete at the top of the pier cap is desired because bearing capacity is limiting the design of the connection between the pier cap and steel bent. Since there is substantial reinforcement in the top layer of the pier cap, increased bearing capacity of the concrete is expected.

APPENDIX A

TENSILE TESTS OF REBAR

The tensile tests on the bars were performed using a loading controlled test machine. Load was controlled using a plot of load against strain, with the strain measured using a Satec Systems Model T-6M Extensometer with an eight inch gage length. An example graph of the rebar loading process is shown in Figure A.1. Bars were loaded at a constant rate up to the yield point of the bars. The initial rate of load application was approximately 2,000 pounds per minute for the #3 bars, and about 10,000 pounds per minute for the #6 bars. After the bars yielded, a plastic deformation of approximately twice the yield strain was applied. The test machine was then turned off, allowing the rebar to unload. After five minutes, the stress in the bar was recorded as the static yield stress, f_{y1} . The bars were loaded two more times, applying a plastic strain of approximately twice the yield strain with each load step. The average static yield strain for the bar was the average of the three static yield points, f_{y1} , f_{y2} , and f_{y3} . For each lot of bars, two different tensile tests were run.

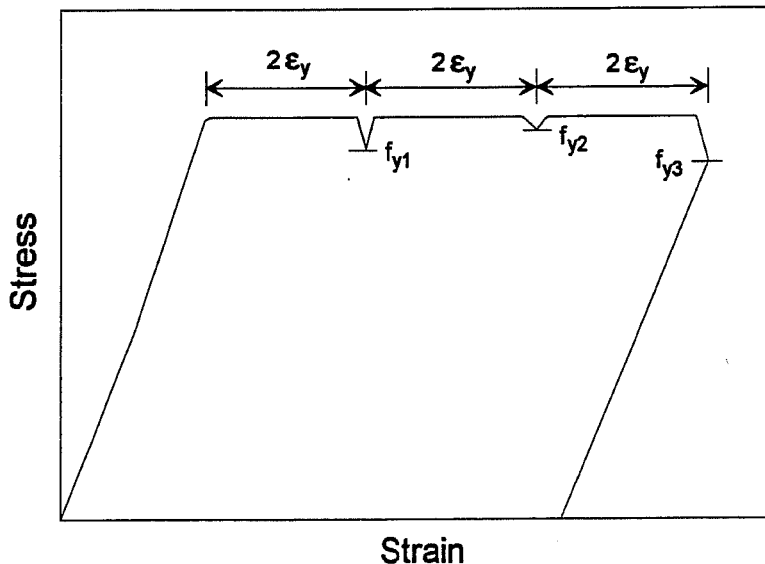


Figure A.1 Typical Stress - Strain Curve for a Tensile Test of Rebar

APPENDIX B

LOAD - DISPLACEMENT GRAPHS

This appendix contains plots of load versus displacement on linear pots 1 through 4 for all tests. The layout of the linear pots is shown in Figure B.1. Load is the resultant load at the tested end of the pier cap, and is a static load reading. Deflections have been shifted as explained in Chapter 3 to remove the scatter in deflections under small loads (loads less than 50 kips). The unloading curve for the specimens is not included.

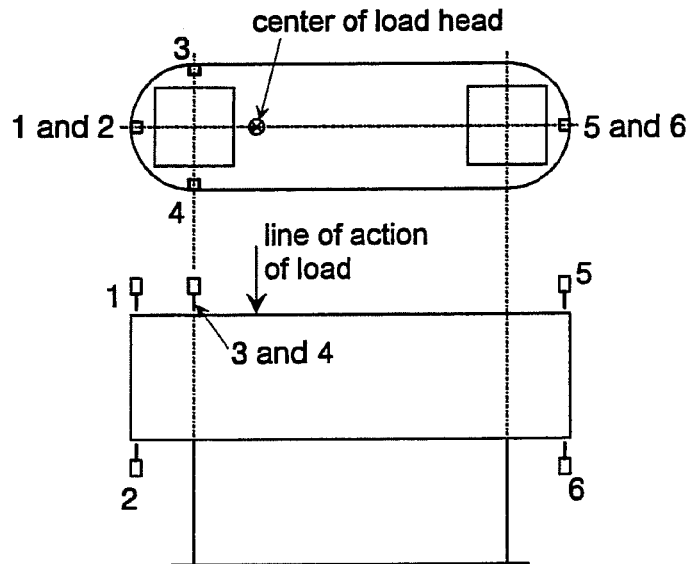


Figure B.1 Location of Linear Pots

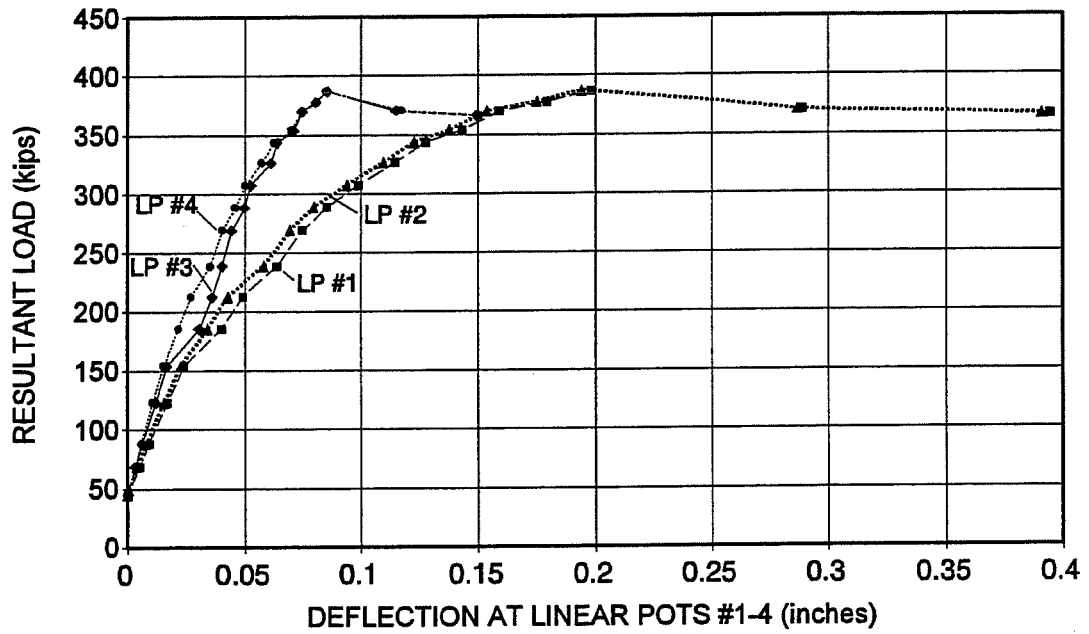


Figure B.2 Resultant Load vs. Deflection at Linear Pots 1 through 4 for Pier A1-1

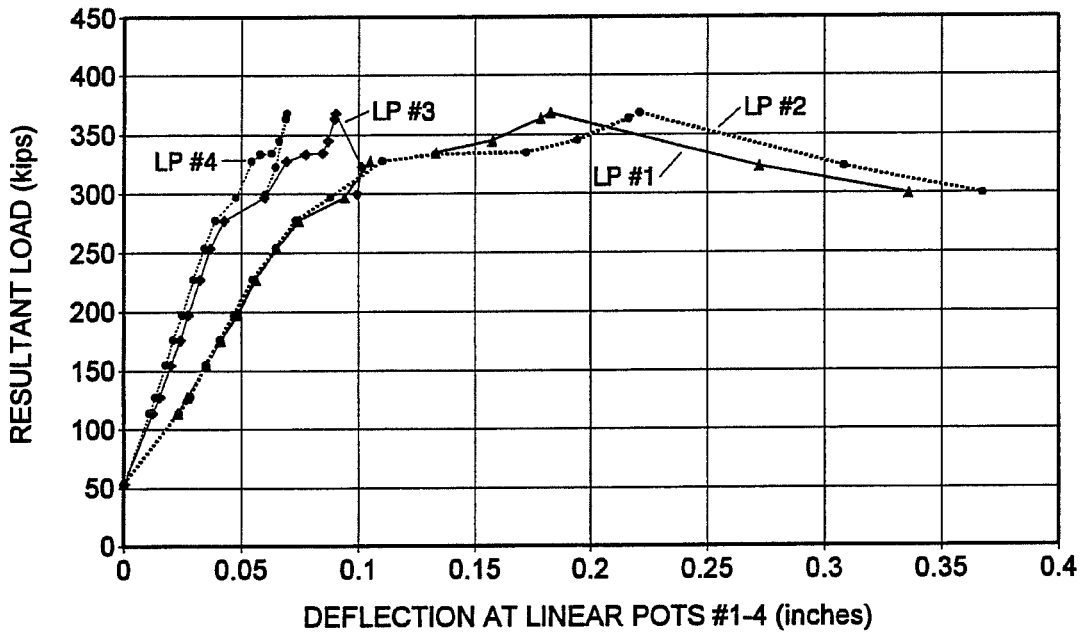


Figure B.3 Resultant Load vs. Deflection at Linear Pots 1 through 4 for Pier A2-2

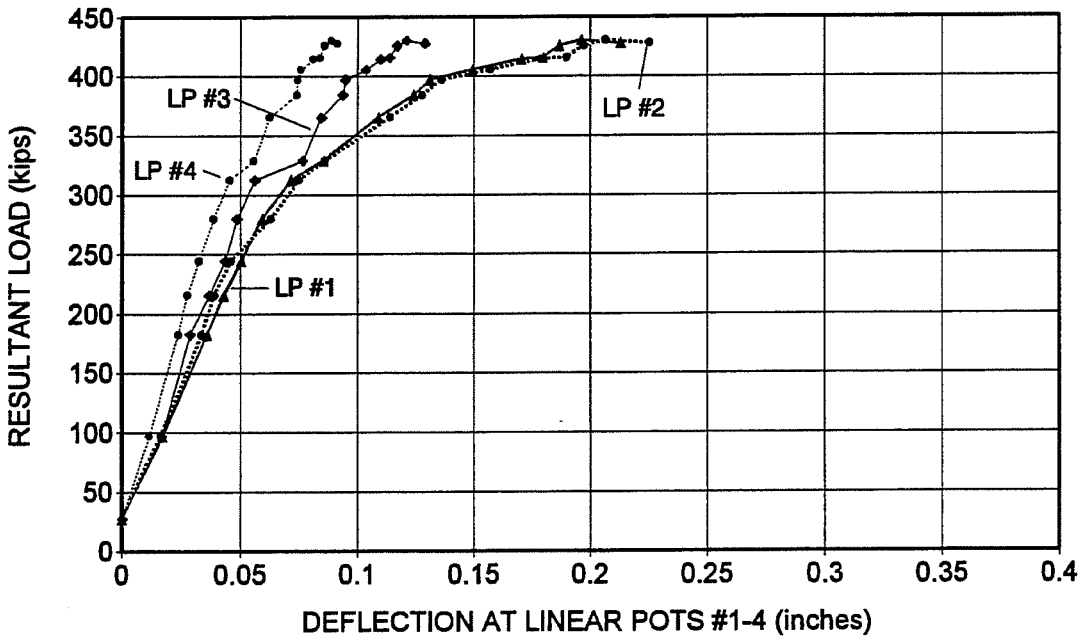


Figure B.4 Resultant Load vs. Deflection at Linear Pots 1 through 4 for Pier A2-3

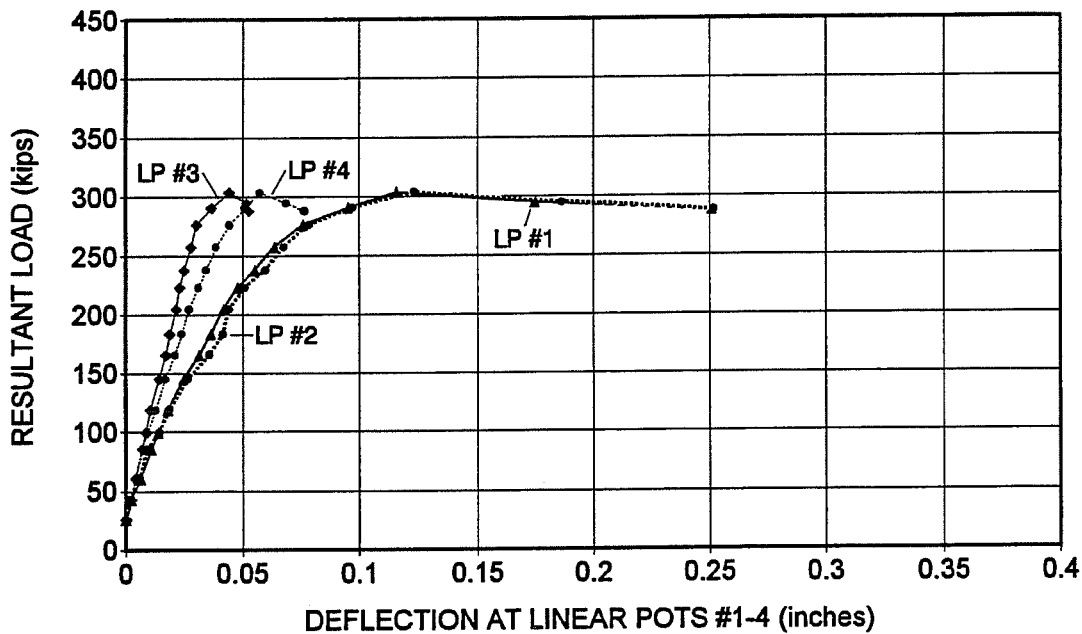


Figure B.5 Resultant Load vs. Deflection at Linear Pots 1 through 4 for Pier B-1

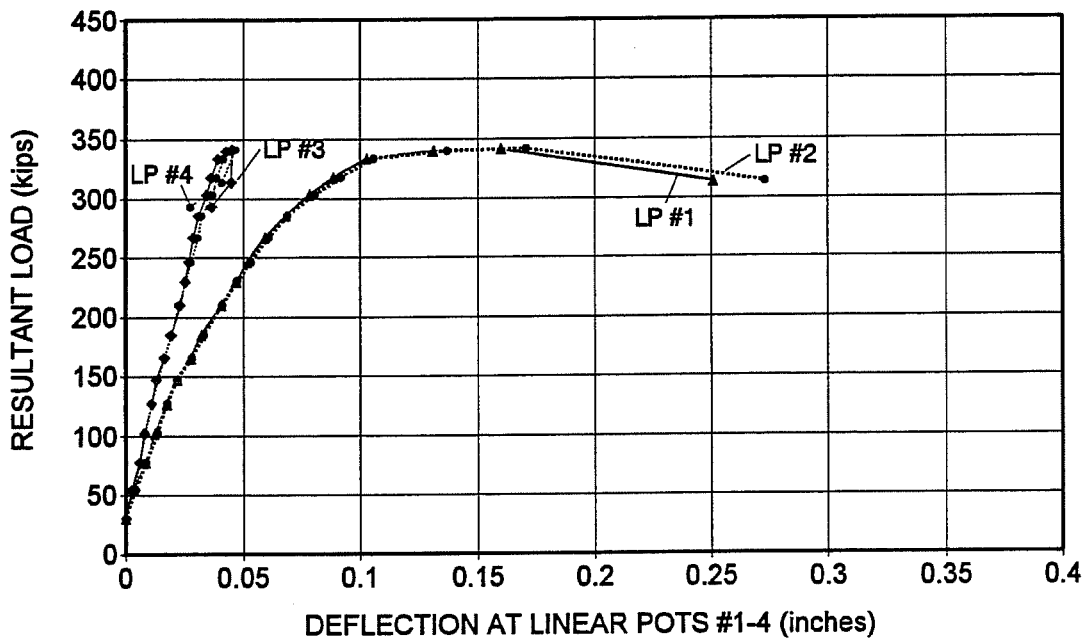


Figure B.6 Resultant Load vs. Deflection at Linear Pots 1 through 4 for Pier B-2

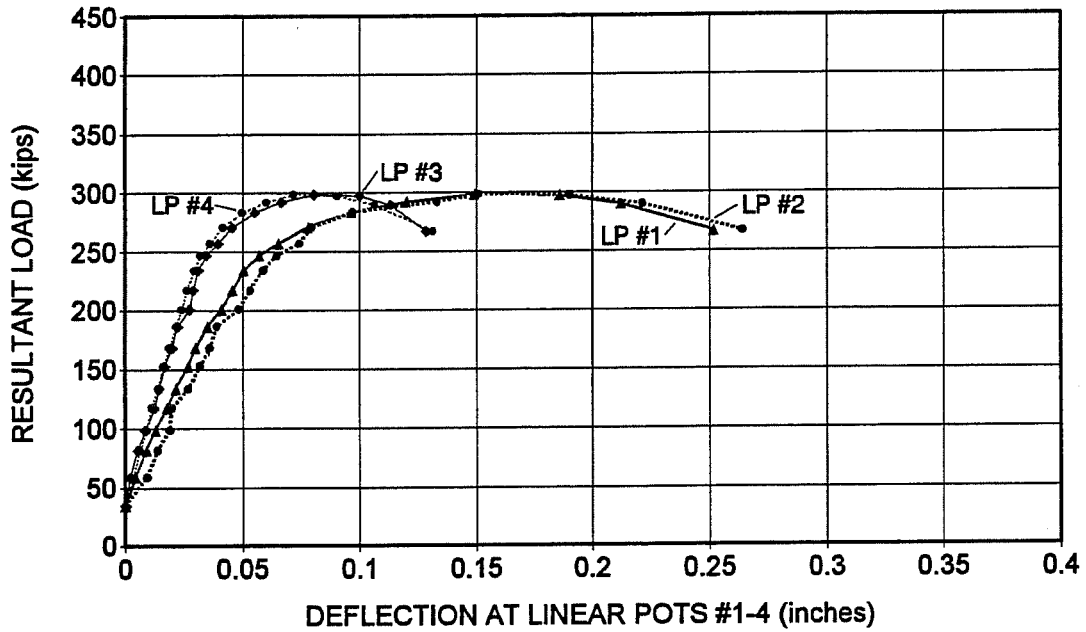


Figure B.7 Resultant Load vs. Deflection at Linear Pots 1 through 4 for Pier C-1

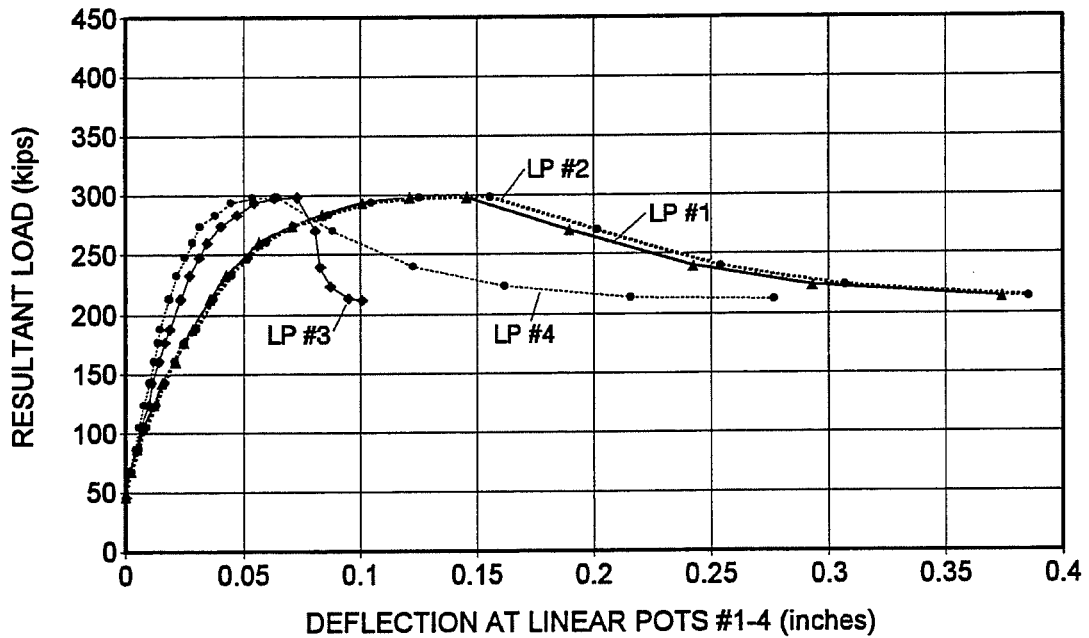


Figure B.8 Resultant Load vs. Deflection at Linear Pots 1 through 4 for Pier C-2

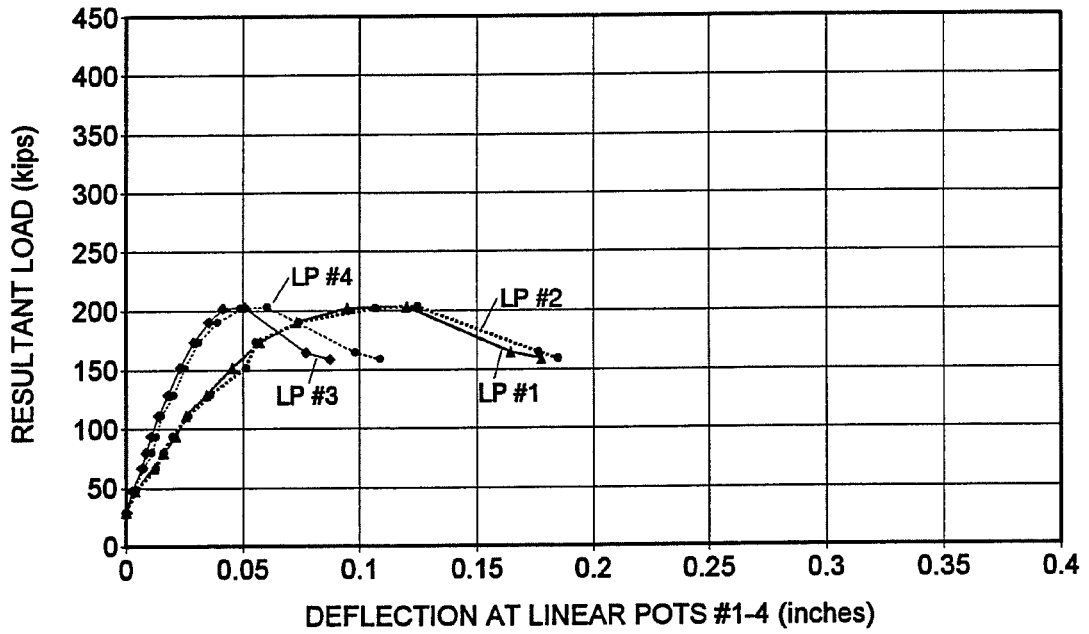


Figure B.9 Resultant Load vs. Deflection at Linear Pots 1 through 4 for Pier D-1

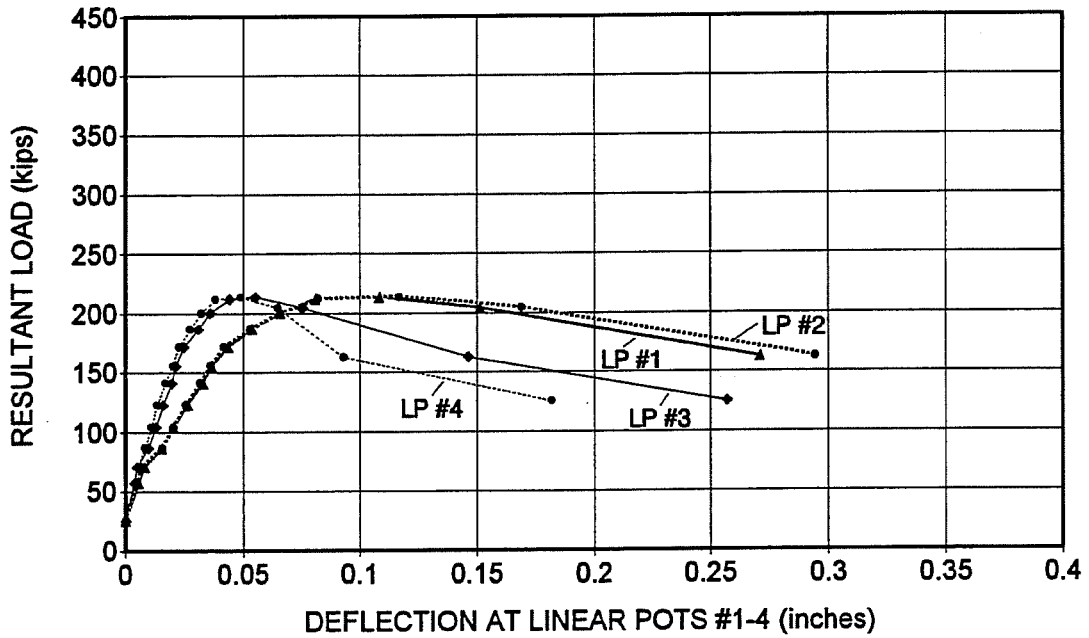


Figure B.10 Resultant Load vs. Deflection at Linear Pots 1 through 4 for Pier D-2

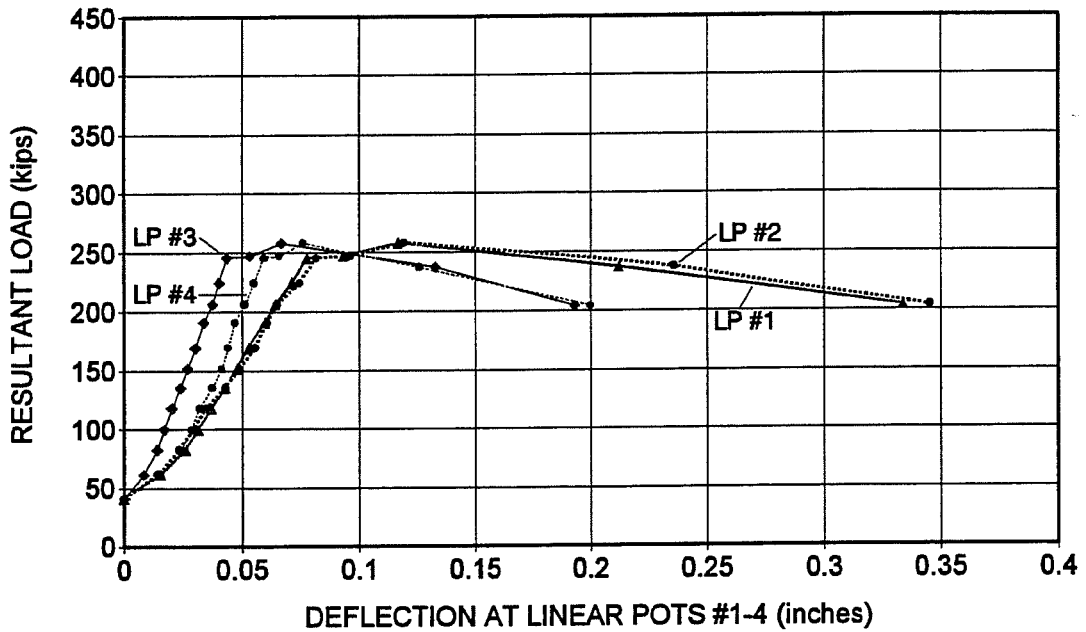


Figure B.11 Resultant Load vs. Deflection at Linear Pots 1 through 4 for Pier E-1

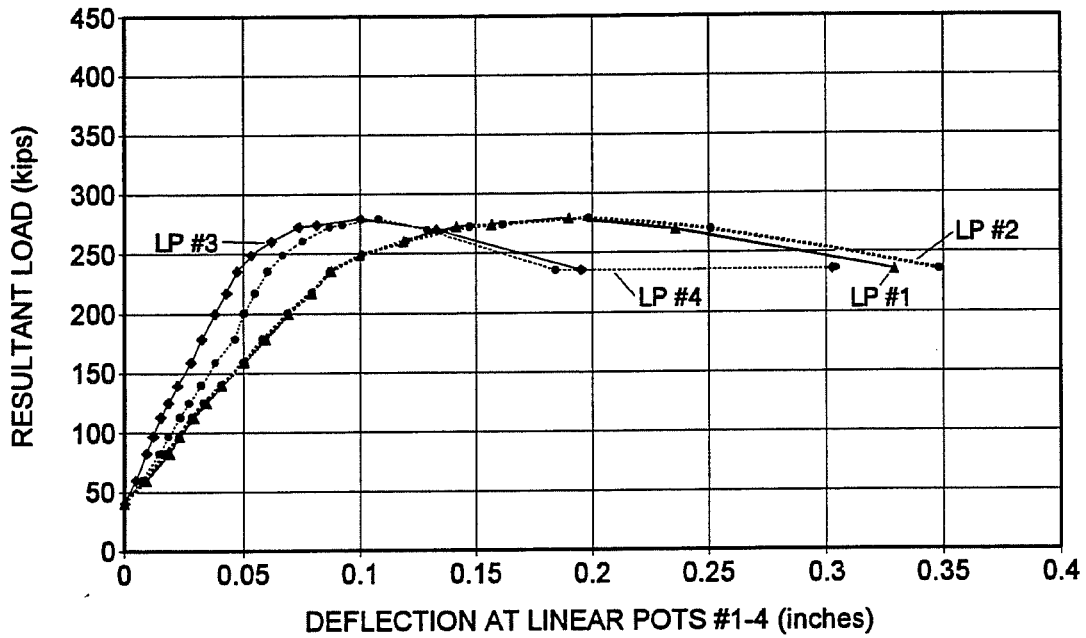


Figure B.12 Resultant Load vs. Deflection at Linear Pots 1 through 4 for Pier E-2

APPENDIX C

PHOTOS OF THE FAILED SPECIMENS

This appendix contains photos of the specimens after failure. Photos show the distribution of cracking on both faces of a specimen, crushing at the cap/column interface, and punching of the base plates. Numbers marked on the specimen are the total load in kips applied to the spreader beam, and not the resultant load at the tested end of the pier cap. The load marked on the specimen is placed at the point where a crack had propagated at that point. Loads marked on the specimens are slightly larger than the static load, as the static load was not reached until crack mapping had been completed. Thus, the loads marked on the specimen are approximately 5 to 10 kips larger than the total static load applied to the spreader beam.

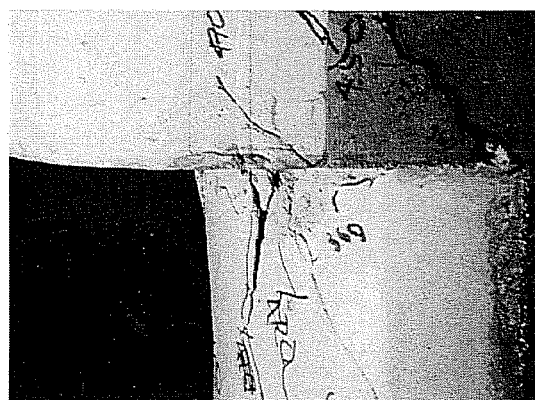
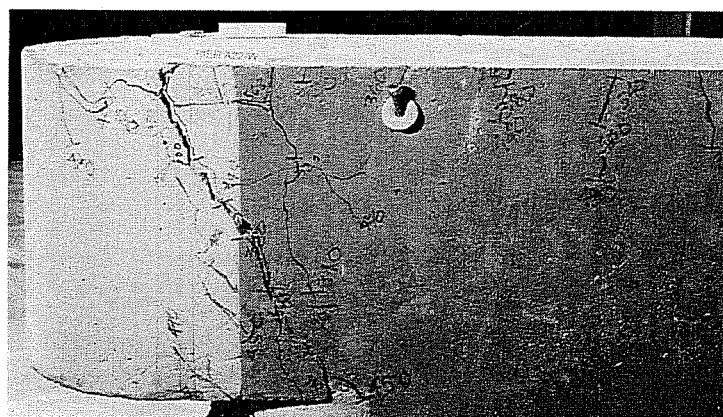
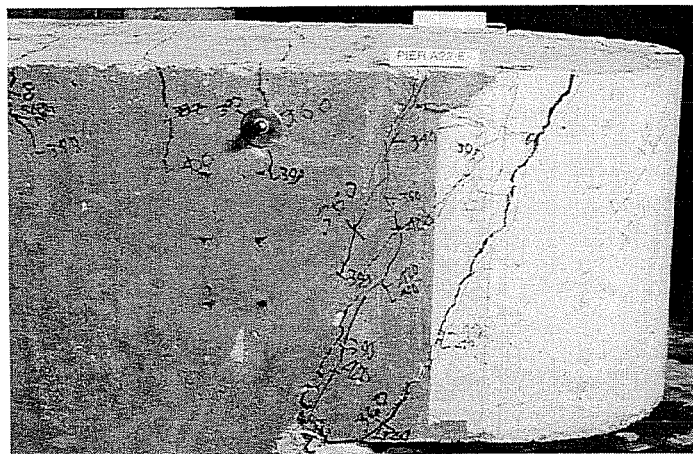


Figure C.2 Damage to Pier A2-2 After Failure

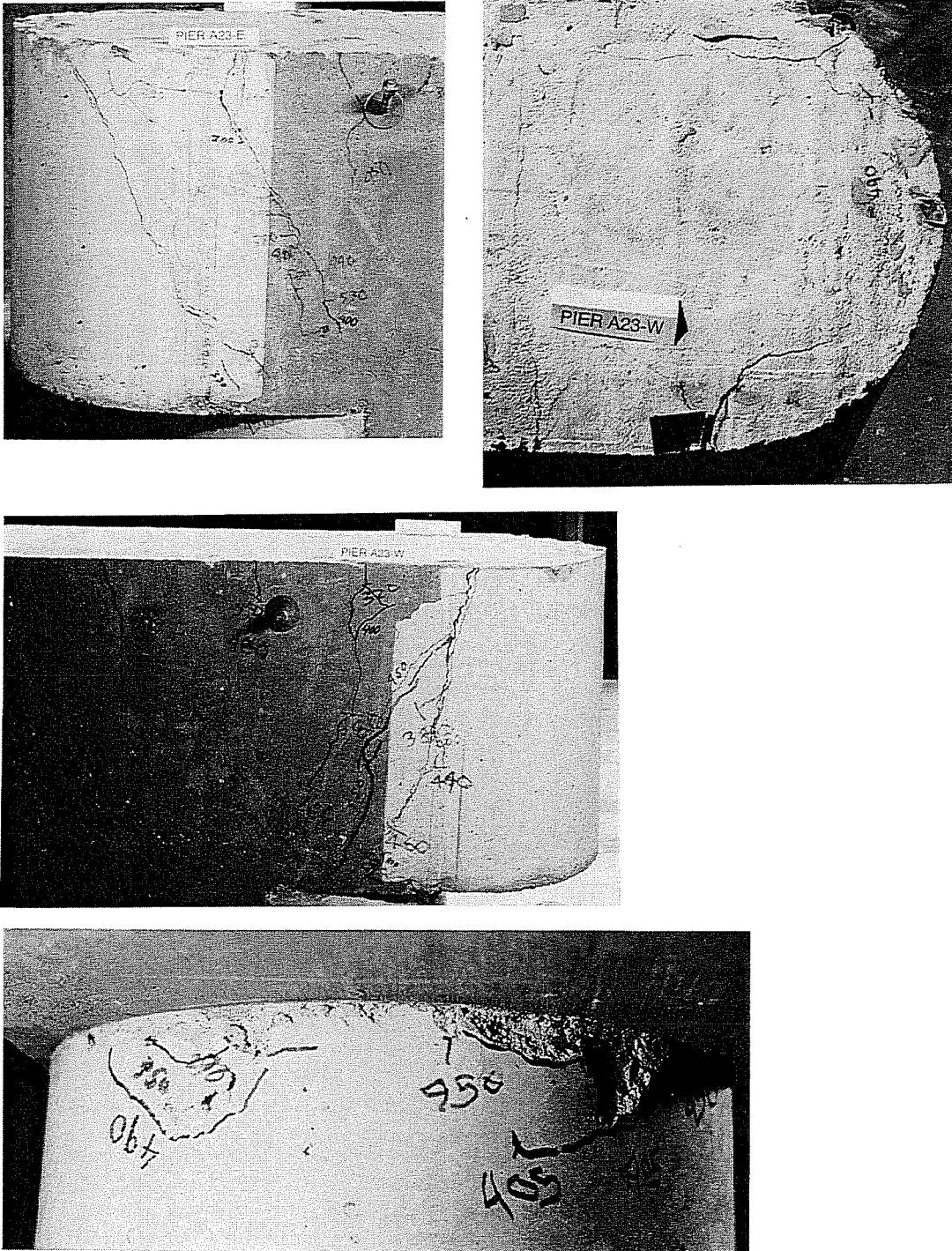


Figure C3 Damage to Pier A2-3 After Failure

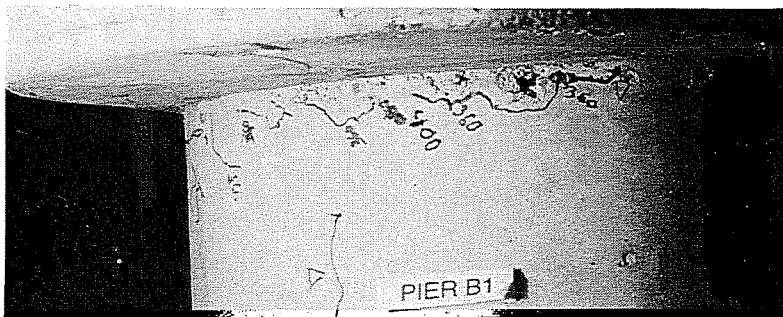
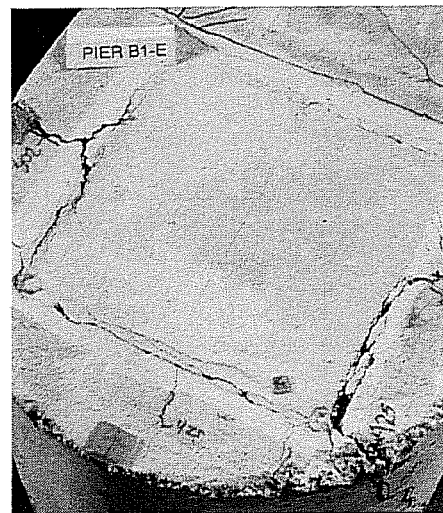
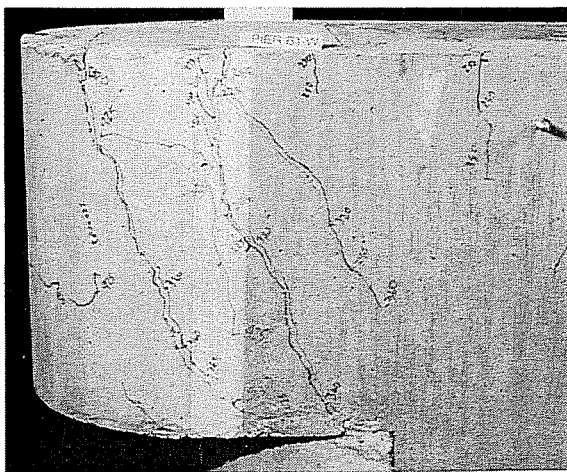
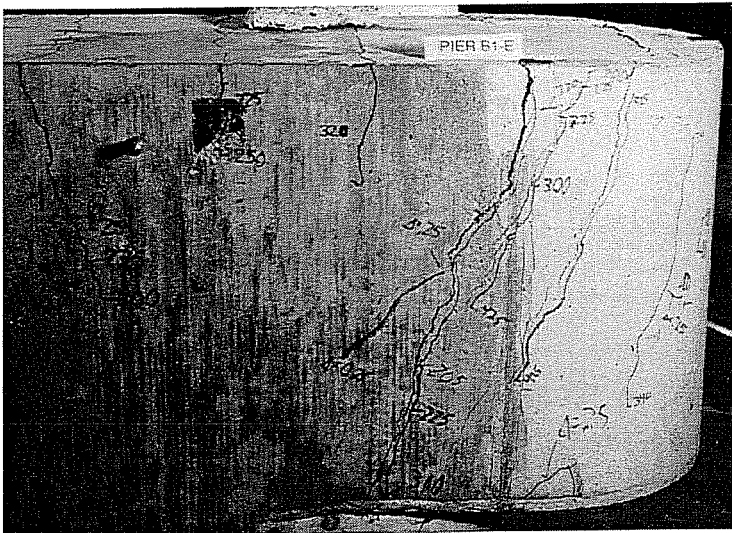


Figure C.4 Damage to Pier B-1 After Failure

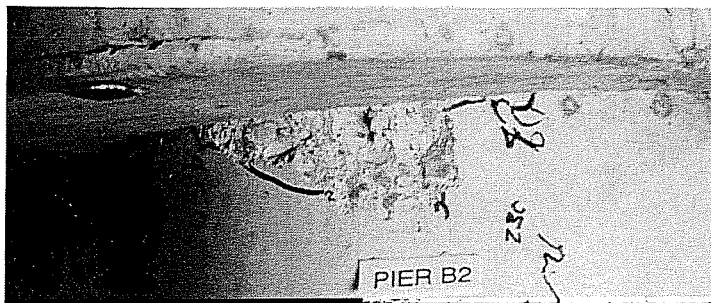
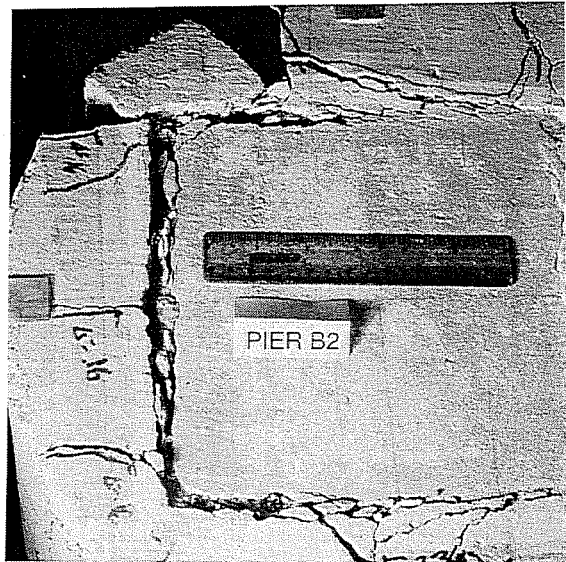
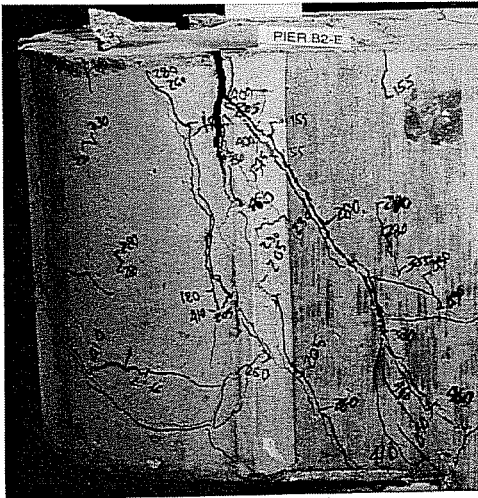
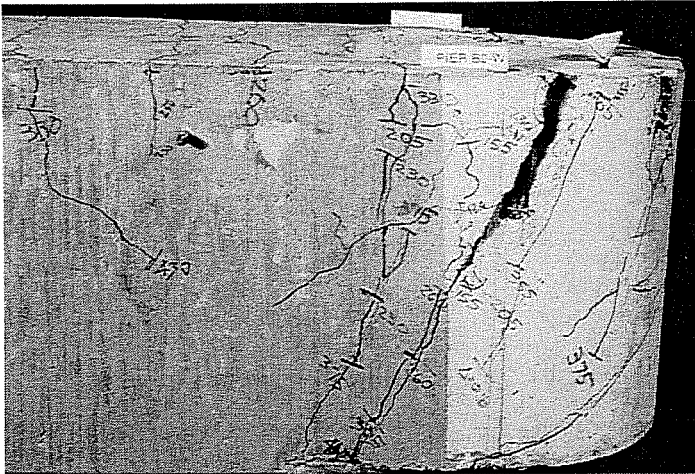


Figure C.5 Damage to Pier B-2 After Failure

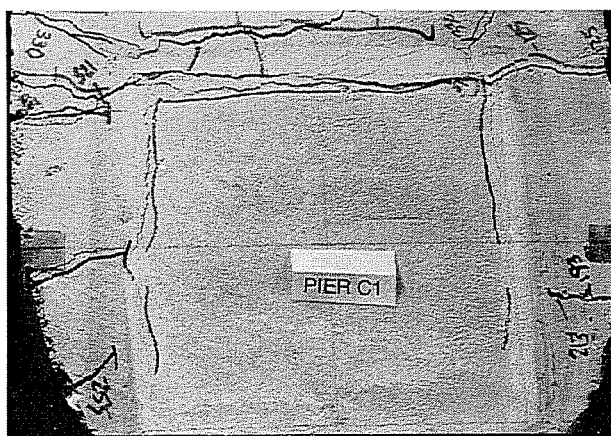
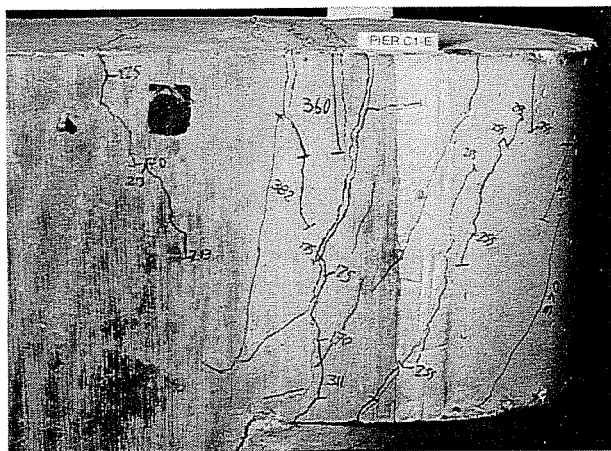
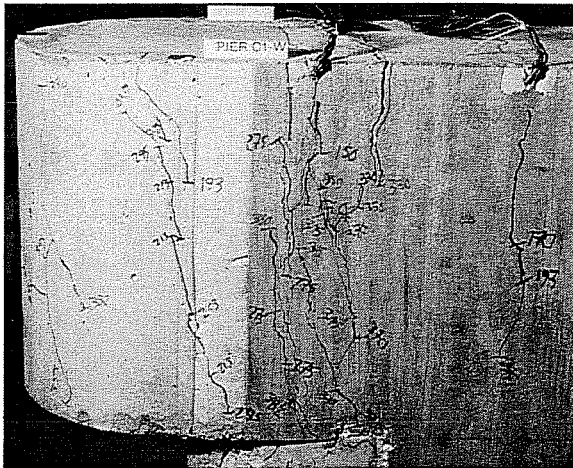


Figure C.6 Damage to Pier C-1 After Failure

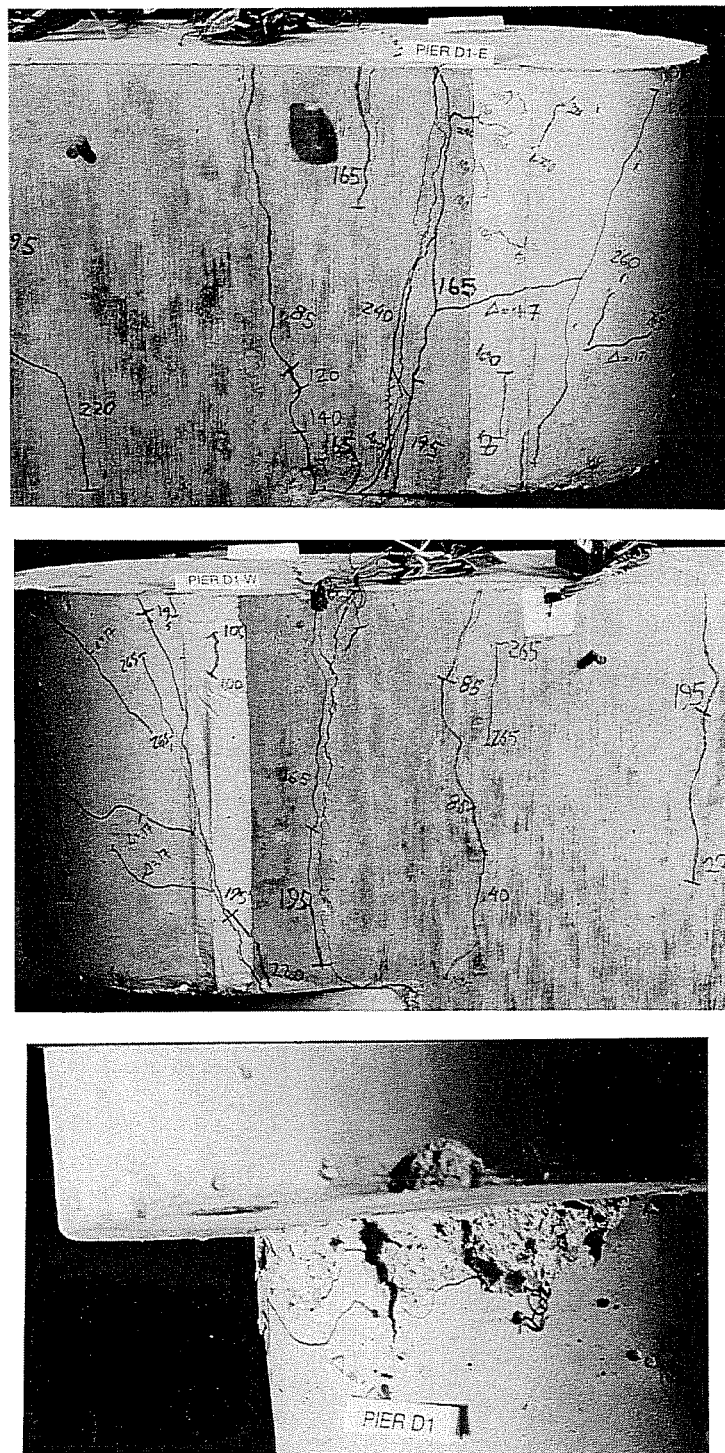


Figure C.8 Damage to Pier D-1 After Failure

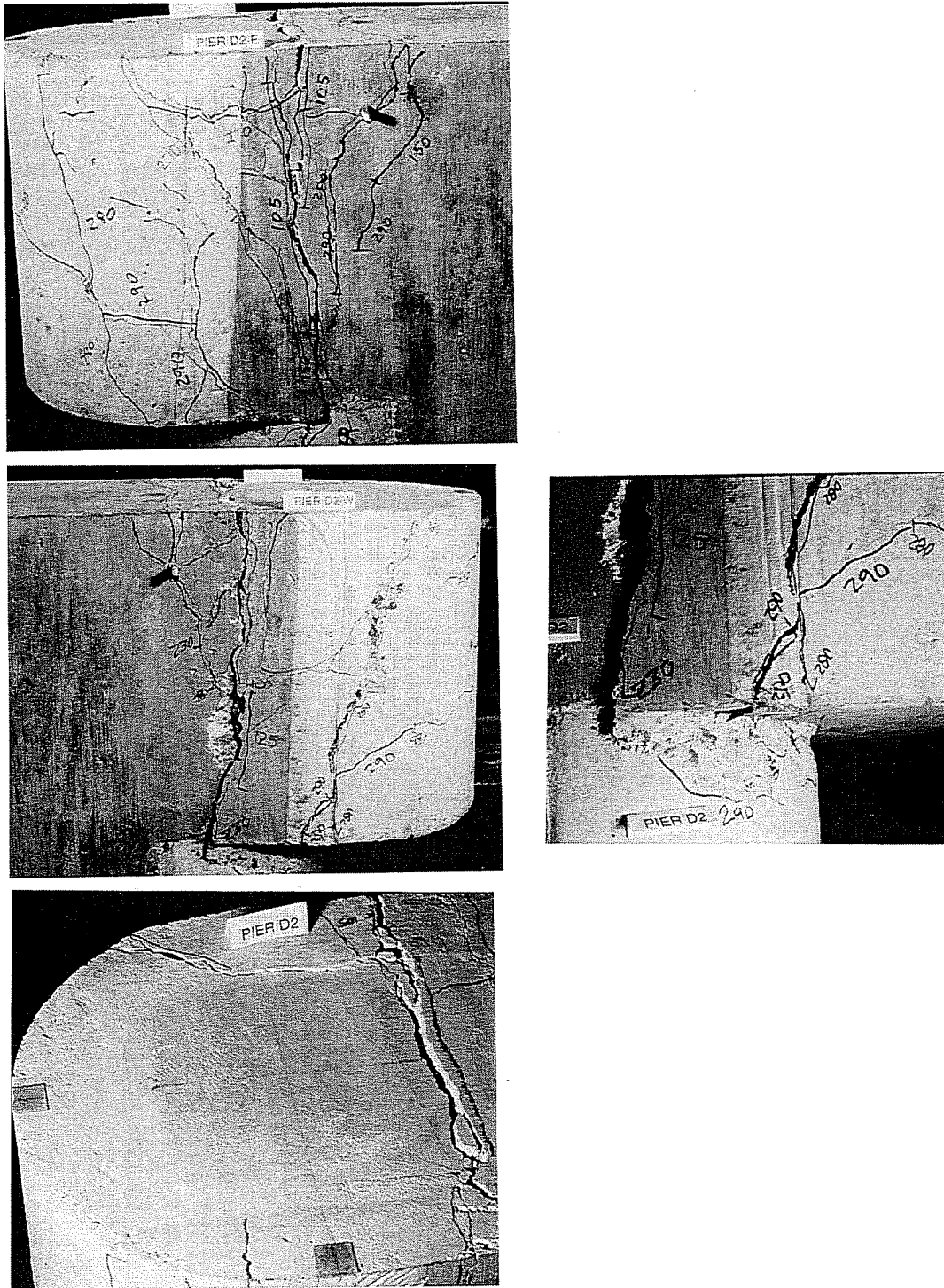


Figure C.9 Damage to Pier D-2 After Failure

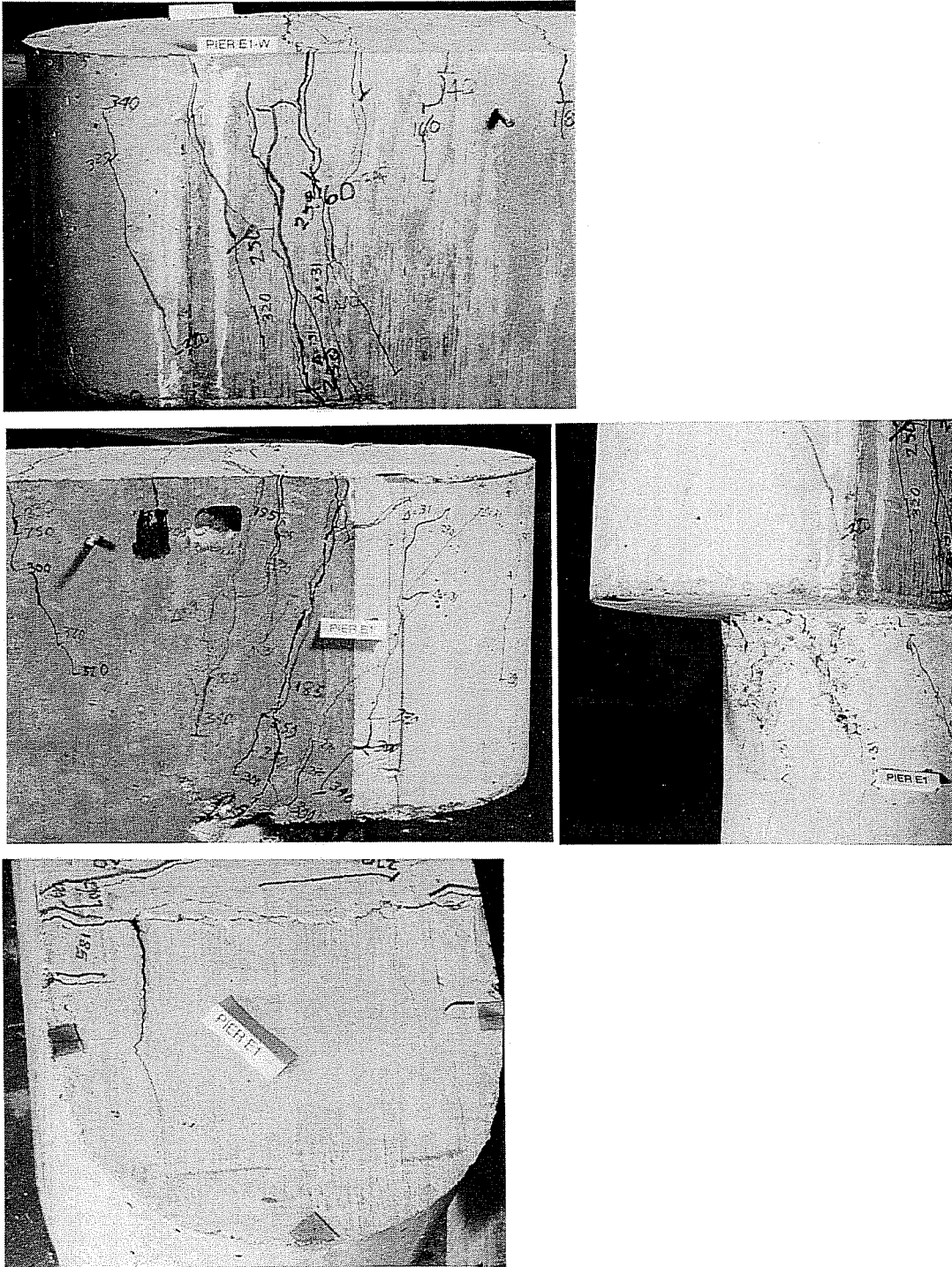


Figure C.10 Damage to Pier E-1 After Failure

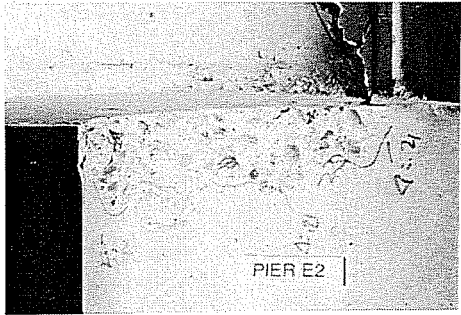
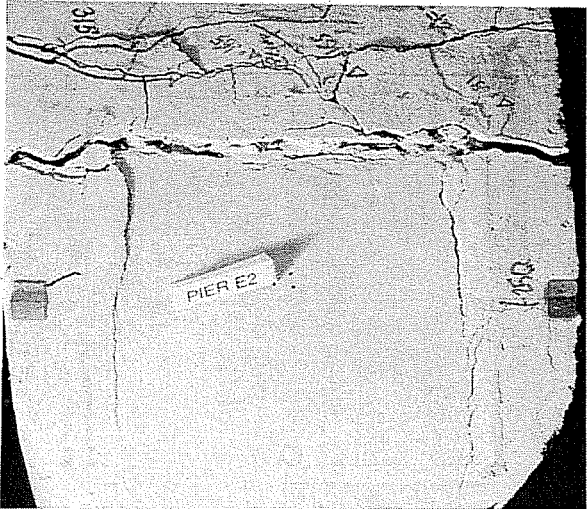
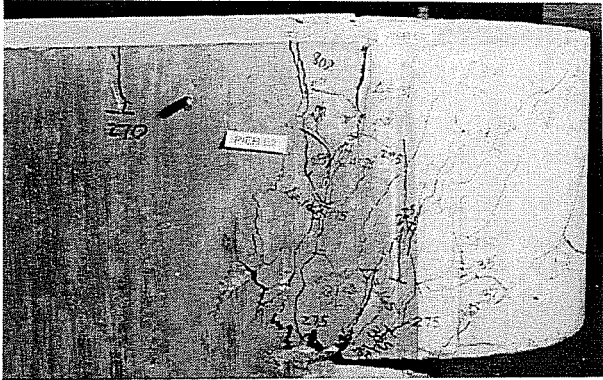
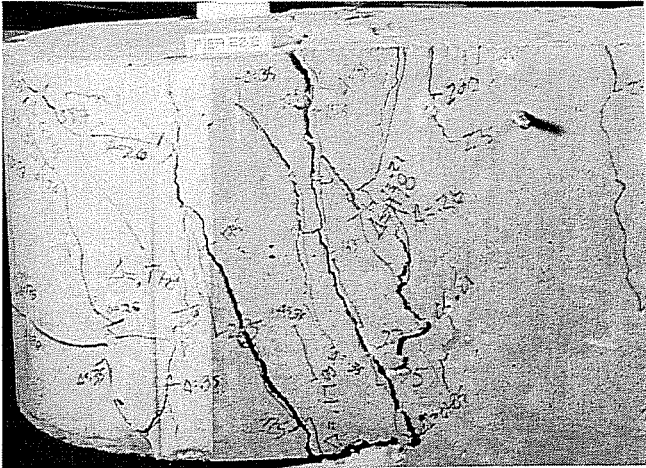


Figure C.11 Damage to Pier E-2 After Failure

APPENDIX D
LOAD- STRAIN GRAPHS

This appendix contains plots of resultant load versus strain for tests on Specimens C and D. The strain gages are located in the top layer of the pier cap on #3 bars as shown in Figure D1. For tests Pier C1 and D1, the strain gages are at the tested end of the specimen, while for tests Pier C2 and D2 the gages are on the end of the specimen subject the smaller load. The unloading curve for the strain gages is included to show the final strain in the bars. For both specimens, the yield strain, 1630 microstrains, is calculated as the experimentally obtained yield stress divided by the modulus of elasticity (47.4 ksi/ 29,000 ksi).

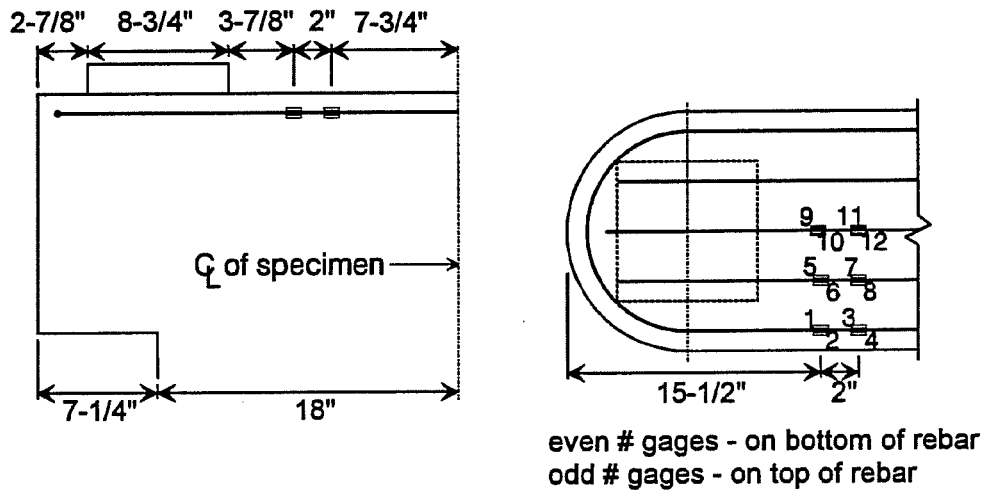


Figure D.1 Location of Strain Gages

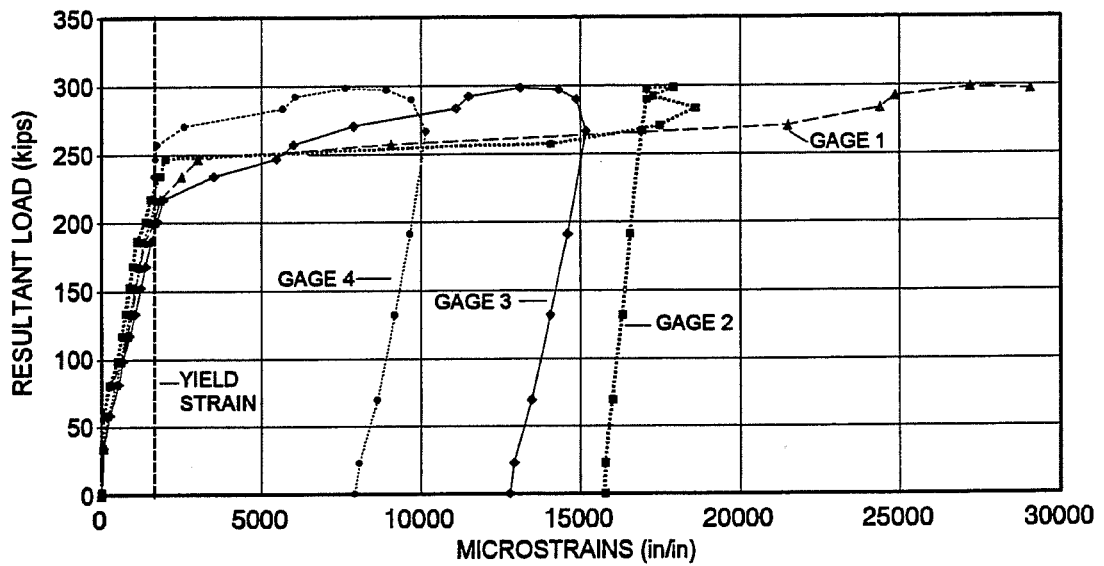


Figure D.2 Resultant Load vs. Strain in Gages 1 through 4 for Pier C-1

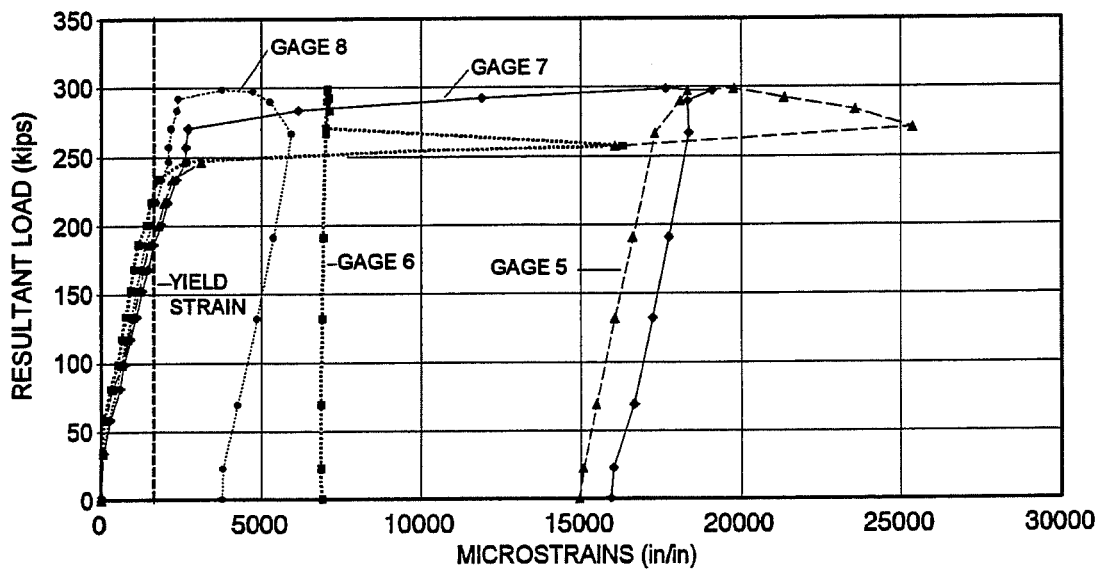


Figure D.3 Resultant Load vs. Strain in Gages 5 through 8 for Pier C-1

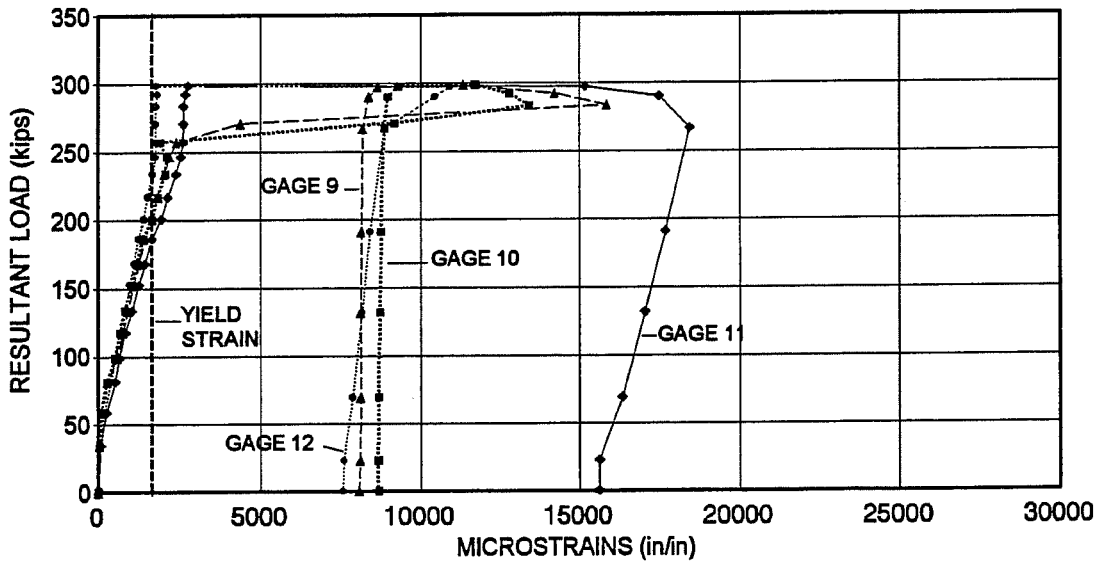


Figure D.4 Resultant Load vs. Strain in Gages 9 through 12 for Pier C-1

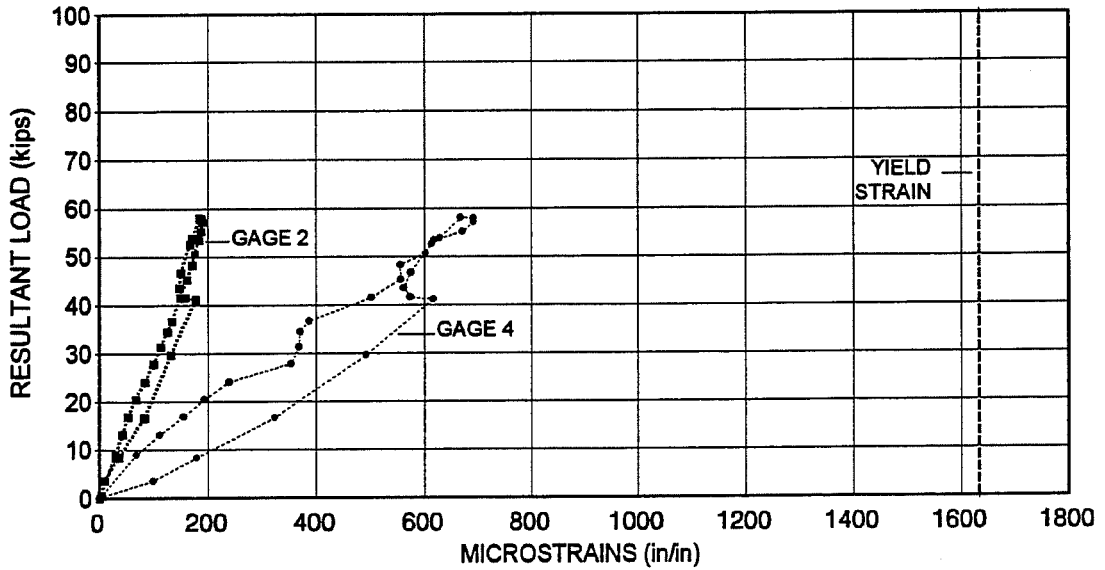


Figure D.5 Resultant Load vs. Strain in Gages 2 and 4 for Pier C-2

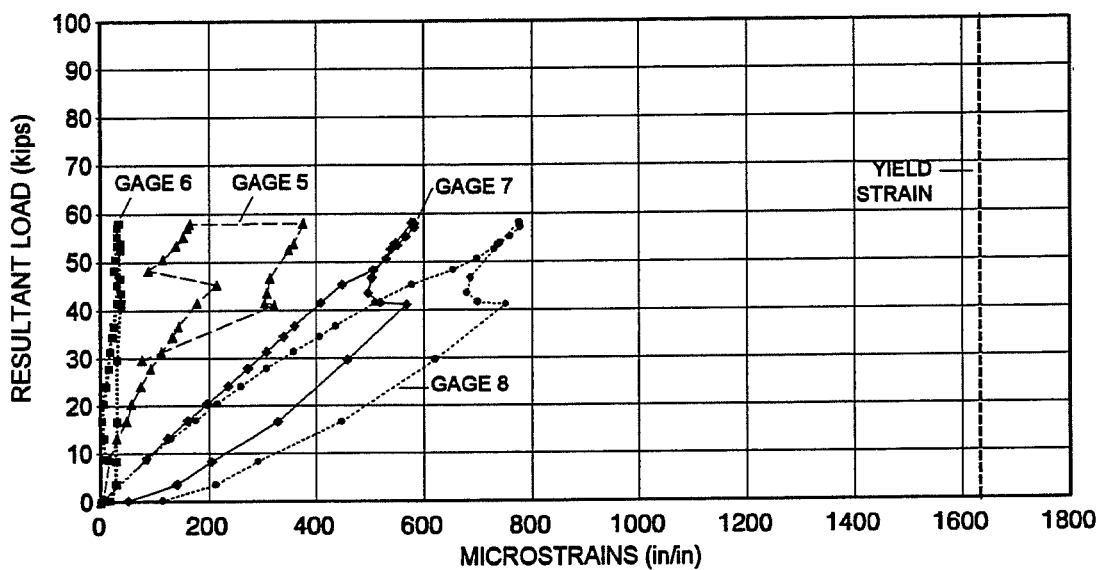


Figure D.6 Resultant Load vs. Strain in Gages 5 through 8 for Pier C-2

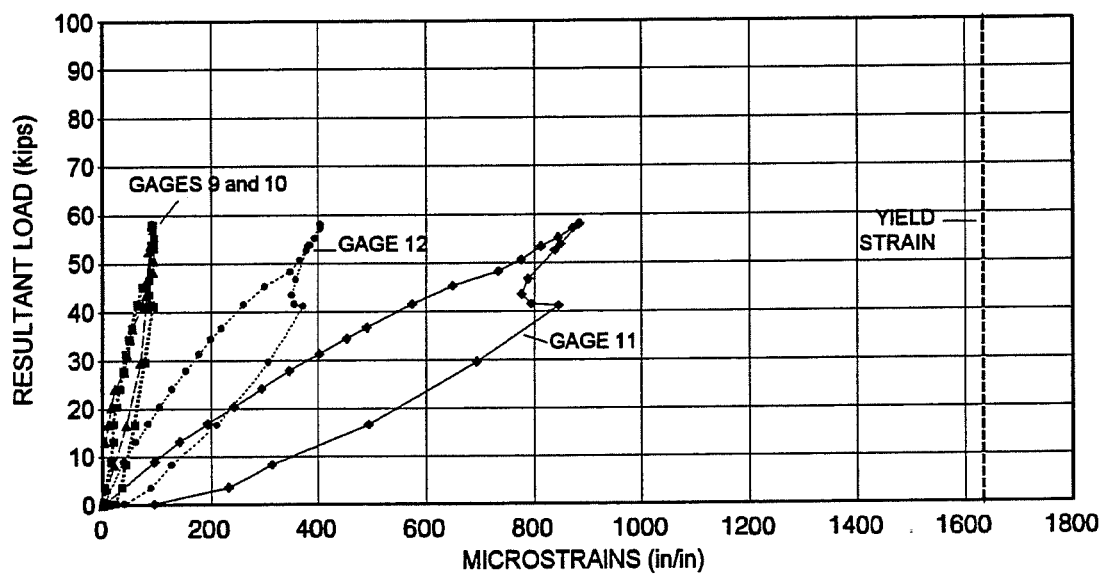


Figure D.7 Resultant Load vs. Strain in Gages 9 through 12 for Pier C-2

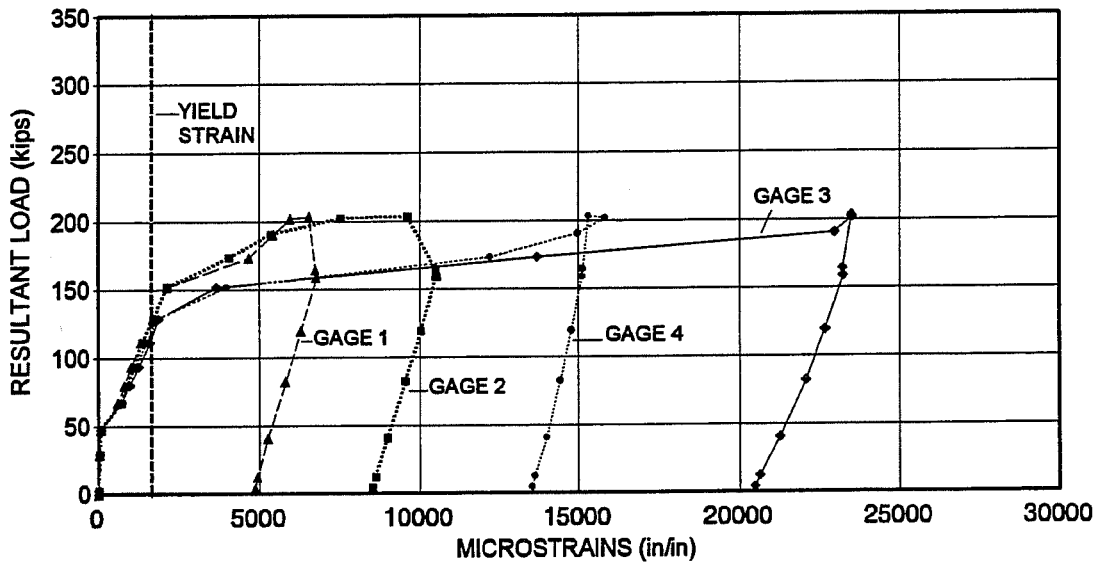


Figure D.8 Resultant Load vs. Strain in Gages 1 through 4 for Pier D-1

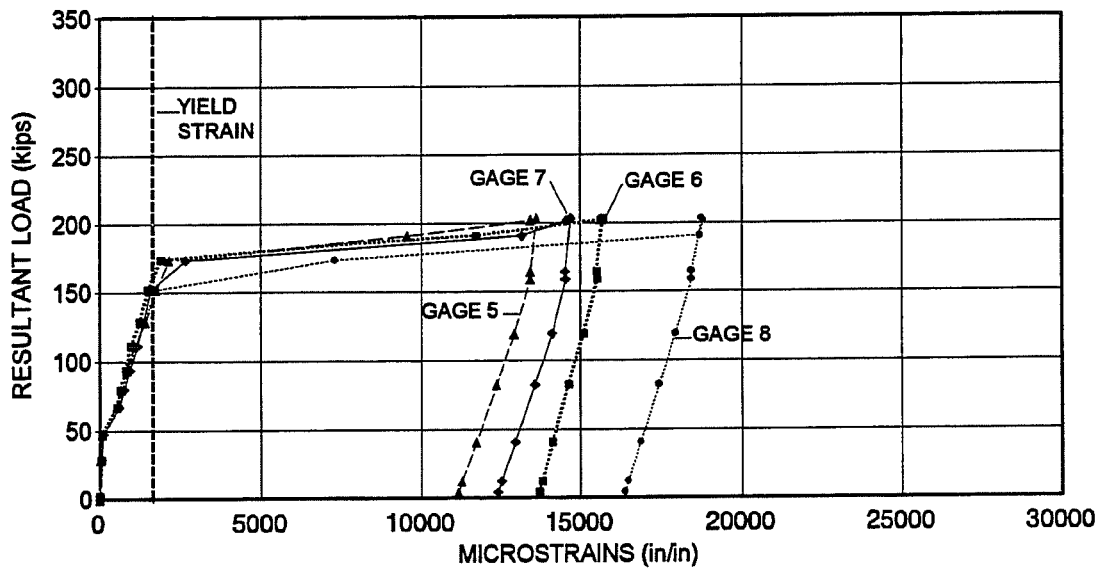


Figure D.9 Resultant Load vs. Strain in Gages 5 through 8 for Pier D-1

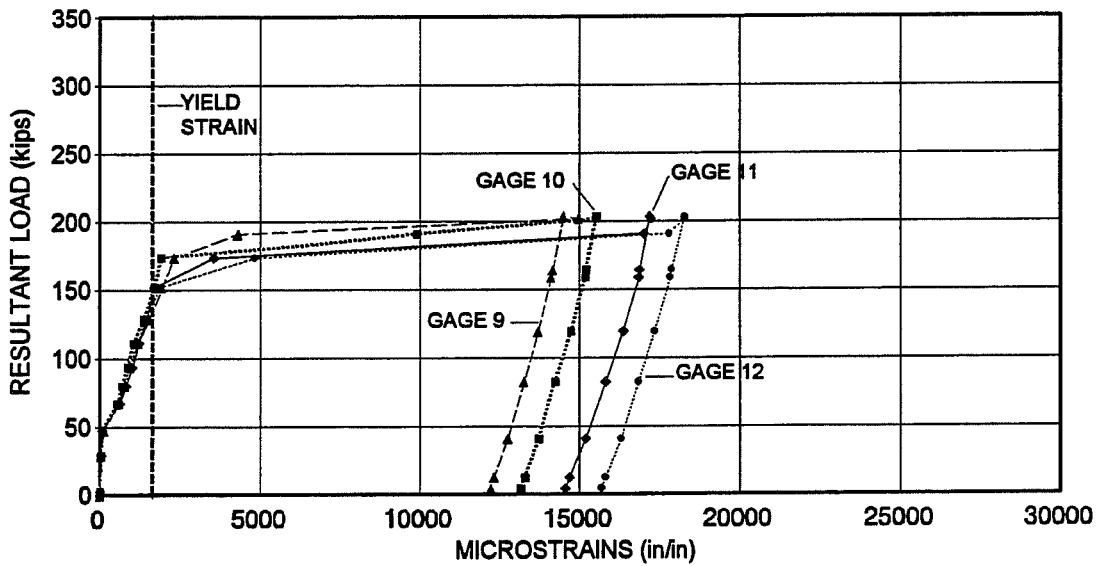


Figure D.10 Resultant Load vs. Strain in Gages 9 through 12 for Pier D-1

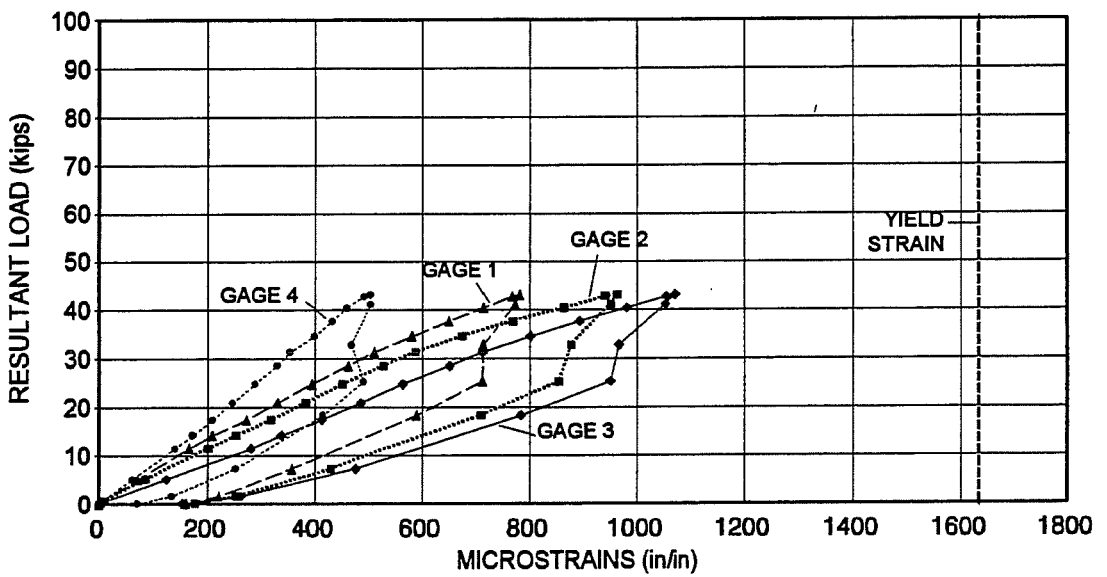


Figure D.11 Resultant Load vs. Strain in Gages 1 through 4 for Pier D-2

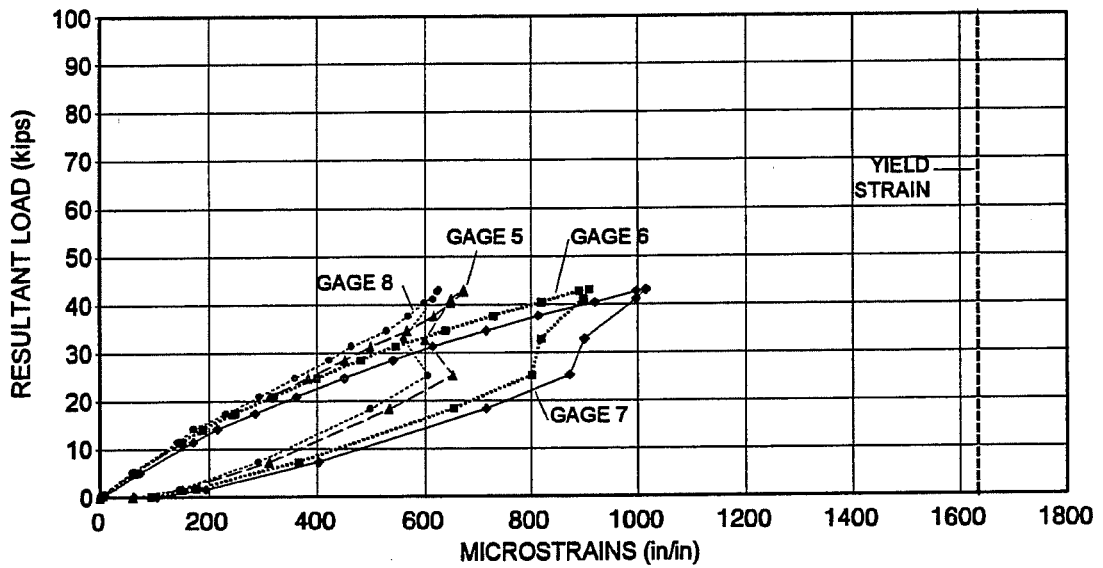


Figure D.12 Resultant Load vs. Strain in Gages 5 through 8 for Pier D-2

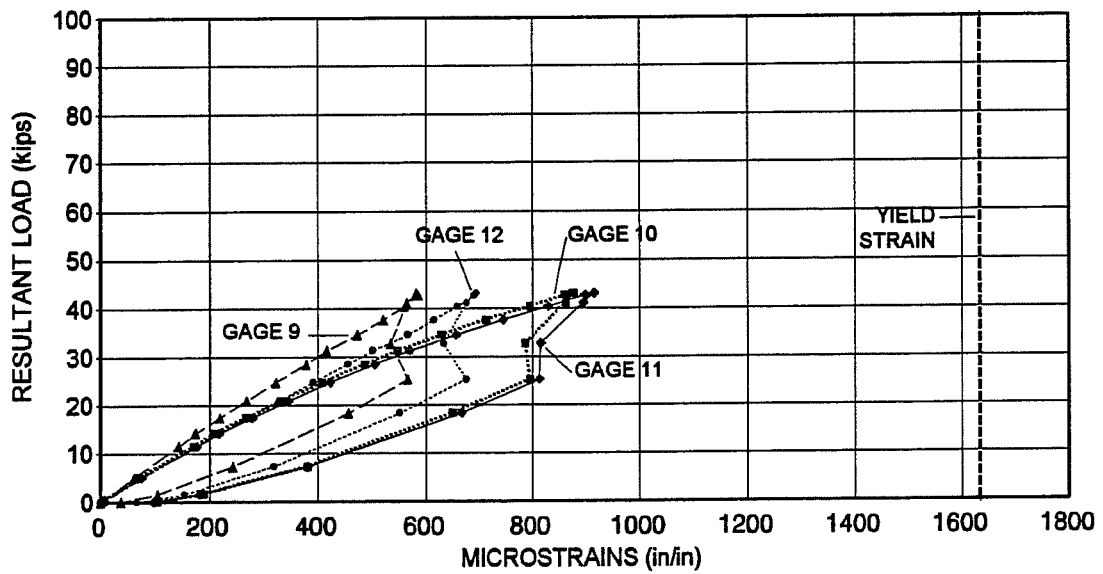


Figure D.13 Resultant Load vs. Strain in Gages 9 through 12 for Pier D-2

BIBLIOGRAPHY

American Association of State Highway and Transportation Officials, *Standard Specifications for Highway Bridges*, Fifteenth Edition, Washington D.C., 1992.

American Concrete Institute, *Building Code Requirements for Reinforced Concrete (ACI 318-89) and Commentary - 318R-89*, Detroit, 1989.

Anderson, R. B., "Behavior of CCT-Nodes in Reinforced Concrete Strut-and-Tie Models", Master's Thesis, University of Texas at Austin, December 1988.

Barton, D. L., "Detailing of Structural Concrete Dapped End Beams", Master's Thesis, University of Texas at Austin, December 1988.

Barton, D. L., Anderson, R. B., Bouadi, A., Jirsa, J. O., and Breen, J. E., "An Investigation of Strut-and-Tie Models for Dapped Beam Details", *Research Report 1127-1*, Center for Transportation Research, The University of Texas at Austin, May 1991.

Bergmeister, K., Breen, J. E., Jirsa, J. O., and Kreger, M. E., "Detailing for Structural Concrete - Draft Report", *Research Report 1127-3F*, Center for Transportation Research, The University of Texas at Austin, October 1990.

Bouadi, A., "Behavior of CCT Nodes in Structural Concrete Strut-and-Tie Models", Master's Thesis, The University of Texas at Austin, December 1989.

Park, R., and Paulay, T., *Reinforced Concrete Structures*, John Wiley & Sons, New York, 1975.

Powers, A. C., "Shear Strength of Pretensioned Concrete Girders in Negative Moment Regions", Master's Thesis, The University of Texas at Austin, May 1989.

Salmon, C. G., and Wang, C. K., *Reinforced Concrete Design*, Fourth Edition, Harper & Row, New York, 1985.

Schlaich, J., Schafer, K., and Jennewein, M., "Towards a Consistent Design of Structural Concrete", *PCI Journal*, May-June 1987, pp. 75-150.

Yura, J. A., *Plastic Design in Metals Class Notes*, The University of Texas at Austin, Spring 1992.

VITA

Richard Johnathan Denio was born in Eau Claire, Wisconsin, on October 26, 1968, the son of Dr. Allen Albert Denio and Valerie Steinmetz Denio. After graduating from Eau Claire Memorial High School in 1986, he enrolled in the pre-engineering program at the University of Wisconsin at Eau Claire. After two years at UW Eau Claire, he transferred to the University of Wisconsin at Madison. While attending UW Madison, he interned with Sargent & Lundy Engineers, Chicago, as a structural engineer. Richard graduated from UW Madison in August of 1991, receiving the degree of Bachelor of Science in Civil and Environmental Engineering. He entered The Graduate School of The University of Texas in September, 1991.

Permanent Address: 433 McKinley Avenue
Eau Claire, Wisconsin 54701

This thesis was typed by the author.

